7-1-2014

Antifungal Activity of Cationic Conjugated Polyelectrolytes and Oligomers against Candida albicans

Laura Ingersol

Student Name Laura Jane Ingersol
Candidate

Graduate Unit (Department) Biomedical Sciences Graduate Program
Department

This thesis is approved, and it is acceptable in quality and form for publication:

Approved by the Thesis Committee:

Chairperson Bridget Wilson

Aaron Neumann

David Witten

Antifungal Activity of Cationic Conjugated Polyelectrolytes and Oligomers against *Candida albicans*

Laura Ingersol

B.A., Biology/Chemistry, University of Colorado at Colorado Springs, 2011

Thesis

Submitted in Partial Fulfillment of the

Requirements for the Degree of

Master's in Science

Biomedical Science

The University of New Mexico

Albuquerque, New Mexico

July, 2014

Antifungal Activity of Cationic Conjugated Polyelectrolytes and Oligomers against *Candida albicans*

by

Laura Ingersol

B.A., Biology/Chemistry, University of Colorado at Colorado Springs, 2011

Abstract

Candida albicans is a human fungal commensal and an opportunistic pathogen. It is a polymorphic fungus that is able to invade host cells and disseminate through tissues. *C. albicans* also form biofilms on medical devices and mucosal surfaces, which aid in the development of drug resistance, tissue colonization and evasion of host immunity. Disseminated candidiasis is associated with high mortality rates, especially in immunocompromised hosts. Concern about resistance to current antifungal therapies has led to a push to develop novel, alternative treatments. In this study, we investigated the antifungal activities of two agents: PPE-DABCO, a poly(phenylene ethynylene) (PPE)-based cationic conjugated polyelectrolyte (CPE), and EO-OPE-1 (DABCO), an oligo-phenylene ethynylene (OPE). Both compounds generate singlet oxygen upon UV-irradiation. The effect of both compounds against *C. albicans* was tested in the dark and with photoactivation using light of the appropriate wavelength for each agent. We demonstrated that both compounds showed enhanced antifungal activity when irradiated with UV-light, reducing the viability of yeast in suspension. Activation of PPE-DABCO with the 405nm confocal laser was also able to significantly reduce the viability of *C. albicans* yeast and hyphal cells. Furthermore, by limiting the time of exposure to the

405nm laser to 20 minutes, we were able to isolate the effects of photoactivation of PPE-DABCO from effects due to phototoxicity, by assessing the subsequent hyphal growth. Neither dark nor light treatment with either compound was able to prevent the biofilm formation of surviving cells. This study provides evidence that PPE-DABCO and EO-DABCO act as potent antifungal agents upon photoactivation, and photoactivation is necessary to achieve full antifungal efficacy to reduce the viability of yeast and hyphae and prevent morphological transitioning.

Table of Contents

List of Tables

List of Figures

Chapter 1. Introduction

1.1 *Candida albicans*: a human fungal commensal and opportunistic pathogen

Candida albicans is a human fungal commensal that commonly colonizes mucosal surfaces and is found as part of the normal flora in greater than half of the population. It is also an opportunistic human pathogen; displaying a pattern of invasiveness into tissues and the bloodstream stemming from an abnormal overgrowth in urinary, gastrointestinal, and respiratory tracts. While this infection is frequently observed in immunocompromised patients, it is becoming increasingly common in healthy individuals as a result of nosocomial infections. (1). *Candida* spp. provides a significant contribution to morbidity and mortality rates; candidemia is associated with mortality rates that are reported as 30-40% (2). Of the *Candida* spp., *C. albicans* is the most prevalent pathogen identified as the cause of nosocomial infections, greater than 50% (3). The risk factors for acquiring candidiasis includes surgery, often involving the use of implanted catheters or other medical devices, administration of immunosuppressive medications, previous use of broad-spectrum antibiotics, or wounds such as burns or skin abrasions (4). Clinical treatment of invasive candidiasis using current antifungals is complicated by resistance to these drugs, either acquired or intrinsic, which contributes to an increase in morbidity, mortality, cost of treatments and duration of hospitalization (5). The pathogenicity of *C. albicans* is mediated by a wide range of virulence factors that enable the infection of a number of host niches. Some of these factors include the ability to switch between morphological forms, the expression of

adhesins and invasins, biofilm formation, thigmotropism, and the secretion of hydrolytic enzymes to degrade host tissue and promote invasion (6).

1.2 Yeast to hyphal morphological transition

C.albicans is polymorphic and can grow as yeast, which are spherical or ovoid in shape and reproduce by budding, pseudohypae, which are ellipsoid-shaped, elongated yeast cells that remain attached to other cells at a defined and constricted site of separation, or as hyphae, the filamentous form of the cells, that have sides that remain parallel along the entire length, and have a tube-like morphology. The switch to hyphal form is regulated by a series of signal transduction cascades that are initiated by numerous environmental factors, such as changes in temperature and pH, limiting nitrogen and carbon in the environment, and the presence of human hormones, such as progesterone, oestrogen, luteinizing hormone (LH) and human chorionic gonadotrophim (hCG) (7, 8, 9). Several transcription factors are activated in this process, including Cph1p and Efg1p, which are targets of the mitogen-activated protein kinase (MAPK) pathway, and the Ras-cAMP pathway, respectively (7, 10). These transcription factors are essential to activation of genes necessary for hyphal development, including *HWP1*, which encodes a GPI-linked cell surface protein that is expressed exclusively in hyphal cells. *HWP1* expression is dependent upon Efg1p (10). Deletion of either Efg1p or Cph1p, results in a defect in hyphal formation in response to an elevation in temperature to 37◦C and addition of serum, environmental triggers that induce hyphal growth in wild-type cells (11).

This ability to switch between morphological forms is associated with virulence (12). The hyphal form is associated with tissue invasion, due in part environmental factors within the host organism that promote the switch to this morphology, including temperature and pH. Furthermore, it has been found that *C. albicans* isolates that are defective in forming hyphae are associated with a decrease in the virulence of the pathogen (13). A study by Lo *et al.* demonstrated that a mutant strain of *C. albicans,* defective in the expression of two genes that are necessary for induction of filamentation, were avirulent in a mouse model (14). However, there is supporting evidence that the ability to switch between morphological forms is a major factor predicting virulence in *C. albicans* isolates. In fact, both yeast and hyphae have been found to be present in infected organs, and the predominance of one form or another depends largely upon the organ that is being infected (15, 16).

1.3 Biofilm formation by *C. albicans*

The ability of *C. albicans* to form robust biofilm structures contributes to the ability of the cells to survive adverse environmental conditions. The transition to hyphal form is not necessary for the formation of a biofilm structure; in fact, biofilms formed from *C. albicans* mutants defective in producing hyphae retain the ability to form dense three-dimensional structures that display similar resistance to amphotericin B (17). Biofilms are characterized as a three-dimensional structural community of microorganisms that are embedded in copious amounts of extracellular matrix. These structures become sessile upon attachment to a surface, which is the primary stage of biofilm development (18). In the case of *C. albicans* biofilms, the formation of the structures can be defined in a series of distinct phases. The first phase, attachment to a

surface, involves cells, usually in the form of yeast, adhering to a surface. Once adhered, the cells begin to enter the second stage of biofilm development, which is typified by cellular proliferation resulting in the formation of microcolonies. The third stage involves the expansion of the microcolonies to form a complex three-dimensional structure. During this stage, the cells begin to grow and produce hyphae, which are an alternative filamentous morphological form of *C. albicans*, and secrete extracellular matrix (ECM), a heterogenous composition of proteins, nucleic acids, carbohydrates and other materials produced or shed by the growing cells (17). The presence of extracellular DNA and other nucleic acids in the ECM is not a unique feature to *C. albicans* biofilm structure, but there is evidence that it may play a role in the ongoing maintenance and stability of mature biofilms, as well as the induction of the yeast to hyphal transition during biofilm development (19, 25). *C. albicans* biofilms can be diverse in structural form and cellular composition, with the surface to which initial adhesion occurs being a major influence on these characteristics.

1.4 *C. albicans* biofilm resistance to antifungals

Biofilms are particularly resistant to antimicrobial compounds. A study by Chandra *et al.* provided evidence that the MICs for amphotericin B, fluconazole, nystatin, and chlorhexidine all increased progressively as *C. albicans* biofilms matured (20). The complexity of biofilm structure and the heterogeneity of biofilm composition create multiple mechanisms for antimicrobial resistance. This is further evidenced by the observation, by our lab, that biofilm development is characterized by heterogeneous cell populations that display discrete growth rates, both in the presence and absence of sub-MIC concentrations of clinically used antifungal drugs. Furthermore, there is evidence

that the presence of persister cells within a biofilm, which are characterized as cells possessing a variant phenotype that confers antimicrobial resistance, possess the ability to produce new resistant biofilm structures following drug treatment (21). Cell growth within biofilms, characterized by both increasing cellular mass, formation of three dimensional structural complexity, and increased metabolic rate, may contribute to the resistance of biofilms to known antifungals, but cannot account for it completely (22). A study conducted by Baillie *et al.*, dispelled the idea that the biofilm growth rate of *C. albicans* alone conferred resistance to the common antifungal amphotericin B (23).

Maturing biofilms also produce copious quantities of extracellular matrix, which is a heterogenous material consisting of carbohydrates, nucleic acids, proteins, phosphorous and other materials produced by the cells; this material may vary in relative abundance of the individual components based upon factors such as maturity of the biofilm or morphological form of the secreting cells (24). Extracellular matrix production may contribute to the resistance of *C. albicans* biofilms to antimicrobial compounds by acting as a diffusion barrier, preventing access of the drugs to cells embedded deep within the biofilm structure. However, there is evidence that suggests that the extracellular matrix produced by *C. albicans* biofilms does not prevent fully the penetration of several common antifungal drugs (24). Extracellular DNA (eDNA) in the ECM has been linked to increased resistance to several clinically used antifungals, and has been demonstrated to play a role in maintaining the integrity of mature *C. albicans* biofilm structures. A study by Martins *et al.* provided evidence that increasing biofilm biomass can be linked to an increase in the eDNA content in the ECM, and biofilm mass decreases upon addition of DNase treatment (25). There is also evidence that DNase

treatment increases the efficacy of amphotericin B against *C. albicans* biofilms, although this form of combination therapy does not appear to increase the susceptibility of biofilms to other antifungals, such as fluconazole (26).

C. albicans biofilms also have several molecular mechanisms by which antimicrobial resistance is achieved, although this is an area requiring further investigation. One such mechanism contributing to azole resistance is the expression of ATP-binding cassette (ABC) transporters and the major facilitator superfamily (MFS) transporters that actively efflux drugs, which contribute to resistance in both biofilms and free-floating cells (27). A recent study using a clinical isolate of *C. albicans* from a hospital in Tunisia, found that azole resistance in this isolate was due to the overexpression of a multidrug efflux pump of the superfamily, Mdr1, due to a gain-of-function mutation (28). However, the presence of certain drug transporters in the cell membrane alone may not confer resistance. A study conducted by Shah *et al.* found that the absence of the Quinidine Drug Resistance (QDR) transporters in the cell membrane did not increase the susceptibility of *C. albicans* to a number of cell wall stressors or common antifungals, although these strains did show defects in both biofilm formation and attenuated virulence (29). Other molecular mechanisms governing resistance in *C. albicans* biofilms have been recently identified, such as the presence of heterozygous-*MTL* (mating type locus) cells within a biofilm (**a**/α), which confers a far less permeable environment for penetration of both antifungal agents and polymorphonuclear leukocytes than biofilms comprised of cells that are homogeneous at this locus. As 90% of *C. albicans* are of the heterozygous *MTL* variety, this type of biofilm is commonly found in both nature and in clinical settings (30).

1.5 *C. albicans* mechanisms of adhesion to host cells

Adhesion is mediated by a family of large cell-surface glycoproteins encoded by the agglutinin-like (*ALS)* genes, which are regulated differently according to whether the cells are growing in planktonic or hyphal forms (20). Furthermore, these genes display altered regulation due to medium changes or growth stages. The Als proteins are linked to beta1,6-glucan within the cell wall, acting as a glycosylphosphatidylinositol (GPI)-module, and are heavily N- and O-glycosylated (36). Also implicated in adhesion is hyphal wall protein 1 (Hwp1), which contains an amino-terminal domain that is exposed on the cell wall surface, and can cross-link with exogenous proteins (37). A study by Younes *et al.* linked Hwp2 with contributing to tolerance to oxidative stress as well as adhesion to human endothelial and epithelial cells, formation of biofilms and chitin content of the cell wall. *C. albicans* strains that were deficient in Hwp2, were less adherent to endothelial and epithelial cells, unable to form wild-type biofilm structures, and more susceptible to oxidative stress by exogenous hydrogen peroxide (38). Other factors influencing adhesion are the relative hydrophobicity of the cell wall, which may influence adhesion to epithelial cells often influenced by the relative glycosylation of mannoproteins within the cell wall (39).

1.6 *C. albicans* mechanisms of invasion into host cells

C. albicans possesses the ability to invade host tissues using two distinct mechanisms: active penetration or induced endocytosis (6). The expression of invasins on the fungal cell surface, proteins on the cell surface of the fungi that mediate binding to host tissues, allow the pathogen to induce host cells to endocytose fungal cells (31). The

two invasins that are implicated in this process are Als3 and Ssa1 (6). Als3, which also functions as an adhesin, binds to E-cadherin on epithelial cells or N-cadherin on endothelial cells to induce endocytosis, by activation of the clathrin-dependent endocytosis pathway (32). Ssa1 is a member of the heat shock protein 70 (Hsp70) family that is expressed on the cell surface; it can directly mediate adherence to and endocytosis by host cells by the same mechanism as Als3 (33). Active penetration of *C. albicans* into host tissues is a less well understood mechanism, but appears to require the hyphal morphology of the pathogen, as well as both the adhesion of fungal cells to host tissues, secretion of hydrolytic enzymes and the application of physical force (34). The importance of hyphal formation in invasion is evidenced in a study by Felk *et al.* in which a strain of *C. albicans* that lacked the expression of the transcription factor Efg1, and could not form hyphae, was not able to invade or damage parenchymal organs in mice (35).

1.7 Secretion of hydrolytic enzymes enhances *C. albicans* virulence

The ability of *C. albicans* to secrete hydrolases following adhesion to host cells is an important virulence factor that is thought to both facilitate penetration into host tissues, as well as increase the availability of extracellular nutrients, and digesting components of the host immune system (34, 40). *C. albicans* produce three main types of hydrolytic enzymes: secreted aspartyl proteinases (Sap), phospholipase B enzymes, and lipases.

The Sap proteins are encoded by 10 *SAP* genes in *C. albicans*, although many other pathogenic *Candida* species also possess some of these genes as well. Sap1-8 are

secreted forms, while Sap9 and Sap10 are bound to the cell surface (6, 40). Sap proteins are differentially expressed based upon environmental cues, such as pH or availability of nitrogen sources, which may partially explain the ability of the pathogen to colonize many different host tissues (41). Furthermore, Sap proteins are differentially expressed depending upon the morphological form of the fungi; for example, *SAP4* and *SAP6* expression is associated with the transition to the hyphal form, while *SAP1* may be regulated by phenotypic switching (42, 41, 40). One of the proposed functions of Sap proteins may be to mediate adherence to host cells (40). The relative level of Sap protein expression may also predict virulence, as evidenced in a study by Felk *et al.* in which *C. albicans* strains that were sufficient in hyphal formation, but lacked Sap proteins associated with hyphal growth, particularity Sap6, were less invasive in a murine model of disseminated candidiasis (43). Recently, there has been some evidence that Sap production may play a role in inducing apoptosis in epithelial cells, by damaging lysosomal membranes following internalization by epithelial cells (44).

The phospholipases are comprised of a group of enzymes that are able to hydrolyze the ester bonds in phospholipids. The specificity of the ester bond that each enzyme is able to cleave lead to the use of grouping and lettering the enzymes A, B, C, and D, which indicate the target bond (45, 46). Phospholipase B (PLB) is the predominant phospholipase in *Candida*, accounting for ~90% of the extracellular phospholipase activity. PLB possesses both hydrolase and lysophospholipase-transacylase (LPTA) activities. The hydrolase activity of the enzyme results in the release of fatty acids from phospholipids and lysophospholipids; the transacylase activity of PLB results in the production of a phospholipid by transfer of a free fatty acid to a

lysophospholipid. This activity is thought to facilitate invasion of the pathogen by leading to cell membrane disruption in host cells, which may cause cell lysis and promote transmigration of the fungi (46).

C. albicans also secrete lipases during invasive growth, which enzymes are capable of catalyzing both the hydrolysis and synthesis of triacylglycerols (47). *C. albicans* possess 10 lipase genes; but differential expression of these genes has been observed, which appears to be partially dependent upon the relative location of infection (48). Lipase 8 has been associated with increased virulence in murine intravenous infection models (47).

1.8 Cell wall composition of *C. albicans*

The cell wall of *C. albicans* that surrounds the cell provides two essential functions; it protects the cell by providing a rigid structure that maintains cellular integrity and interacts with the surrounding environment to provide cues to the cell that helps ensure survival (50). Localized externally to the cell membrane of the fungi, it is comprised of a multipart organized structure that primarily consists of beta-glucans (β1,3 and β1,6-glucan), which are complex glucose polymers (50).The beta-glucans form around 50-60% of the cell wall structure and are largely responsible for providing the structural rigidity that provides both cellular shape and protection (51, 49) The beta-glucans are enriched in the inner portion of the cell wall. They contribute to a pliable highly branched network of beta1,3-glucan that attaches to both chitin and beta-1,6-glucan via the multiple reducing ends of the branched polymer (50). The reducing ends of the beta-glucans also have a role in facilitating the attachment of multiple types of cell

wall proteins (50), primarily glycosylphosphatidylinositol (GPI)-dependent and Pir cell wall proteins (49). Soluble glucans are also shed by the fungal cell wall and can enter into the blood stream of patients during active fungal infections, and are responsible for the activation of a number of host immune responses (52). The second most abundant components of the *C. albicans* cell wall are mannoproteins, which comprise about 30-40% of the structure. They are mainly found in the outer layer of the cell wall, whereas the inner cell wall layer consists mainly of the fibril network of glucan and chitin (53). The mannoproteins mediate adherence of the cells to various surfaces, including tissues of host organisms, as well as possessing a role in modulation of the immune response within the host organism (50). Chitin is of relatively low abundance within the cell wall, comprising a mere 0.6-3% of the structure, but is of utmost importance in the maintenance of cell wall rigidity, primarily due to the interactions with the beta-glucan network of fibrils (51). Increased chitin content within the cell wall can also allow the integrity of the cell wall to be maintained in instances when the synthesis of beta1,3-glucans is compromised, either because of mutations or defects in the synthesis pathway caused by exposure to certain types of antifungal drugs, particularly echinocandins, which inhibit the production of 1,3-beta-D-glucan by interference with the catalytic subunit of Beta (1,3)-glucan synthase, Fks1 (54, 55). In addition to increasing chitin content within the cell wall, *C. albicans* can achieve further structural stability by increasing the linkages between chitin and beta1,6-glucans (49, 56, 57). Cell wall proteins are a major factor influencing the composition of the cell wall. These proteins are usually heavily *O*-mannosylated at both serine and threonine residues, which facilitates convalent attachment of these proteins to the beta-1,6-glucan fibrils; without

the *O*-mannosylation of these proteins, cells will undergo heavy cell wall remodeling by upregulation of chitin and beta1,3-glucan (53). The modification of cell wall proteins begins in the ER, due to the activity of five nonredundant isoforms of protein-O-mannosyltransferases (Pmt1, Pmt2, Pmt4, Pmt5, Pmt6) prior to partial extension of the *O*-mannosylation in the Golgi by mannosyltransferases (58). Defects in any of these enzymes can lead to various negative consequences to the cell, including increased antifungal sensitivity, changes in internal turgor pressure to combat weakening of the cell wall, lowered virulence, and changes in the ability to form hyphae (59, 60 ,61).

The ability of *C. albicans* to undergo dynamic cell wall remodeling in response to stress partially responsible for the robustness of this pathogenic fungi even in adverse environments. One such mechanism by which *C. albicans* senses environmental stress and compensates by undergoing cell wall remodeling is by activating the cell wall integrity (CWI) pathway. Much of what is understood about this pathway has been elucidated in studies involving *S. cerevisiae*. The CWI pathway is a kinase cascade that is tightly regulated by a series of GTPase-activating proteins and guanyl nucleotide exchange factors (GEFs); when this cascade is initiated, it leads to the activation of transcription factors that lead to cell wall remodeling (62). Two cell wall-associated stress sensors, Wsc1 and Mid2, initiate the cascade by binding to Rom2, which acts as a GEF for Rho1 (63, 62, 64). Activation of Pkc1 by Rho1 begins the activation of the MAPK cascade, ultimately ending in the phosphorylation of Rlm1 and SBF, two transcription factors that stimulate the expression of genes necessary for cell wall synthesis (65, 66, 62). SBF is a heterodimer comprised of two proteins Swi4 and Swi6, and is of primary importance during the G1/S transition (67). The importance of Rlm1 in

cell wall biogenesis and maintenance is evidenced in a study by Delgado-Silva *et al.* in which deletion of this transcription factor lead to significant cell wall remodeling, including an increase in chitin and a concurrent reduction in mannans, and an increased sensitivity to compounds associated with the induction of cell wall stress, including calcofluor-white and caspofungin (68).

C.albicans also possesses a mechanism which allows yeast to respond to additional osmotic stress known as the high-osmolarity glycerol (HOG) pathway (69). This pathway may be activated by two different input branches. The first is the Sho1 branch, which responds to severe hyperosmotic stress using two plasma membrane proteins, Sho1 and Msb2. Once initiated the Rho GTPase Cdc42 is activated, along with Ste20 and Ste50. Ste20 activates the MAPKKK Ste11, which subsequently activates Pbs2 , which activates Hog1 (70, 69). The second branch also leads to Pbs2 activation, but involves the transmembrane protein Sln1 and the regulatory response proteins Ypd1 and Ssk1 (71). Once initiated, this pathway results in the activation of two redundant MAPKKKs, Ssk2 and Ssk22, which activate Pbs2. Activation of Hog1 results in the transcriptional activation of genes that are critical for the cellular response to osmotic stress (67). Although the CWI pathway is the primary pathway that is involved in cell wall construction, the Hog1 pathway is also activated under conditions of cell wall damage, and both pathways are necessary for cell survival in these circumstances (67).

1.9 Current antifungal treatments for invasive candidiasis

Prior to the introduction of echinocandins, only three classes of antifungal drugs have been clinically used to treat *Candidiasis* and other fungal infections: the polyenes

(amphotericin B); the azoles (ketoconazole, itraconazole, fluconazole, and voriconazole); and flucytosine (72). The use of these drugs clinically, as well as increasing reports of resistance in clinical isolates, demonstrated a need for standardization of the techniques used for antifungal susceptibility testing. The protocols for assessing susceptibility for both yeast and filamentous fungi were established by the Clinical and Laboratory Standards Institute in 2002 (73, 74). However, susceptibility testing results do not always accurately predict the clinical responses to different antifungal therapies. This observation in antibacterial susceptibility testing resulted in the implication of the "90-60 rule", in which it is predicted that isolates deemed susceptible will respond to treatment around 90% of the time, and isolates found to be resistant will respond to treatment around 60% of the time (72). While the refinement of susceptibility testing is necessary, this approximation is a clinically useful predictive tool that aids treatment of fungal infections. However, increasing resistance to antifungals is a major clinical concern that necessitates the development of new antifungal therapies that can be applied in a clinical setting.

The antifungal class of azoles, which includes both the imidazoles and the triazoles, combat fungal infections by preventing the biosynthesis of ergosterol through inhibition of lanosterol 14-α-demethylase (75). Ergosterol is the main sterol component of the fungal cell membrane, and is analogous to cholesterol in mammalian cells; inhibition of the biosynthetic pathway causes ergosterol depletion in the membrane as well as a toxic buildup of methylated sterol intermediates. Azoles act by targeting C14 lanosterol demethylase (76). This leads to growth inhibition of the cell, and in some cases, cell death (77). However, there is considerable difficulty in successfully treating

fungal biofilms with azoles, as biofilms show considerable resistance to these compounds compared to the MICs used against planktonic cells; almost 1000 fold increase over the MIC needed to kill cells in suspension was needed to inhibit *C.albicans* biofilms in one study (78). Beta-1,3-glucan, present in the ECM of *Candida* biofilms, is implicated in fluconazole resistance, by binding to and sequestering the drug before it has the opportunity to diffuse to the cells located deep within the biofilm structure (79, 78). It has been demonstrated that azoles have the ability to induce the accumulation of reactive oxygen species (ROS) in planktonic cells, particularly miconazole. However, the ability of these compounds to induce ROS accumulation varies widely, and some compounds may not cause enough to induce cell death (80, 81). The mechanism by which this occurs seems to include an inhibition of perioxidase and catalase, which break down ROS (81). One concern associated with use of azoles for irradiation of biofilms is the presence of persister cells, which remain viable following treatment with supra-MIC concentrations due to heritable phenotypic differences in these cells. This is often evidenced by the biphasic killing pattern that is associated with azole treatment, particularly miconazole, in which a fraction of the original cell population remains viable and resistant following drug treatment (79). A study by Bink *et al.* demonstrated that miconazole-tolerant persister cells were linked to a ROS-detoxifying effect due to expression of superoxide dismutases within the cells of a *C.albicans* biofilm; inhibition of genes associated with production of superoxide dismutases resulted in a reduced number of persister cells in miconazole-treated biofilms (82). However, though azoles are effective antifungal drugs against planktonic cells, only miconazole has effective activity against *C. albicans* biofilms, and often results in biphasic killing, leading to the emergence of persister cells

(79). Additionally, resistance can also be achieved by either overexpression of or mutations of the target of the drug, C14 lanosterol demethylase . Resistance in *Candida spp.* has also been attributed partially to overexpression of the genes encoding the drug efflux pumps of the ABC and MFS classes, including *CDR1, CDR2 and MDR1* (76).

Flucytosine is a commonly used clinical antifungal. It is endocytosed by the cell and subsequently converted into its metabolically active form, 5-fluorouracil. This compound then inhibits cell growth by inhibition of both protein synthesis and DNA replication). However, *C.albicans* commonly show resistance to this antifungal; with about 10% displaying intrinsic resistance, and around 30% developing resistance during clinical treatment using this compound (76). Resistance is associated with mutations in the *FCy2* gene, which encodes purine-cytosine permease, which is necessary for successful uptake of the drug by the cell, in the *FCy1* gene, encoding cytosine deaminase converts flucytosine to its active form, 5-flurouracil, or in the *FUR1* gene, encoding phosphoribosyltransferase, which converts 5-fluorouracil to 5-fluorouridine monophosphate (76). A recent study by Gopinathan *et al.* examined antifungal resistance *Candida* isolates from two hundred vaginal candidiasis patients in Chennai, and found that mutant *FUR1* was present in all species that displayed flucytosine resistance. Furthermore, the incidence of resistance to this antifungal drug was prevalent among all the isolates and a greater percentage were resistant to 5-flucytosine than the other antifungals tested, around 41.66% (83). Due to high prevalence of clinical resistance to this antifungal, combination antifungal therapy has often been employed when using this drug in a clinical setting. However, there is evidence that treatment with flucytosine can contribute to other antifungal resistance, particularly to azoles. A recent study conducted

by Steier *et al.* demonstrated that subinhibitory concentrations of flucytosine antagonized fluconazole activity in different isolates of *C. glabrata.* The mechanism behind this antagonism was due to flucytosine activation of Pdr1, a transcription factor that upregulates the expression of *CDR1,* a multidrug transporter encoding gene (84). The activation of this gene is associated with azole resistance in *C. glabrata (*86). The contribution of resistance to flucytosine to resistance to azoles has been established in other *Candida* species as well. *C. lusitaniae* isolates that contained mutations in *FCY1* or *FCY2,* displayed resistance to fluconazole as well (87).

In contrast to flucytosine, resistance of *Candida* isolates to amphotericin B, is not as commonly observed. Amphotericin B is an agent of the polyene class of antifungals; which are naturally occurring polyketides produced by *Streptomyces* spp (88). It effectively binds to ergosterol in the cell membrane of fungi to form pores, which can eventually lead to cell death (76). Resistance to this class of antifungals is defined as displaying a MIC that is greater than 2ug/mL (76). The molecular mechanisms contributing to resistance to amphotericin B are poorly understood, but usually associated with changes in the molecular composition of the cell membrane, particularly decreases in ergosterol content. This decrease is usually due to gene mutations in genes that encode enzymes that are involved in ergosterol synthesis, usually *ERG3,* leading to a concurrent increase in the content of other sterols in the cell membrane (76). Resistance in both *Candida* and *Cryptococcus* clinical isolates was associated with a low level of ergosterol content in the cell membrane (89).

Echinocandins have gained widespread clinical use as antifungal drugs to their ability to inhibit fungal cell wall synthesis in most species of *Candida*, and are

particularly useful against *Candida* that displays antifungal resistance to other clinical drugs (55). The fungicidal activity of this class of large lipopeptides is due to the inhibition of beta-1,3-glucan production, by targeting the catalytic subunit of Fks1 within the beta-1,3-glucan synthase complex (55). These compounds are chemically modified from naturally produced fungal products. They are thought to intercalate into the phospholipid bilayer of the cell membrane of exposed fungi using the N-linked acyl lipid side chains present in each agent, although the exact chemical composition of this side chain varies with each (90). This class of drugs is clinically effective, and causes relatively few adverse effects in patients, due in part to the lack of a mammalian target. The echinocandins also display far fewer drug interactions than other antifungal classes of drugs, such as azoles (72). There is evidence that caspofungin, an echinocandin, is more effective against *C. albicans* biofilms than either fluconazole or amphotericin B (91). There are several distinct drugs in this class of antifungals, but for all agents within this class, susceptibility is defined as possessing drug minimum inhibitory concentrations (MICs) of ≤2ug/mL. Furthermore, the MIC_{90}, or the MIC at which 90% of *Candida* isolates are susceptible are usually less than 2ug/mL (90). However, although resistance rates to echinocandins are fairly low, instances of resistance has been observed both in clinical and laboratory settings (92). Resistant strains of *C. albicans* are often found to contain specific point mutations at two hot spots in the FKS1 gene, usually at the serine at position 645, which lead to amino acid substitutions that occasionally, but not always, confer resistance (90). Studies have shown that elevated chitin content within the cell wall of various species of *Candida* also confers resistance to echinocandins, likely due to increased stability of the cell wall that prevents lethal amounts of damage from occurring

(93). A paradoxical effect on growth on strains of *Candida* is well-reported in the literature, at which isolates are found to be capable of growing at concentrations far exceeding the MICs of different agents. This effect seems to rely in part, on the ability of the isolate to remodel the cell wall to contain more chitin than is usually observed. A study by Shields *et al.* revealed that several varieties of *Candida* exhibited paradoxical growth when treated with caspofungin, an echinocandin, but this effect was eliminated using both chitin synthase inhibitor nikkomycin Z and calcineurin pathway inhibitors (94).

Although these antifungal drugs are distinct in form and function, they have been all found to the ability to induce the production of reactive oxygen species (ROS) in fungal cells (79). Among the azoles, miconazole is particularly effective at inducing ROS accumulation within planktonic fungal cells (95). In addition, miconazole is the only agent within this class that has produced significant levels of ROS accumulation in biofilm cells. However, ROS accumulation did not result in increased apoptosis nor did quenching of ROS lead to enhanced survival of *C. albicans* biofilm cells (96). Autooxidation of amphotericin B can lead to oxidative damage and death of *C. albicans*, evidenced by a study by Sokol-Anderson *et al.* in which treatment with this antifungal under hypoxic conditions reduced the oxidative damage to the cells by 80%. This study demonstrated that catalase and superoxide dismutase conferred a protective effect to *C. albicans*, allowing them to resist killing by amphotericin B (97).

Finding methods to increase ROS accumulation in *Candida* planktonic and biofilm cells, in order to promote apoptosis, is currently being pursued as a possible alternative antifungal treatment. One such method is the use of photodynamic

inactivation, which typically uses a compound that acts as a photosensitizer, producing ROS in response to activation by light of the appropriate wavelength (79). This method has been known to possess the ability to eliminate different types of microorganisms since the early 1900's, but the increases use of antibiotics since the mid-20th century caused this form of therapy to fall into disuse. It began to be reevaluated as an antimicrobial therapy after increases in antibiotic resistance made finding alternative clinical strategies necessary (98). To enhance the selectivity of these compounds, they are often engineered to either be taken up by target cells or to attach to them in some manner (104). Studies involving *C. albicans* suggest this form of therapy works faster than other antifungal treatments, and can be effectively used to eliminate microorganisms showing resistance to other agents (98).

Antimicrobial photodynamic therapy (APDT) begins when light of a specific wavelength is absorbed by the photosensitizing compound; this causes the promotion of the compound from the ground state to a photoactive triplet state, in which the molecules of the compound can pass either excess energy or their electrons to nearby biomolecules. This can occur by one of two mechanisms. The first mechanism utilizes the localized production of cytotoxic radicals from nearby substrates, the second generates singlet oxygen from molecular oxygen, which can then react with nucleic acids, proteins or other biomolecules (98). Singlet oxygen production can lead to cellular damage through many targets, including inactivation of enzymes leading to disruption of cellular processes and peroxidation of lipids, causing membrane disruptions and possibly leading to lysis of cellular membranes; however, the exact photosensitivity effect on cells varies depending upon factors such as media composition (99).

Clinically, the only photosensitizing compounds used to date are phenothiazinium salts, such as methylene blue and Toluidine Blue, which are often used together and activated with red light. This therapy is often used to sterilize during dental procedures and to treat periodontitis (98). However, the effectiveness of APDT against fungal cells has been established, making this form of alternative treatment attractive as a potential method of combating fungal infections, particularly superficial ones. A recent study conducted by Pereira *et al.* indicated that photodynamic inactivation using methylene blue as a photosensitizer was effective as significantly decreasing viability of biofilm cells formed by different microorganisms, including *C. albicans* (100). Furthermore, a study by Zeina *et al.* provided evidence that ketatinocytes exposed to methylene blue and visible light, had kill rates that were 18-200 fold lower than that for cutaneous microbial species under identical conditions, indicating that this form of treatment could be used without severe damage occurring to nearby tissues (101, 102).

There has been little evidence that APDT has mutagenic effects on treated cells, and as the therapy is nonspecific and damages many cellular components, complete resistance from repeated use would be unlikely to occur (103, 98). Singlet oxygen reacts strongly with nucleic acids, which could have a potential mutagenic effect, however, this effect does not prevent killing of *D. radiodurans*, a bacteria with a DNA repair mechanism efficient enough to allow the organism to survive doses of ionizing radiation, by APDT (105).

The main mechanisms of fungal resistance to APDT are the same mechanisms that govern other types of drug resistance, particularly those related to efflux of the drugs. The ABC and MFS transporters in *C. albicans* have been reported to decrease the

effectiveness of APDT using methylene blue (106). This would suggest that targeting photosensitizers to the outside of fungal membranes may be effective at circumventing resistance mechanisms in fungal cells. Intrinsic mechanisms of resistance seem to be the main factors contributing to the resistance of microorganisms to APDT. *C. albicans* possess an oxidative stress response against ROS, such as expression of catalase Cta1 and superoxide dismutases, Sod1 and Sod 5 (107, 108). The expression of catalase is thought to enhance the pathogenicity of *C. albicans* by allowing the fungi to be less sensitive to oxidative damage by neutrophils and exogenous peroxide, and strains that did not express catalase were less virulent in a murine model of disseminated candidiasis (107). Sod proteins convert superoxide radicals into hydrogen peroxide, which is less toxic to the cell. Sod1 (CuZnSOD) expression in *C. albicans* is primarily confined to the cytosol; this species also expresses Sod3 (MnSOD) in the mitochondria. In addition to these Sod proteins, *C. albicans* also express Sod4, Sod5 and Sod6. Sod5 is upregulated during the transition from yeast to hyphal morphology, during both osmotic and oxidative stress, and when grown in certain media (109, 108). Sod5 is an important virulence factor; strains deficient in expression were more sensitive to oxidative damage by hydrogen peroxide and less virulent in a mouse model of infection (108). Resistance to oxidative damage may also be achieved via alternative mechanisms. *C. albicans* express six major heat shock proteins (HSPs), which respond to environmental stresses such as oxidative stress, nutrient deprivation or temperature elevation by preventing the aggregation of damaged or misfolded proteins, which can potentially lead to cell death (6). Expression of HSPs is upregulated when the transcription factor Hsf1 becomes hyperphosphorylated as a cellular response to stress; it then activates the transcription of genes that contain

heat shock elements (HSEs), including those encoding various HSPs. Hsf1 activation and subsequent upregulation of HSPs is necessary for full virulence of *C. albicans* in a mouse model of systemic candidiasis (110). The expression of small heat shock proteins (sHSPs) may also contribute to the ability of *C. albicans* to resist oxidative stress. Thus far, six sHSPs have been identified in *C. albicans*; they function to prevent the aggregation of damaged or misfolded proteins, which may become toxic to the cell (6). sHSPs may contribute to the pathogenicity of *C. albicans* as well. A study by Mayer *et al.* demonstrated the critical role of Hsp21 in resistance of oxidative and thermal stresses, hyphal development, defects in adhesion and invasion into endothelial and epithelial tissues, and resistance to killing by neutrophils (111). However, it remains to be elucidated whether these intrinsic mechanisms of responding to oxidative stress confers resistance to APDT using various photosensitizing compounds.

APDT continues to be a promising alternative treatment for bacterial and fungal infections, particularly in strains that are resistant for other antimicrobial treatments. The development of new photosensitizing compounds may lead to more effective clinical treatments for invasive candidiasis, but this is an area that requires further elucidation.

1.10 Cationic conjugated polyelectrolytes and oligomers as antimicrobial agents

The development of antimicrobial cationic compounds has been investigated as an alternative treatment to traditional antimicrobial agents. The positive charges are able to effectively interact with surfaces, polymers, peptides and particles; which can confer antimicrobial properties by causing disruption to membranes. In addition, many of these

compounds display low toxicity to mammalian cells, which is of utmost importance when considering the possible use of agents clinically (112).

There are several aspects that influence the mechanisms of antimicrobial activity and efficacy. The molecular weight of the agent may influence the permeability of the compound through the cell wall. The presence of a counterion may influence the solubility of the compound. The relative hydrophobicity and hydrophilicity of the agent and the overall structure and geometry may also affect the activity, interactions with cellular structures, solubility, and permeability of the compound (113).

In this study, we tested two photoactivatible biocidal compounds, one (PPE)-based cationic conjugated polyelectrolyte (CPE), PPE-DABCO, and one oligo-phenylene ethynylene (OPE), EO-OPE-1 (DABCO). The PPEs and OPEs are conjugated electrolytes, containing double or triple bonds separated by a single bond. These compounds form ions in solution and are fluorescent (114, 115).

The antibacterial properties of PPE-based cationic conjugated polyelectrolyte were first described by Lu *et al.* In this study, they demonstrated the effectiveness of the light-induced biocidal activity following the coating of the agent to the surface of both Gram negative and Gram positive bacteria (115). The antimicrobial properties of (PPE)-based cationic conjugated polyelectrolytes (CPEs) have been found to correlate to the length of the polymerized chain; the shortest polymer (n=7) tested in one study showed the greatest degree of antibacterial activity against both Gram negative and Gram positive bacteria (116).

Previous work by Wang *et al.* revealed that (PPE)-based cationic conjugated polyelectrolytes (CPEs) and oligo-phenylene ethynylenes (OPEs) were effective at breaching the outer membrane of bacterial cells and interacting with the cytoplasmic membrane, creating damage to the cell surface. This interaction was effective at killing bacterial cells, even in the absence of photoactivation of the compounds (117). It has been demonstrated that while Gram negative bacteria exposed to CPE and OPE compounds in the dark show evidence of damage to the cell envelope, plasma membrane and some damage to the cytoplasm, Gram positive bacteria remained intact upon exposure to the same compounds in the dark, and the agents bound to and disrupted the cell wall only (118). This indicates that the mechanism by which these agents are able to inflict damage to cells in the absence of photoactivation depends on the cellular structure and organization of the organism.

In addition, both the CPE and OPE compounds possess light-activated biocidal activity, which is mediated by the ability of the agents to generate singlet O_2 upon irradiation with UV-visible light. A study by Wang *et al.* demonstrated that *E. coli* exposed to CPEs and OPEs in the presence of UV-light showed evidence of covalent modifications to both plasmid DNA and proteins, which was attributed to oxidative pathways activated by the generation of singlet oxygen and other ROS (118).

1.11 Antifungal activities of PPE-DABCO and EO-DABCO

Previous work by Wang *et al.* has demonstrated the effectiveness of both PPE-DABCO and EO-DABCO against *S. cerevisiae*. Both compounds were effective at

significantly reducing the viability of vegetative yeast cells in the dark; and upon UV-irradiation, both compounds demonstrated even more potent antifungal activity (119).

In this study, we tested the antifungal activity of PPE-DABCO and EO-DABCO against a clinically relevant pathogenic fungus, *C. albicans*, to determine whether these compounds could effectively reduce the viability of the yeast in the dark and upon light activation of the compounds. Furthermore, we tested the ability of the compounds to inhibit the yeast to hyphal transition of these cells, as that is an important factor that contributes to the virulence of the fungi, and the ability of fungi to form biofilms. We saw reductions in the viability of the yeast upon photoactivation of the compounds, but treatment with the agents in the dark failed to reduce viability significantly. We also demonstrated that light-irradiation of the compounds could inhibit the yeast to hyphal transition of *C. albicans*. We were able to localize both of the compounds to the cell wall of both yeast and hyphal cells and photoactivate the agents using the 405nm confocal laser, which allowed us to directly visualize and subsequently quantify changes to the cells over time. However, treatment with the compounds, either in the dark or upon photoactivation, did not reduce the ability of persister cells to form mature biofilm structures, complete with hyphal development. We were able to conclude that these two compounds are able to act as potent antifungal agents upon photoactivation, reducing both the viability of yeast cells, as well as inhibiting the yeast to hyphal transition of individual cells.

Chapter 2 Materials and Methods

2.1 Antifungal testing of PPE-DABCO and EO-DABCO

This study utilized concentrations of PPE-DABCO and EO-DABCO at 20µg/mL. These concentrations were based on the previous antifungal testing concentrations used by Wang *et al.* in which all compounds were tested at a concentration of 10µg/mL. (119). We doubled the concentration after preliminary testing with 10µg/mL with each compound was not deemed significantly effective (data not shown).

2.1.1 Synthesis of PPE-DABCO and EO-DABCO

The synthesis of these compounds has been described previously (114, 117, 120, 121). The structures of these compounds are included in Table 2.1.

Table 2.1. Structures of Biocidal Compounds

Structure	Name of Compound
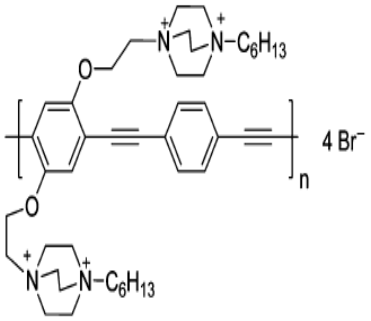	PPE-DABCO
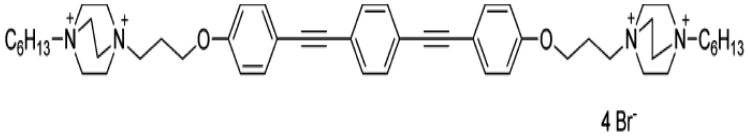	EO-OPE-1 (DABCO)

2.1.2 CFU assay

C. albicans 5314 were grown overnight (16-18h) in 5mL YPD broth (scraping taken from LiN2 ATCC stock) at 30C in the orbital shaker, 300rpm. For light exposure experiments, 100µL of the yeast suspension was added to 900µL of PBS in VWR Glass Vials, Short Form Style, Phenolic Cap on, 0.5 Dr. For dark experiments, 100µL of yeast suspension was added to 900µL of YPD broth in VWR-International 14mL sterile round-bottom culture tubes (60818-689). Either PPE-DABCO or EO-DABCO was added to a final concentration of 20µg/mL; untreated controls included for both dark and light exposure experiments. The light irradiation experiments were carried out in a photoreactor (4 UV-lamps, LZC-ORG, Luzchem Research Inc., Ottawa, Canada). LZC-420 (centered at ~420 nm) was used to activate PPE-DABCO and UVA (centered at ~350 nm) was used to activate EO-DABCO for 30min at room temperature. For dark exposure experiments, yeast were incubated with or without the compounds for 2h on orbital shaker, 30C, 300rpm. Following exposure, cultures were diluted 1:10^4 in PBS, and 50µL of each dilution was plated onto YPD agar plates. Plates were incubated overnight (16-18h) at 37C. Colonies were counted by ImageJ (1.48p, Java 1.7.0_07 (64-bit), NIH) analysis of digital photographs. Both the light and dark experiments were performed in triplicate.

2.1.3 Confocal imaging of *C. albicans* cultures to assess yeast to hyphal transition

C. albicans 5314 were grown overnight (16-18h) in 5mL YPD broth (scraping taken from LiN2 ATCC stock) at 30C in the orbital shaker, 300rpm. For light exposure experiments, 100µL of the yeast suspension was added to 900µL of PBS in VWR Glass

Vials, Short Form Style, Phenolic Cap on, 0.5 Dr. Either PPE-DABCO or EO-DABCO was added to a final concentration of 20µg/mL. The light irradiation experiments were carried out in a photoreactor (4 UV-lamps, LZC-ORG, Luzchem Research Inc., Ottawa, Canada). LZC-420 (centered at ~420 nm) was used to activate PPE-DABCO and UVA (centered at ~350 nm) was used to activate EO-DABCO for 30min or 60min at room temperature. . Following exposure, cultures were diluted 1:10^4 in PBS, and 50µL of each dilution was plated onto YPD agar plates. Plates were incubated for four days at 37C. A small loop of each sample was added to RPMI+300mg/L L-glutamine+0.165M MOPS+0.2% glucose (pH 7.4) in a MatTek dish. Samples of each irradiated culture were incubated either at room temperature for 1h in the dark, or at 37C for 3h or 24h in the dark and immediately imaged on an Olympus FV1000 confocal microscope (PLAPON 60X O NA:1.42, 0.207µm/pixel x 0.207µm/pixel, Z depth 20 slices, 1.5µm/slice, Sampling speed 2.0µs/pixel). A scraping from the original stock of *C. albicans* 5314 was also used to grow a 24h biofilm for comparison purposes, by suspending the cells in the same RPMI media and using this suspension to directly seed a MatTek dish. The samples grown to 24h were first stained with 20µg/mL calcofluor-white prior to imaging; all other samples were unstained. Analysis of images was performed in ImageJ (1.48p, Java 1.7.0_07 (64-bit), NIH).

2.1.4 Growth of 25h *C. albicans* biofilms under static conditions

C. albicans 5314 were grown overnight (16-18h) in 5mL YPD broth (scraping taken from LiN2 ATCC stock) at 30C in the orbital shaker, 300rpm. For light exposure experiments, 100µL of the yeast suspension was added to 900µL of PBS in VWR Glass Vials, Short Form Style, Phenolic Cap on, 0.5 Dr. For dark experiments, 100µL of yeast

suspension was added to 900µL of YPD broth in VWR-International 14mL sterile round-bottom culture tubes (60818-689). Either PPE-DABCO or EO-DABCO was added to a final concentration of 20µg/mL; untreated controls included for both dark and light exposure experiments. Cultures were exposed to either 420nm light to activate PPE-DABCO, or UVA light to activate EO-DABCO for 30min at room temperature. For dark exposure experiments, yeast were incubated with or without the compounds for 2h on orbital shaker, 30C, 300rpm. Following exposure, yeast were counted with a hemocytometer. Yeast were resuspended in RPMI+300mg/L L-glutamine+0.165M MOPS+0.2% glucose (pH 7.4) at 1e6 yeast/mL. For biofilm growth an Ibidi Culture-Insert for self-insertion (69842) was placed into the center of a MatTek Glass Bottom 35mm Microwell Dish, No. 1.5 coverglass (0.16-0.19mm), using sterilized tweezers. Yeast suspensions were added to dishes by injecting 70µL into the center of each side of insert. Biofilms were grown for 25h at 37C; calcofluor-white was then injected into each biofilm at a final concentration of 20µg/mL. Biofilms were immediately imaged on an Olympus FV1000 confocal microscope. Experiment was performed in triplicate per condition; three fields per biofilm were analyzed using ImageJ (1.48p, Java 1.7.0_07 (64-bit), NIH).

2.1.5 Live cell localization of PPE-DABCO and EO-DABCO in the cell wall of *C. albicans*

C. albicans 5314 were grown overnight (16-18h) in 5mL YPD broth (scraping taken from LiN2 ATCC stock) at 30C in the orbital shaker, 300rpm. The yeast were counted with a hemocytometer and 1.0e6 yeast were washed in 1mL PBS one time at 10,000xg for 5min. The pellet was resuspended in1mL RPMI+300mg/L L-

glutamine+0.165M MOPS+0.2% glucose (pH 7.4) containing 20uM fluorescein. 150µL of yeast were added to each of two channels of an Ibidi µ-slide $VI^{0.4}$ luer (80601) using a pipette. The slide was incubated at 30C for 1h to allow yeast to adhere. Following the 1h incubation, either PPE-DABCO or EO-DABCO was added to one of the channels of the slide at a final concentration of 20µg/mL. The slide was immediately imaged on an Olympus FV1000 confocal microscope (PLAPON 60X O NA:1.42, 0.207µm/pixel x 0.207µm/pixel, Z depth 20 slices, 1.5µm/slice, Sampling speed 2.0µs/pixel), with the imaging chamber heated to 37C. The PPE-DABCO or EO-DABCO and untreated cultures were imaged as follows. Images of the untreated cultures were imaged initially, immediately prior to beginning a 2h imaging session where the cultures treated with either EO-DABCO or PPE-DABCO were imaged every 5 minutes with the 405nm laser (14%, HV 830V, Gain 1); the 473nm laser was used to visualize the fluorescein to generate a negative image of the growing cells that was used for image processing (1%, HV 610V, Gain 1). Immediately following the 2h of imaging, the same initial field of the untreated culture was again imaged with the same settings for comparative purposes. Analysis of images was performed in ImageJ (1.48p, Java 1.7.0_07 (64-bit), NIH).

2.1.6 Live cell imaging of *C. albicans* biocidal testing of PPE-DABCO

C. albicans 5314 were grown overnight (16-18h) in 5mL YPD broth (scraping taken from LiN2 ATCC stock) at 30C in the orbital shaker, 300rpm. The yeast were counted with a hemocytometer and 1.0e6 yeast were washed in 1mL PBS one time at 10,000xg for 5min. The pellet was resuspended in1mL RPMI+300mg/L L-glutamine+0.165M MOPS+0.2% glucose (pH 7.4) containing 20uM fluorescein. 150µL of yeast were added to each of two channels of an Ibidi µ-slide $VI^{0.4}$ luer (80601) using a

pipette. The slide was incubated at 30C for 1h to allow yeast to adhere. Following the 1h incubation, PPE-DABCO was added to one of the channels of the slide at a final concentration of 20µg/mL. The slide was immediately imaged on an Olympus FV1000 confocal microscope with the imaging chamber heated to 37C. The PPE-DABCO and untreated cultures were imaged as follows. For the experiments in which PPE-DABCO treated cultures were continuously exposed to the 405nm laser (14%, HV 830V, Gain 1), a single field of the untreated culture was imaged at the initial time point and after 2h of hyphal growth in the dark. During the two hours between these images, a single field of the PPE-DABCO treated culture was imaged every 5 minutes for 2h with the 405 laser (PLAPON 60X O NA:1.42, 0.207µm/pixel x 0.207µm/pixel, Z depth 20 slices, 2.0µm/slice, Sampling speed 2.0µs/pixel); the 473nm laser was used to visualize the fluorescein to generate a negative image of the growing cells that was used for image processing (1%, HV 610V, Gain 1). This experiment was performed twice and analyzed using the surface-rendering feature of Imaris software (X63, 6.1.5, Bitplane, Zurich, Switzerland) and Minitab® (16.2.4, LEADTOOLS © 1991-2004, LEAD Technologies, Inc.). A single control experiment was performed using the exact imaging conditions as above, with the only change being the omission of PPE-DABCO treatment to the culture. The single control experiment was analyzed using ImageJ (1.48p, Java 1.7.0_07 (64-bit), NIH).

For the experiments controlled for phototoxicity effects, a single field of the PPE-DABCO culture and untreated culture were exposed to the 405nm laser (14%, HV 830V, Gain 1) to activate the PPE-DABCO for a total of 4 scans per field (1024x1024, 0.207µm/pixel, Z depth 20 slices, 1.5µm/slice, scanning speed 2.0µs/pixel). The cultures

were simultaneously scanned with the 473nm laser to fluoresce the fluorescein. Following this scan, the 405nm laser was shut off, and the PPE-DABCO and untreated fields previously exposed to the 405nm laser, along with a PPE-DABCO and untreated field not previously exposed to the 405nm laser, continued to be scanned for a following 2h, Z-stacks of each field taken every 10min (PLAPON 60X O NA:1.42, 0.207µm/pixel x 0.207µm/pixel, Z depth 20 slices, 1.5µm/slice, Sampling speed 2.0µs/pixel). The 473nm laser was used to visualize the fluorescein to generate a negative image of the growing cells that was used for image processing (1%, HV 610V, Gain 1). Experiment was performed in triplicate. Analysis of images was performed in ImageJ (1.48p, Java 1.7.0_07 (64-bit), NIH).

2.1.7 7-AAD viability assay

C. albicans 5314 were grown overnight (16-18h) in 5mL YPD broth (scraping taken from LiN2 ATCC stock) at 30C in the orbital shaker, 300rpm. For light exposure experiments, yeast suspension (1e6 cell/mL in PBS) were transferred to VWR Glass Vials, Short Form Style, Phenolic Cap on, 0.5 Dr. For dark experiments, , yeast suspension (1e6 cell/mL in PBS) were transferred to 1.5uL polypropylene centrifuge tubes. PPE-DABCO was added to a final concentration of 20µg/mL to cultures suspended in PBS at 1e6 cells/mL. Cultures were incubated with PPE-DABCO for 30 minutes prior to washing 3 times in PBS by centrifugation at 10,000xg for 5 minutes, followed by siphoning off the supernatant and resuspending cells in PBS, at 1e6cells/mL. Untreated controls included for both dark and light exposure experiments. The light irradiation experiments were carried out in a photoreactor (4 UV-lamps, LZC-ORG, Luzchem Research Inc., Ottawa, Canada). LZC-420 (centered at ~420 nm) was used to

activate PPE-DABCO treated cultures and untreated cultures for 30min at room temperature. For dark exposure experiments, yeast were incubated, following pretreatment with PPE-DABCO and washing, for 30 minutes at room temperature in the dark. Following exposure, 70µL of each sample was inoculated into a single side of an Ibidi Culture-Insert for self-insertion (69842) placed into the center of a MatTek Glass Bottom 35mm Microwell Dish, No. 1.5 coverglass (0.16-0.19mm), using sterilized tweezers. 7-AAD (Invitrogen, A1310) was added to a final concentration of 10µg/mL, and calcofluor-white was added to a final concentration of 10µg/mL, to each sample. Images were taken using a laser-scanning confocal microscope (UPLSAPO 10X 2 NA:0.40, 0.124µm/pixel x 0.124µm/pixel, 2.0µm/Z slice, Sampling speed 2.0µs/pixel). Images were analyzed using ImageJ (1.48p, Java 1.7.0_07 (64-bit), NIH). Both the light and dark experiments were performed in triplicate, three fields per sample per repeat were analyzed.

2.1.8 7-AAD viability assay-confocal 405nm laser activation of PPE-DABCO

C. albicans 5314 were grown overnight (16-18h) in 5mL YPD broth (scraping taken from LiN2 ATCC stock) at 30C in the orbital shaker, 300rpm. For light exposure experiments, yeast suspension (1e6 cell/mL in PBS) were transferred to VWR Glass Vials, Short Form Style, Phenolic Cap on, 0.5 Dr. For dark experiments, , yeast suspension (1e6 cell/mL in PBS) were transferred to 1.5uL polypropylene centrifuge tubes. PPE-DABCO was added to a final concentration of 20µg/mL to cultures suspended in PBS at 1e6 cells/mL. Cultures were incubated with PPE-DABCO for 30 minutes prior to washing 3 times in PBS by centrifugation at 10,000xg for 5 minutes, followed by siphoning off the supernatant and resuspending cells in PBS, at 1e6cells/mL.

70µL of each sample was inoculated into a single side of an Ibidi Culture-Insert for self-insertion (69842) placed into the center of a MatTek Glass Bottom 35mm Microwell Dish, No. 1.5 coverglass (0.16-0.19mm), using sterilized tweezers. 7-AAD (Invitrogen, A1310) was added to a final concentration of 10µg/mL. Untreated samples were included in each experiment. One field of the untreated culture and one field of the PPE-DABCO treated culture were imaged using a laser-scanning confocal microscope ((UPLSAPO 10X 2 NA:0.40, 0.124µm/pixel x 0.124µm/pixel, 2.0µm/Z slice, Sampling speed 2.0µs/pixel) with the 405nm laser (7%, HV 830V, Gain 1) for 8 scans each at 8 minute intervals. Calcofluor-white was added to each sample at a final concentration of 10µg/mL, and the previous fields were scanned again, along with one field of the untreated culture and one field of the PPE-DABCO treated culture that was not previously exposed to the 405nm laser. For the final scans, the 405nm laser was lowered to 2%. Images were analyzed using ImageJ (1.48p, Java 1.7.0_07 (64-bit), NIH). Experiment was performed in triplicate.

Chapter 3. Results and Discussion

3.1. Effect of PPE-DABCO and EO-DABCO on *C. albicans* viability in the light and dark

In order determine the level of effectiveness of the antifungal activity of PPE-DABCO and EO-DABCO against a laboratory strain of *C. albicans* in both the light and dark, the ability of *C. albicans* to form colonies on YPD agar was used to assess effectiveness of the compounds at reducing the viability of yeast. We first exposed suspension cultures of *C. albicans* to 20ug/mL of either PPE-DABCO or EO-DABCO for 2h in the dark prior to plating dilutions on YPD agar and incubating overnight at 37C. The resultant colonies were quantified and normalized to the untreated control plates. As seen in Figure 3.1, exposure to neither compound resulted in any significant reduction in CFUs per plate.

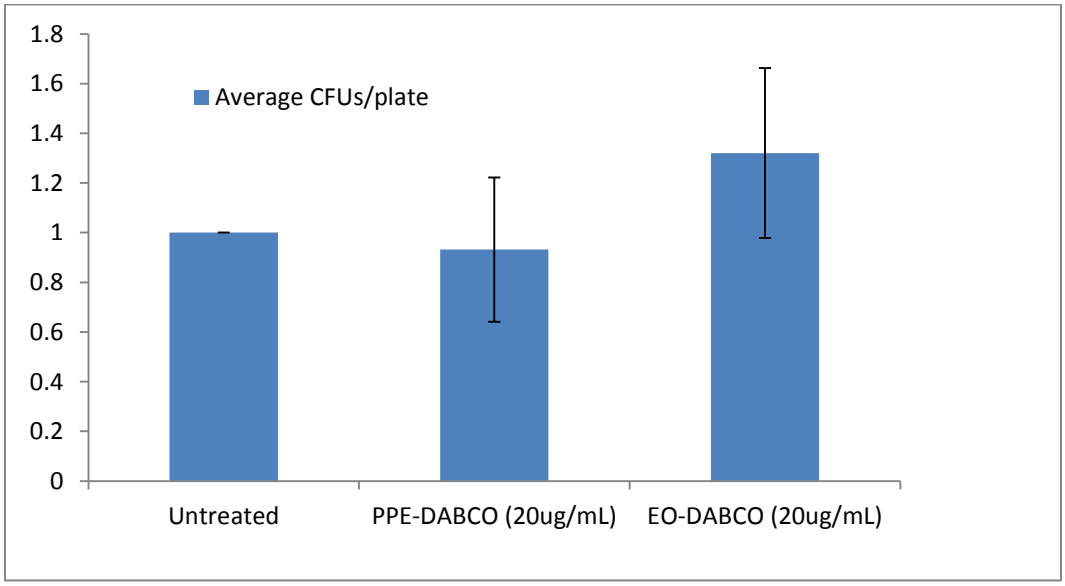

Figure 3.1. Exposure of *C. albicans* to PPE-DABCO (20ug/mL) or EO-DABCO (20ug/ml) in the dark. *C. albicans* were exposed to indicated concentrations of either PPE-DABCO (20ug/mL) or EO-DABCO (20ug/ml) in the dark for 2h prior to diluting samples 1:10^4 and plating on YPD agar. Plates were

incubated at 37C overnight (18-20h) prior to quantification. This experiment was performed in triplicate; error bars represent standard deviation.

We then decided to test the antifungal activities of PPE-DABCO and EO-DABCO upon 30 minute light exposure by assessing colony formation on YPD agar plates following treatment (Figure 3.2). Upon 30 minutes of exposure to UV-light, the cultures exposed to 20ug/mL of EO-DABCO showed an average 72.6% reduction in CFUs/plate and an average reduction of percent area cellularity per plate of 82.8% from the original untreated cultures. The cultures treated with 20ug/mL PPE-DABCO and exposed to 420nm light for 30 minutes showed an average reduction of CFUs/plate of 95.4% and an average reduction of percent area cellularity per plate of 91.5% over the untreated culture that was unexposed to light. However, while the reduction in the colonies formed by *C. albicans* treated with either compound was observable, a distinct phototoxic effect of exposure to UV-light and 420nm light was observable in cultures untreated with either compound. Exposure to UV-irradiation caused an average reduction in the number of CFUs/plate of 2.6% and a reduction in the average percent area cellularity per plate of 54.5% vs. the untreated control unexposed to the light. Furthermore, the untreated cultures exposed to 420nm light for 30 minutes displayed an average reduction in the number of CFU/plate of 64.1% and an average reduction in the percent area cellularity per plate of 72.5% over the untreated controls unexposed to light irradiation. However, the phototoxic effects alone did not account fully for the reduction of colony formation in cultures treated with either compound. The cultures treated with EO-DABCO prior to irradiation showed a 70.0% decrease in the average CFUs/plate and a 28.4% decrease in the average percent area cellularity per plate compared to the UV-

irradiated untreated controls. In addition, the cultures treated with PPE-DABCO and exposed to light displayed a 31.4% decreased in the average number of CFUs/plate and a 19.1% decrease in the percent area cellularity per plate compared to the 420nm light irradiated controls.

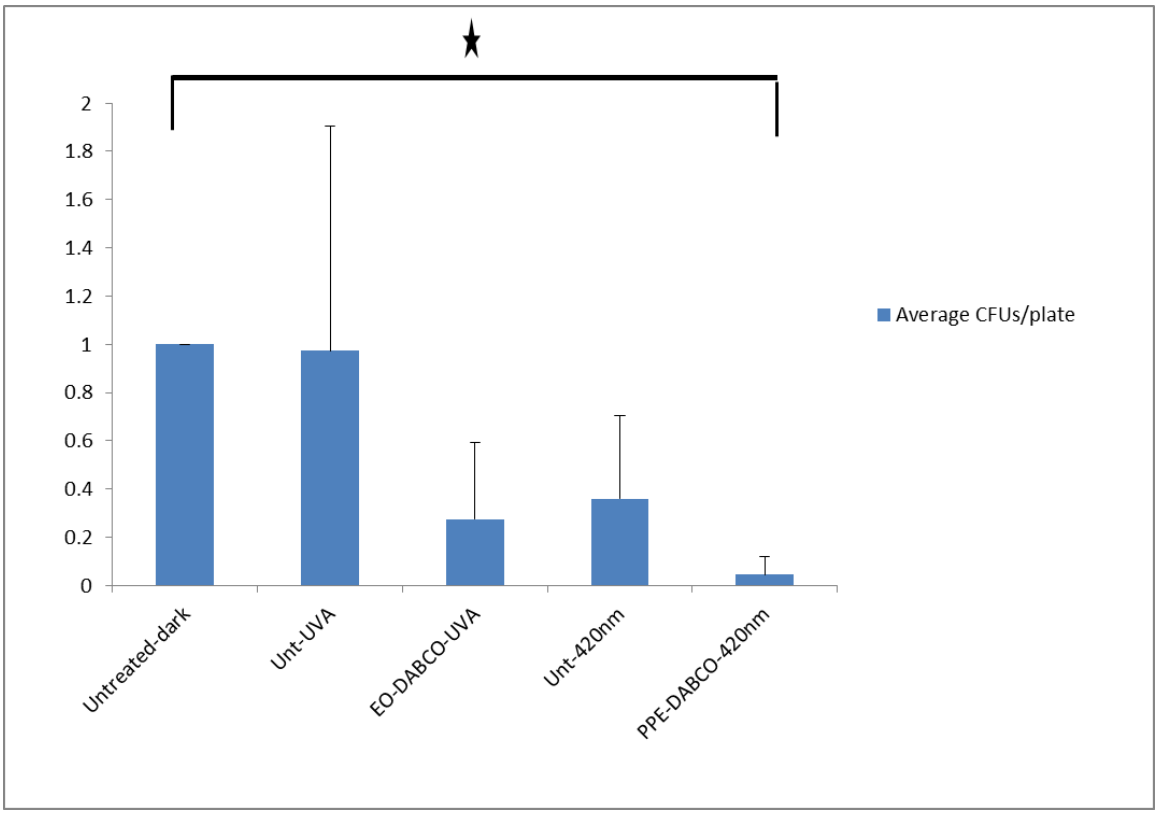

Figure 3.2. Light activation of EO-DABCO and PPE-DABCO leads to a reduction in *C. albicans* colony formation on YPD agar plates. *C. albicans* were exposed to UV-light irradiation or 420nm-light irradiation for 30 min to activate EO-DABCO (20ug/mL) or PPE-DABCO (20ug/mL), respectively. Untreated controls were concurrently exposed to UV-light irradiation or 420nm-light irradiation for 30 min at identical concentrations of yeast/mL, as indicated in the methods section. All samples were diluted 1:10^4 prior to plating on YPD agar, and incubated overnight (~18-20h) at 37C. Experiment performed in triplicate. Statistical significance assessed via a 2-sample, unequal variance T-test. Star indicates p-value<0.05.

After determining that photoactivation of the compounds caused a reduction in CFUs, we then wanted to assess the viability of yeast exposed to 20ug/mL PPE-DABCO, both in the dark, and after photoactivation of the agent with 420nm light. We wanted to determine if photoactivation of the compounds were causing an increase in cell death. We

pre-treated *C. albicans* cultures with 20ug/mL PPE-DABCO for 30 minutes in the dark, prior to exposing the cultures to 420nm light for 30 minutes. Following light irradiation, we performed a viability test using 7-AAD at 10ug/mL (Figure 3.3-3.4). As 7-AAD is excluded from cells with an intact cell membrane, it can be used to detect cells that have increased membrane permeability, a marker of dead or dying cells.

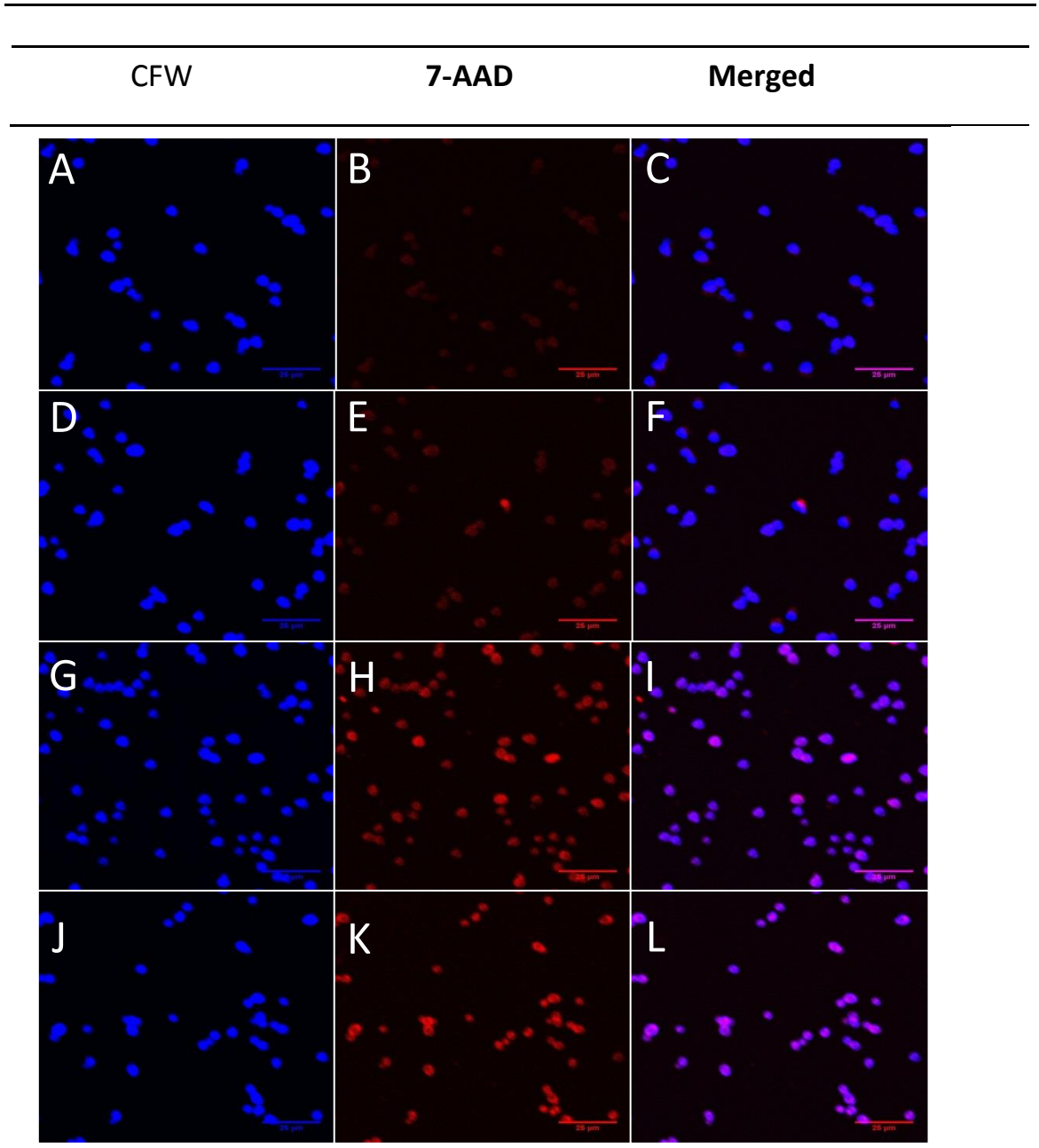

Figure 3.3. Confocal images of *C. albicans* viability test with 7-AAD. (A-C) Untreated dark culture. (D-F) Untreated culture exposed to 420nm light irradiation for 30min. (G-I) PPE-DABCO (20ug/mL) treated dark culture. (J-L) PPE-DABCO (20ug/mL) treated culture exposed to 420nm light irradiation for 30min. Images analyzed using ImageJ (1.48p, Java 1.7.0_07 (64-bit), NIH).

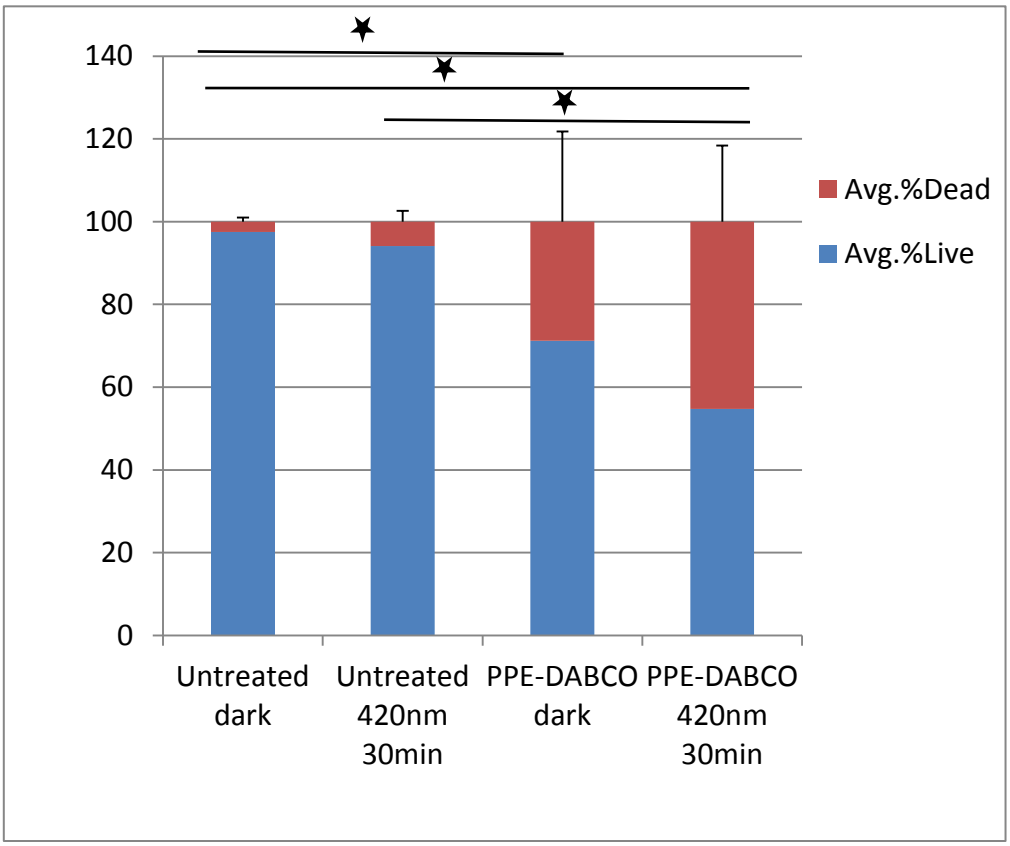

Figure 3.4. *C. albicans* viability test with 7-AAD. Quantification of images represented in Figure 3.3. Experiment performed in triplicate; three fields per sample per experiment were quantified. Images analyzed using ImageJ (1.48p, Java 1.7.0_07 (64-bit), NIH). Statistical significance assessed via a 2-sample, unequal variance T-test. Star indicates p-value<0.05.

The result of the 7-AAD viability test further supports our previous observation that the viability of *C. albicans* yeast in suspension decreases significantly upon photoactivation of PPE-DABCO. A significant decrease in viability was also observed in cultures treated with PPE-DABCO in the dark, which was previously unobserved by our CFU assay. For the viability assay, we pretreated the cultures of *C.albicans* with PPE-DABCO for 30 minutes in the dark, prior to washing away the excess agent and exposing the cultures to 420nm light-irradiation. As we were able to still able to achieve significant decreases in viability upon photoactivation of the compound, we concluded that singlet oxygen generated by excess agent in solution could not fully explain the decrease in

viability; which indicates that some interaction of the agent with the cell itself is likely and this interaction may be critical for the accumulation of enough reactive oxygen species to induce apoptosis. Furthermore, although our CFU assay indicated that some level of phototoxicity may be occurring in untreated cultures exposed to 420nm light (Figure 3.2), the viability assay with 7-AAD indicated that there is not a significant increase in apoptotic or necrotic cells in untreated samples undergoing light-irradiation. That may indicate that any phototoxicity effects on untreated cultures may not involve an increase in cell death.

From these results, we were able to conclude that light irradiation is necessary to achieve the full antifungal effects of these compounds. While we did observe a highly reproducible phototoxic effect of light irradiation on the untreated suspensions of *C. albicans* in our CFU assay, it is unclear what is mechanistically occurring. The presence of the photo-activated agents did effectively reduce colony formation over these untreated controls, indicating a light-inducible antifungal effect of these compounds can effectively reduce the numbers of viable yeast in suspension. This was further supported by a significant reduction in the viability of *C.albicans* yeast that were exposed to PPE-DABCO and irradiated with 420nm light.

3.2 Localization and activation of PPE-DABCO and EO-DABCO in the cell wall

To ascertain whether the localization of PPE-DABCO and EO-DABCO could be detected using a confocal microscope, live-cell laser-scanning confocal imaging using a 405nm laser was used to visualize the compounds relative to the cells, taking advantage of the inherent fluorescent properties of the compounds. Both PPE-DABCO and EO-

DABCO signals could be detected both yeast and growing hyphae (Figure 3.5 C-F**).** The signal from the EO-DABCO was less intense than that of the signal from the PPE-DABCO when activated by the 405nm laser, but that can possibly be attributed to differences in the optimal activation wavelengths between the two compounds: ~420nm for PPE-DABCO and UVA wavelengths for EO-DABCO. However, we were not able to ascertain whether the signal was localized exclusively to the cell wall of the cells. More experiments are required to determine the extent to which these compounds are able to penetrate the cell. Interestingly, the 405nm laser was able to photoactivate both compounds and inhibit hyphal growth, as evidenced by the presence of shortened hyphae after 2h of growth and the failure of many of the yeast to undergo the transition to hyphal form. However, this could be due to an increase in cell death, as evidenced by previous experiments. Surprisingly, what appears to be cell debris in the cultures treated with PPE-DABCO and activated with the 405nm laser is visible in the 2h images, but was not present in either the untreated controls, nor the EO-DABCO treated cultures, which may indicate distinct differences in mechanistically how treatment of *C. albicans* with the compounds inhibits hyphal growth or possibly induces cell death (Figure 3.5 C and D). As a control for these experiments, untreated samples of the same *C. albicans* culture were incubated under identical conditions, and imaged at the initial time point and following 2h growth (Figure 3.5 A and B). The untreated yeast were able to undergo the transition to hyphal form in this time period, with no observable yeast after 2h. This indicates that photo-activation of these compounds during live cell imaging could serve as a novel method of directly observing the effects of these compounds on an individual cellular level.

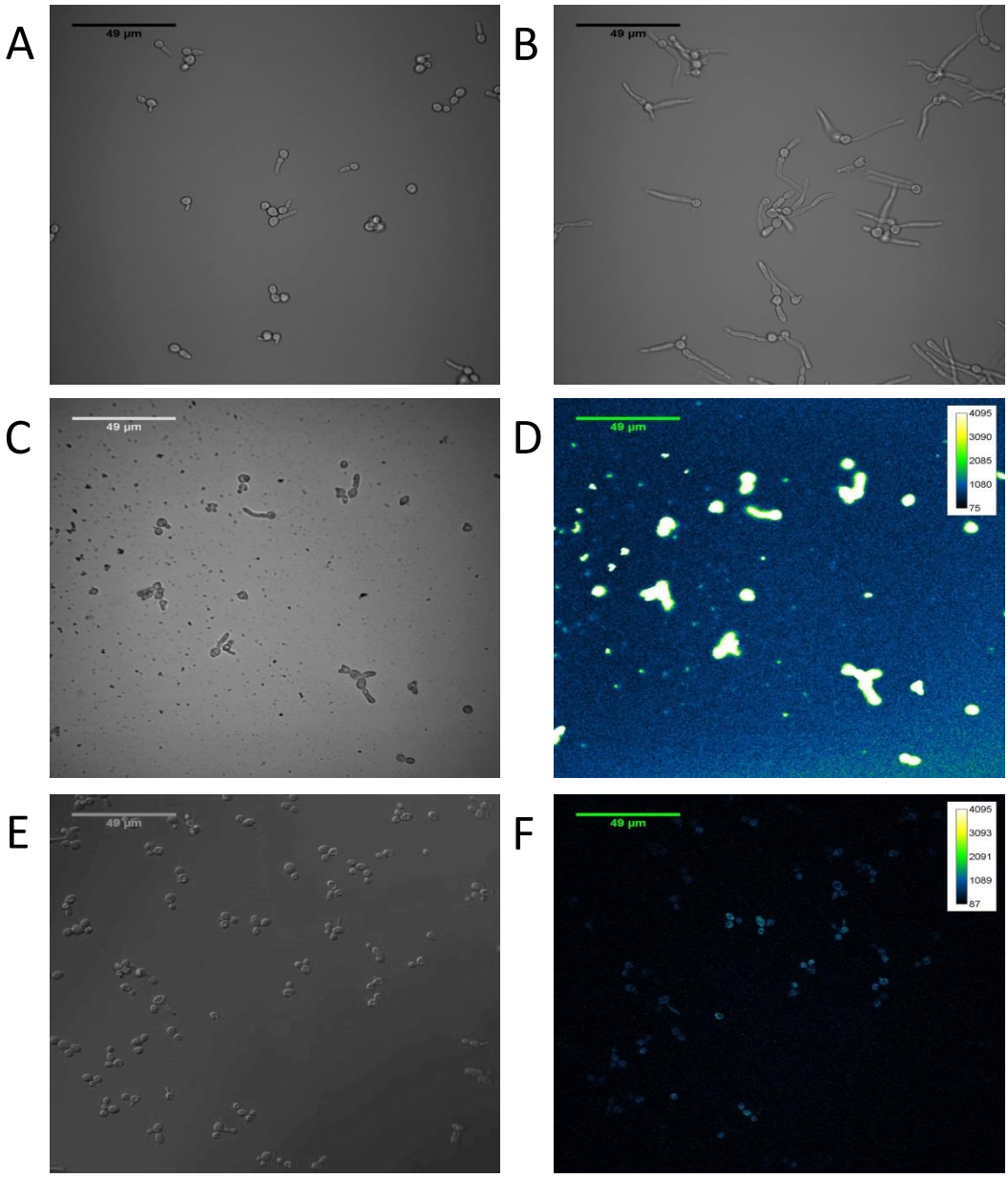

Figure 3.5 Live cell imaging of *C. albicans* allows visual localization of PPE-DABCO and EO-DABCO in the cell wall of yeast and activation with the 405nm laser inhibits hyphal development. A) Initial DIC image of an untreated culture and B)DIC image of untreated culture following 2h of hyphal growth. C) DIC image of culture treated with PPE-DABCO (20µg/mL) following 2h of growth and D) Fluorescent signal from PPE-DABCO activated with 405nm laser. E) DIC image of culture treated with EO-DABCO (20µg/mL) following 2h of growth and F) Fluorescent signal from EO-DABCO activated with 405nm laser.

3.3 Live cell imaging reveals activation of PPE-DABCO inhibits yeast to hyphal transition in *C. albicans*

The dual observation that the 405nm confocal laser could be used to both localize PPE-DABCO to visualize localization of the compound to activate the compound and inhibit the hyphal growth of *C. albicans* led to the conclusion that the dynamics of hyphal development during activation of the compound could be directly visualized on the basis of individual cells. As many of our previous experiments tested the biocidal activity of these compounds on the level of a population of cells, the dynamic temporal responses of individual cells upon activation of this compound remained unclear. To better elucidate these responses, we performed a series of live-cell experiments, in which the 405nm laser was allowed to activate the PPE-DABCO present in the cell wall of the yeast every five minutes for 2h. Images were taken every five minutes for two hours. The fluorescein included in the culture was excluded by the cells, generating a negative image of the cells that was used to quantify the data using ImageJ (1.48p, Java 1.7.0_07 (64-bit), NIH). (Figure 3.6). Prior to beginning the imaging session, the yeast were allowed to adhere to the surface of the slide for 1h. Once adhered, little to no movement of the original yeast cell occurred, which allowed tracking of the growth of the surface-rendered cells from frame to frame of the 3D-projected image (Figure 3.7). This was verified by tracking the location of the centroid of the Imaris surface-rendered object, defined by both the x and y position, during the two hours of growth (Figure 3.8). This allowed us to easily quantify the differences in area (µm^2) and volume (µm^3) of individual surface-rendered objects over time, which gave us an objective method for assessing the temporal effects of activation of PPE-DABCO on the growing hyphae (Figure 3.9 A and B). As the centroid

of each surface rendered object remained consistent throughout the 2h of imaging, we were able to quantify differences in growth in all three spatial dimensions over time, in terms of both volume and area of the surface-rendered objects (Figure 3.10 A-F). In all three dimensions, both surface area and volume of the detected objects were reduced over the 2h time period, which indicates that growth of hyphae over time is not occurring in the PPE-DABCO treated yeast that are exposed to the 405nm laser every 5 minutes for 2h. In contrast, untreated cultures of *C.albicans* showed an increase in both area and volume of surface-rendered objects over a 1h growth period at 37C, during a live cell confocal experiment (Figure B2). The effect of photoactivation of PPE-DABCO on cell growth is quantifiable within 20 minutes of intermittent exposure to light irradiation, which suggests that the effect leading to an inhibition of hyphal development occurs rapidly upon activation of PPE-DABCO. We also grew untreated control samples concurrently and imaged the untreated and PPE-DABCO treated samples initially and after 2h of growth. As shown in Figure 3.11, the untreated control samples increased in the total area and volume of surface-rendered objects over the two hour growth period. The samples treated with PPE-DABCO and exposed to the 405nm laser decreased in total area and volume over the same time period. Images at 2h were taken of another field of the PPE-DABCO treated sample that was unexposed to the 405nm laser in two of three experiments; hyphae grew effectively in PPE-DABCO treated cultures unexposed to the 405nm laser (Figure A.5). The reduction in area and volume of cultures exposed to photoactivated PPE-DABCO indicates that the cells may be undergoing form of cell death, although the mechanism by which this is occurring needs to be further elucidated.

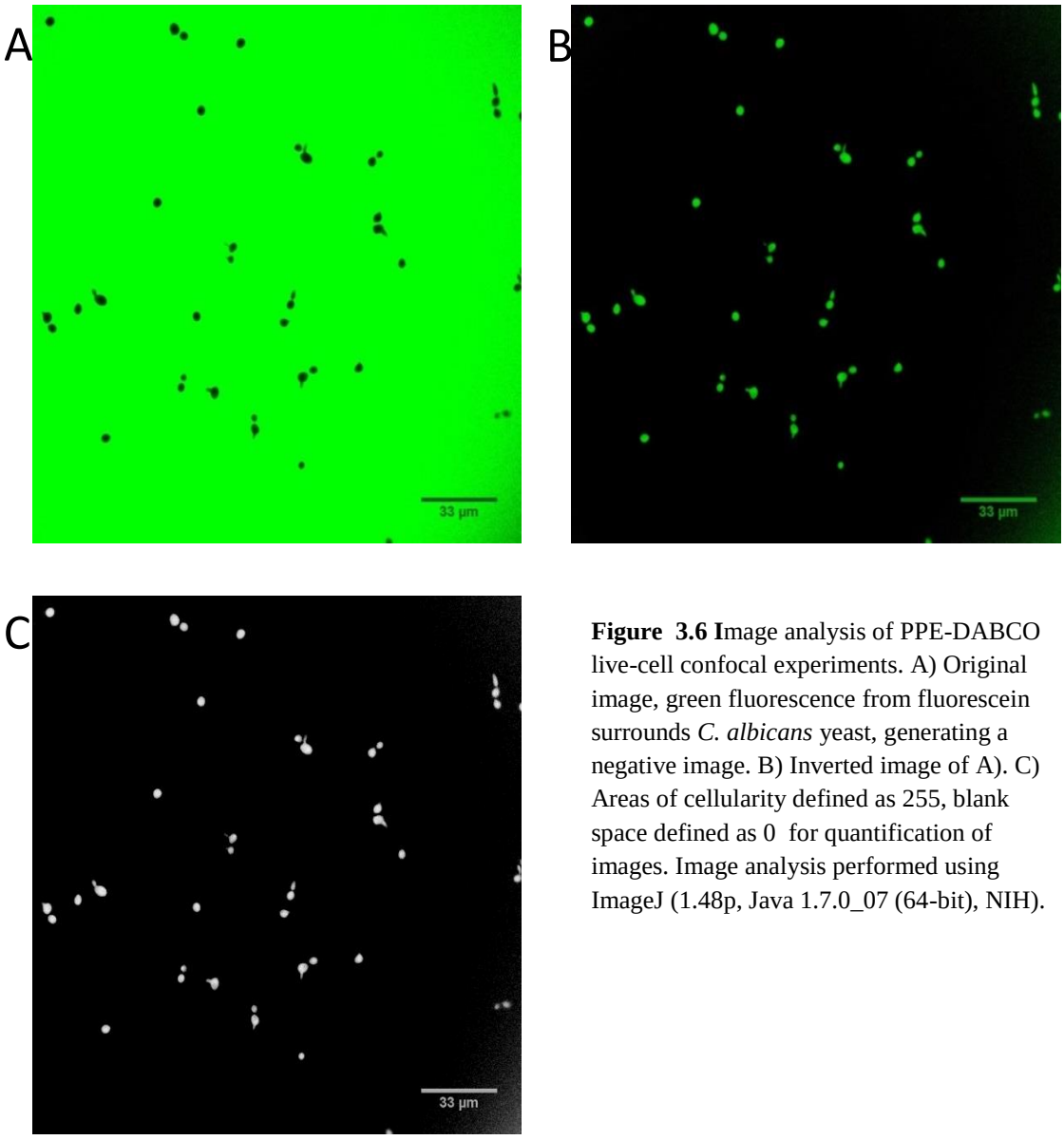

Figure 3.6 Image analysis of PPE-DABCO live-cell confocal experiments. A) Original image, green fluorescence from fluorescein surrounds *C. albicans* yeast, generating a negative image. B) Inverted image of A). C) Areas of cellularity defined as 255, blank space defined as 0 for quantification of images. Image analysis performed using ImageJ (1.48p, Java 1.7.0_07 (64-bit), NIH).

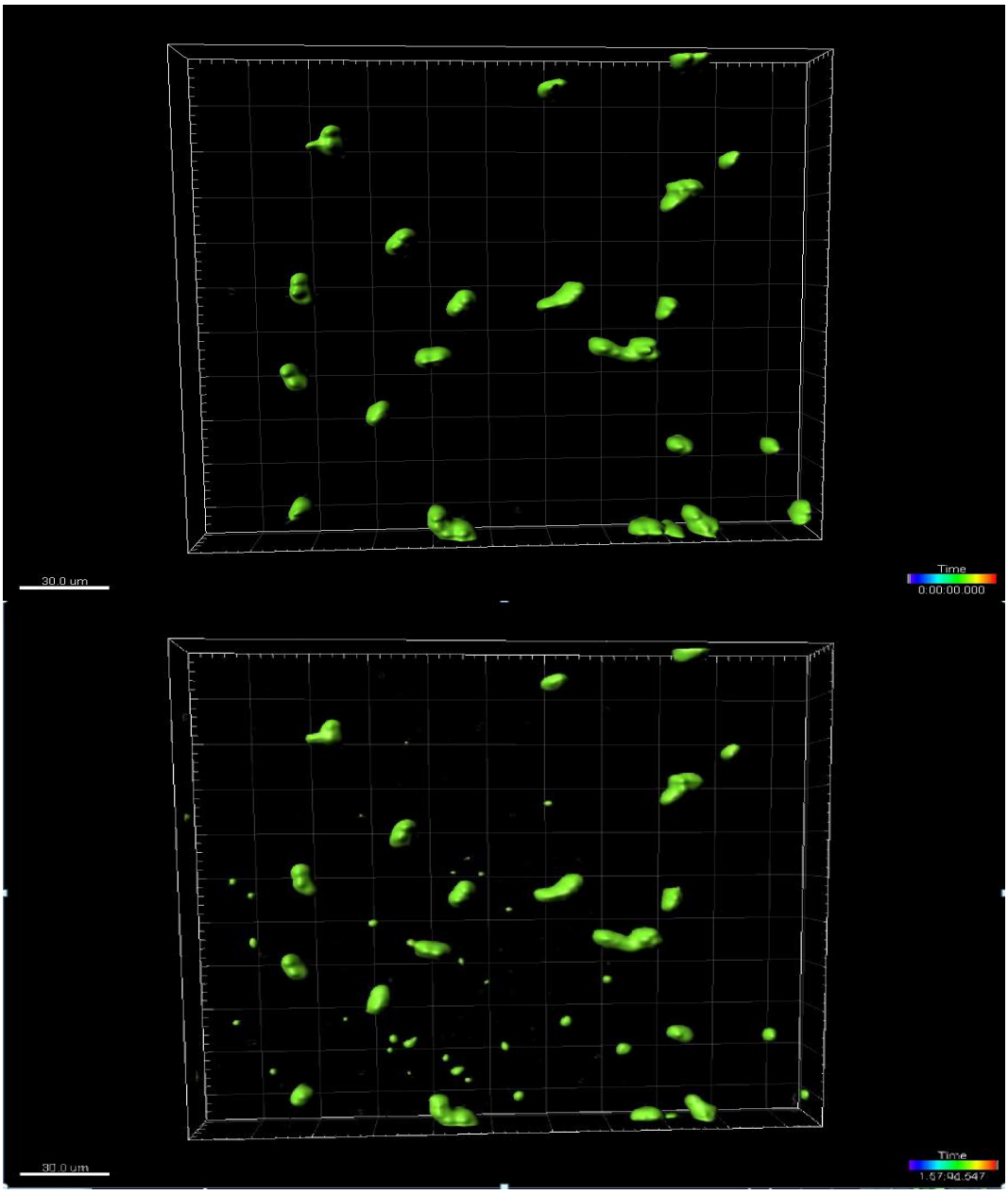

Figure 3.7 Imaris 4D surface rendering of *C.albicans* cultures treated with PPE-DABCO and continuously imaged with 405nm laser. A) Initial image and B) Image following 2h of growth. Experiment performed in triplicate.

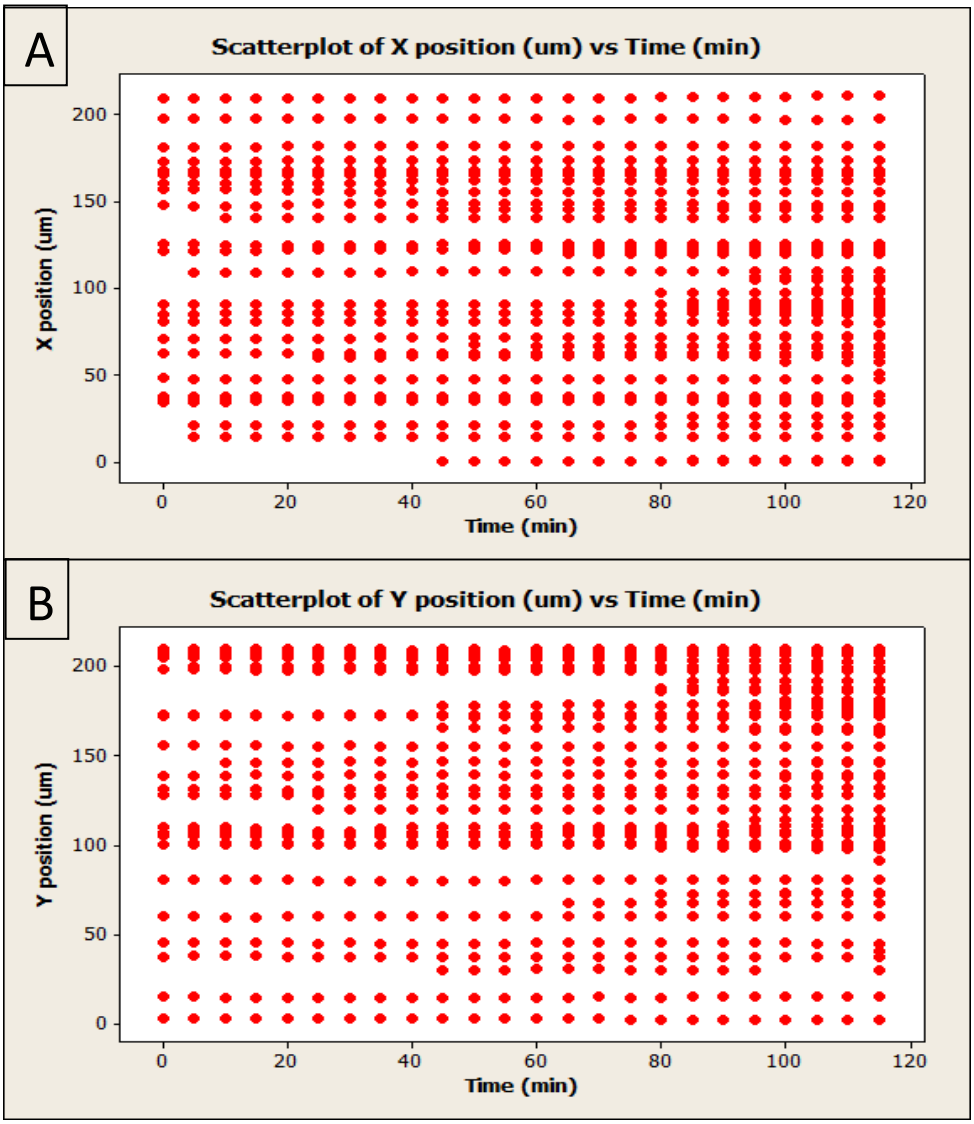

Figure 3.8 Centroid position of Imaris surface-rendered objects can be tracked over time. A) Scatterplot of X position (um) of identified surface rendered objects over time (min) B) Scatterplot of Y position (um) of identified surface rendered objects over time (min). Representative of a single experiment.

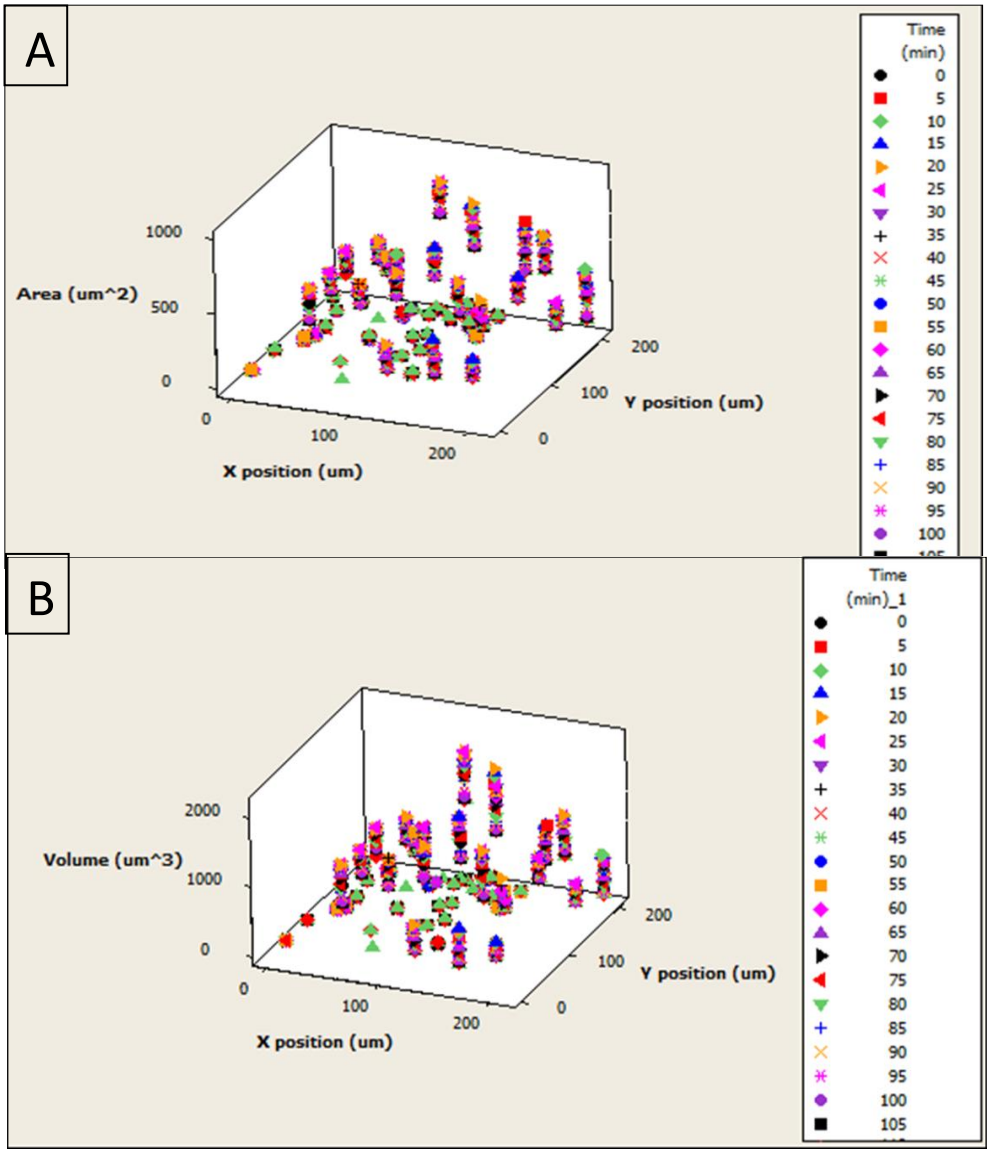

Figure 3.9 Live-cell imaging and activation of PPE-DABCO with the 405nm confocal laser allows spatial and temporal analysis of *C. albicans* hyphal growth. A) Area (μm$^{\wedge 2}$) and B) Volume (μm$^{\wedge 3}$) vs. centroid position of surface rendered object over time (min) of a single experiment.

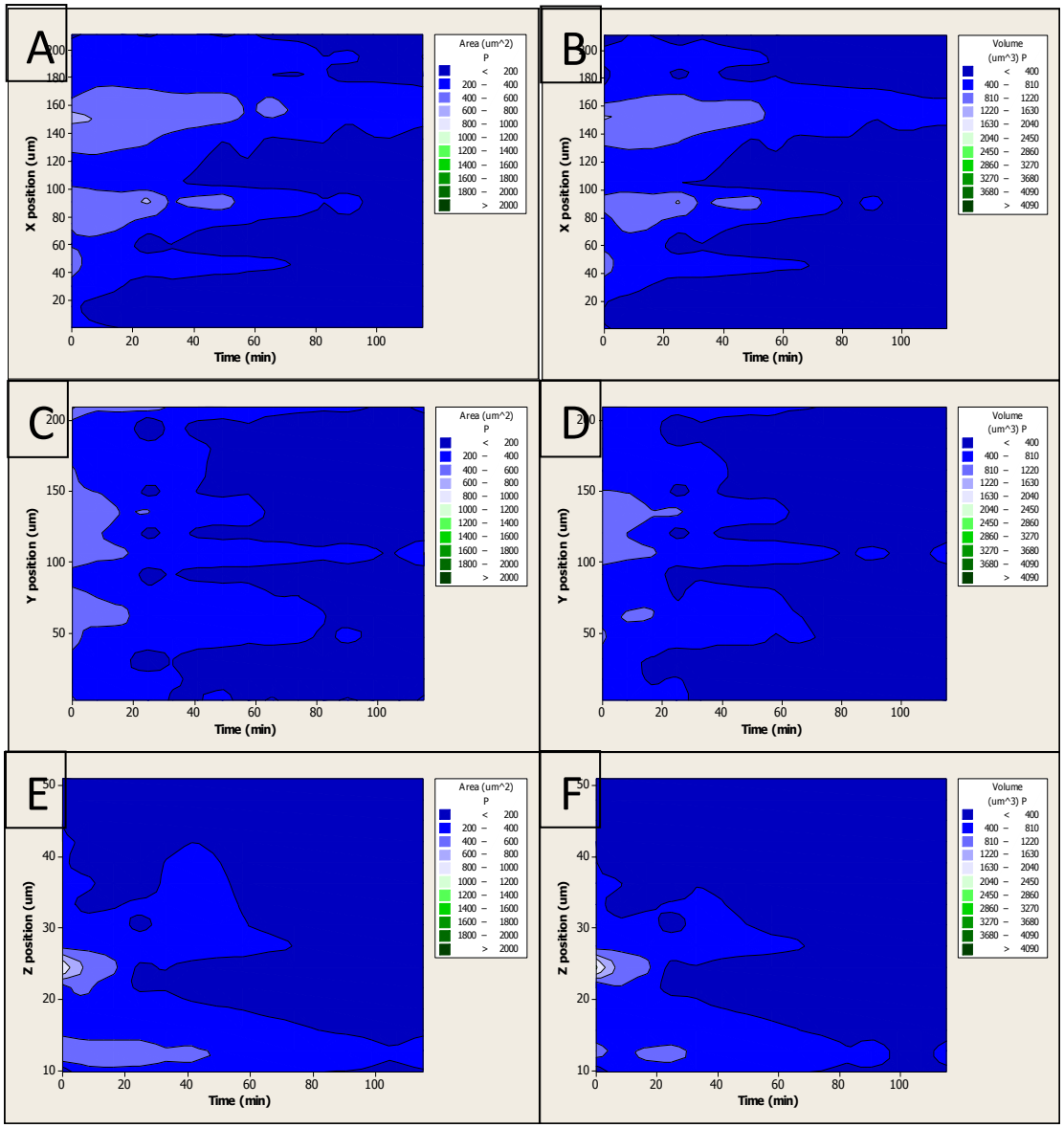

Figure 3.10 Live-cell imaging and activation of PPE-DABCO with the 405nm confocal laser allows spatial and temporal analysis of *C. albicans* hyphal growth. A) Area (μm^2) and B) Volume (μm^3) of surface-rendered cells vs. X position (μm) over time (min). C) Area (μm^2) and D) Volume (μm^3) of surface-rendered cells vs. Y position (μm) over time (min). E) Area (μm^2) and F) Volume (μm^3) of surface-rendered cells vs. Z position (μm) over time (min).

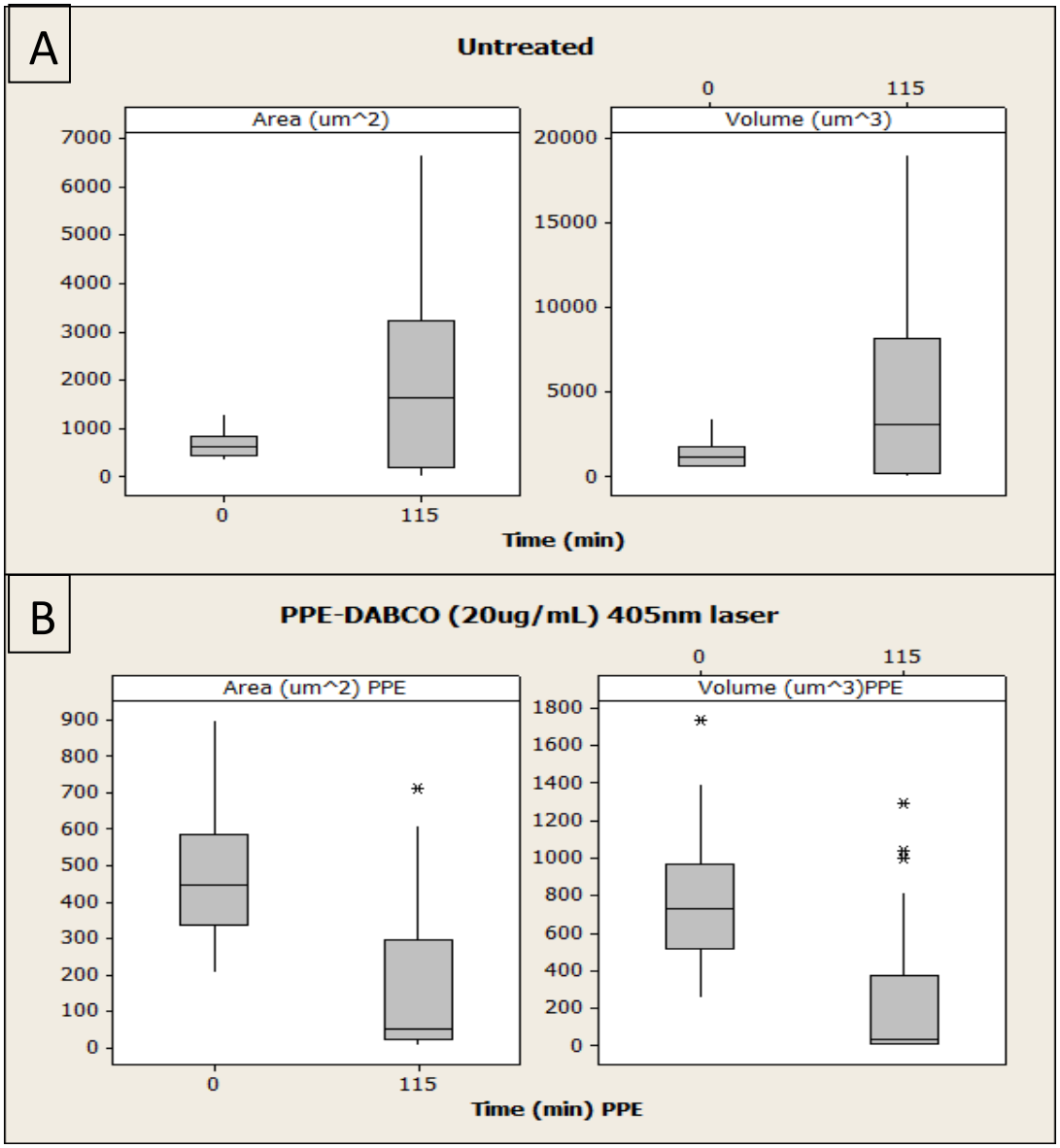

Figure 3.11 Quantification of initial and final area and volume of untreated and PPE-DABCO growth. Quantification of (A) untreated controls grown without 405nm laser activation concurrently and (B) PPE-DABCO (20µg/mL) activated with the 405nm laser every 5 minutes for 2h. Figure shows area (μm^2) and volume (μm^3) of Imaris surface rendered objects initially and after 2h of growth at 37C. Data representative of 3 independent experiments. Untreated controls were from the same *C. albicans* culture as the PPE-DABCO treated cells, and plated on the same an Ibidi µ-slide $VI^{0.4}$ luer in separate channels. Growth and imaging of untreated controls performed concurrently to the treated samples.

3.4 Effect of PPE-DABCO on hyphal growth is distinct from phototoxicity effects

While the previous experiments provided evidence that activation of PPE-DABCO using the 405nm confocal laser could inhibit hyphal growth, it remained unclear if the effect was due to activation of the compound or phototoxicity effects of irradiating the *C. albicans* cultures with a high energy light source. A control experiment to assess phototoxicity of irradiation every 5 minutes for 2h using the 405nm confocal laser revealed that an untreated *C. albicans* culture imaged under the same conditions also showed evidence of inhibited hyphal growth, compared to a control culture which was unexposed to the 405nm laser (Figure 3.12).

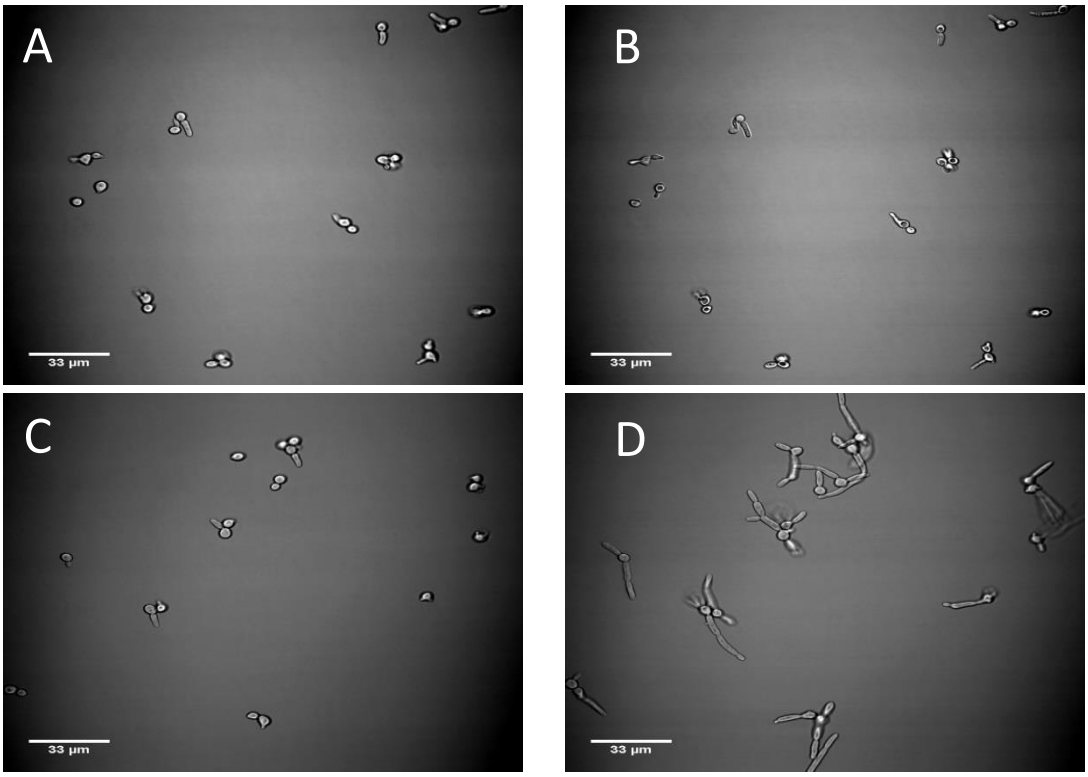

Figure 3.12 Exposure every 5 minutes for 2h to 405nm confocal laser inhibits hyphal growth in untreated *C. albicans* cultures. A) Initial DIC image of untreated culture exposed to 405nm confocal laser and B) DIC image after 2h of growth with 405nm laser. C) Initial DIC image of untreated culture grown in dark conditions D) DIC image after 2h of growth under dark conditions.

Therefore, in an attempt to isolate the specific effect of PPE-DABCO activation from the phototoxicity effects of the laser we undertook a series of experiments in which a single field of a PPE-DABCO treated culture and an untreated culture of *C. albicans* was irradiated with the 405nm laser for a 20 minute period. The rationale for the 20 minute exposure time to the 405nm laser was based on our previous time course data that suggested that the effects leading to hyphal development inhibition may occur within this time frame. Images of each were taken every five minutes during this period. Following this pretreatment, the 405nm laser was disengaged and these two fields, along with a field of a PPE-DABCO treated culture and untreated culture, continued to be imaged for 2h of hyphal growth, with images taken every 10 minutes during this period. The fluorescein included in the culture was excluded by the cells, generating a negative image of the cells that was used to quantify the data using ImageJ (1.48p, Java 1.7.0_07 (64-bit), NIH). (Figure 3.6). Both the untreated cultures as well as those treated with 20ug/mL PPE-DABCO that were unexposed to the 405nm light prior to the 2h of recorded growth displayed similar growth patterns (Figure 3.13). A slight phototoxicity effect of pre-exposure to the 405nm laser on the untreated culture is evidenced by a delay in hyphal growth rate (Figure 3.13 A and C), but the phototoxicity effect alone did not completely inhibit hyphal development. Strikingly, the 20 minute pre-exposure to the 405nm laser caused a drastic inhibition of hyphal growth of *C. albicans* cultures treated with PPE-DABCO, with little to no detectable hyphal growth in the 2h following light-irradiation (Figure 3.13 A and E). Furthermore, reductions in total area cellularity of the light exposed PPE-DABCO treated cultures over this period of time suggests that some form of cell death may be occurring, although this observation needs to be further explored for

validity. The results of these experiments provide strong evidence that PPE-DABCO treatment alone cannot significantly hinder hyphal development in *C. albicans*. Additionally, while there are observable phototoxicity effects of untreated cultures due to exposure to the 405nm confocal laser, these effects alone cannot account for the complete inhibition of hyphal development. This indicates that light activation of PPE-DABCO is the primary cause for the inability of *C. albicans* yeast to undergo the transition to hyphal morphology under these particular growth conditions. The mechanism by which this may be occurring remains to be elucidated with further studies.

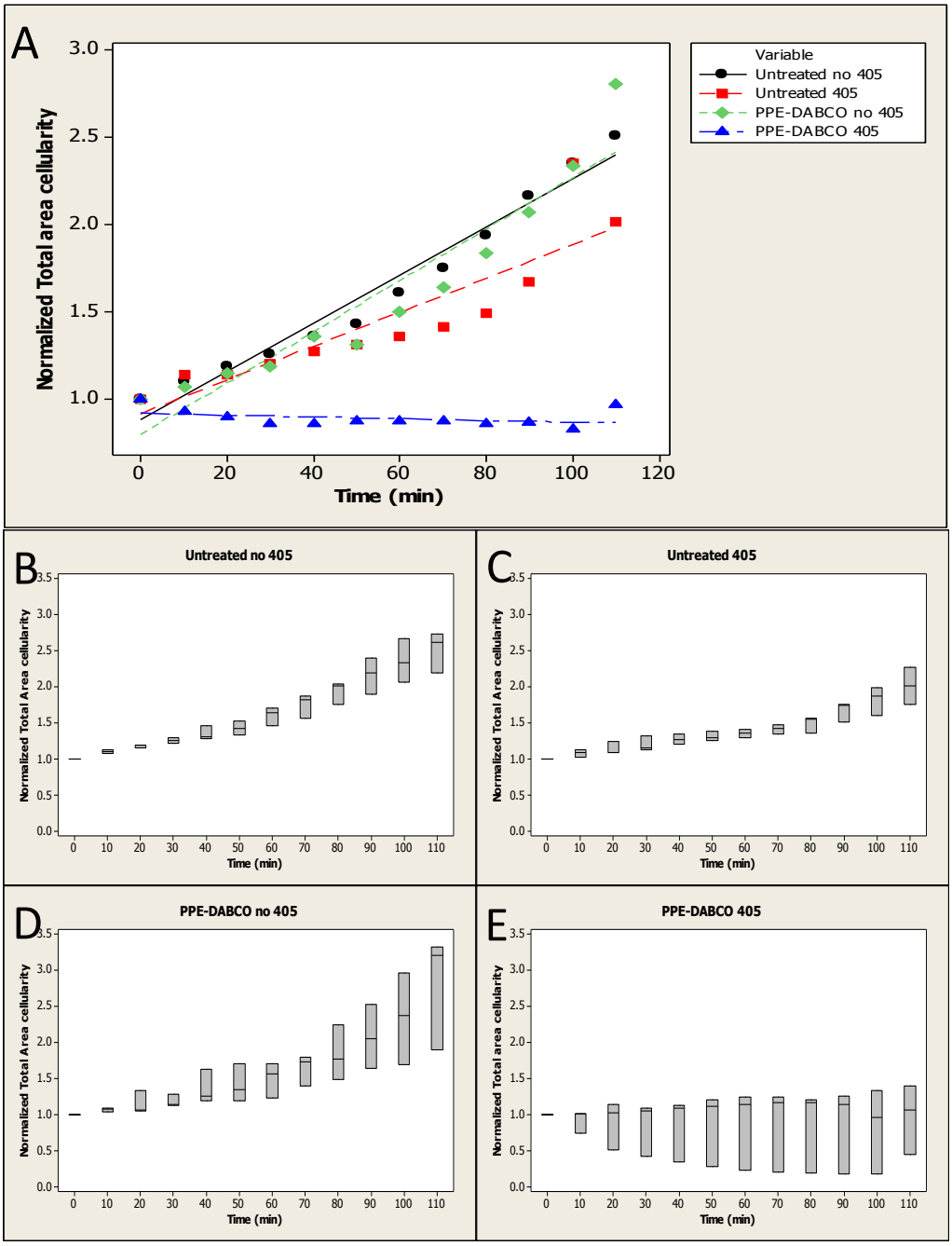

Figure 3.13 Activation of PPE-DABCO with 405nm confocal laser for 20 minutes is effective at inhibiting hyphal growth in C. albicans. *C. albicans* cultures were treated with or without 20µg/mL PPE-DABCO, then exposed intermittently to a 405nm confocal laser for 20 minutes. Following exposure, cultures were induced to grow hyphae for 2h without exposure to the 405nm laser. Untreated and PPE-DABCO treated controls that did not receive any exposure to the 405nm laser were included for comparison. A) Scatterplot of normalized total area cellularity (per imaged field) vs. time (min) of each of the four conditions. (B-E) Boxplots representing the normalized change in total area cellularity (per imaged field) over time. Graphs are representative of compiled data from three independent experiments.

3.5 Effect of PPE-DABCO on viability following 405nm confocal laser exposure

The inhibition of hyphal growth in cultures exposed to the 405nm confocal laser during PPE-DABCO treatment, as well as the appearance of probable cell debris in the confocal images over time, illustrated the possibility that photoactivation of the agent with the 405nm laser may lead to cell death. To assess the effect of 405nm photoactivation of the compound on the viability of *C.albicans*, we performed a live-cell 7-AAD viability assay following a 30 minute pretreatment with PPE-DABCO and a thorough washing of the cells to remove the excess agent. We scanned a single field of an untreated culture and a PPE-DABCO treated culture using the 405nm laser every 8 minutes, for a total of 8 scans apiece. We then stained the cells with calcofluor-white and imaged the fields again, along with a single field each of the untreated and PPE-DABCO treated cultures which were not previously exposed to the 405nm laser. We saw a significant reduction in the viability of the fields treated with PPE-DABCO and photo-activated with the 405nm laser (Figures 3.14 and 3.15). Furthermore, due to the washing of the cells, this reduction in viability cannot be attributed to the singlet oxygen generation resulting from photo-activation of free agent in solution, but by the activation of PPE-DABCO in direct contact with the cell. We saw a reduction in viability in fields that were treated with PPE-DABCO but that were unexposed to the 405nm laser, but this reduction was not found to be significant. The effect of the 405nm laser on the viability of the untreated culture was minimal and not significant; indicating that phototoxicity alone cannot explain the reduction in viability seen in the photoactivated PPE-DABCO treated cultures.

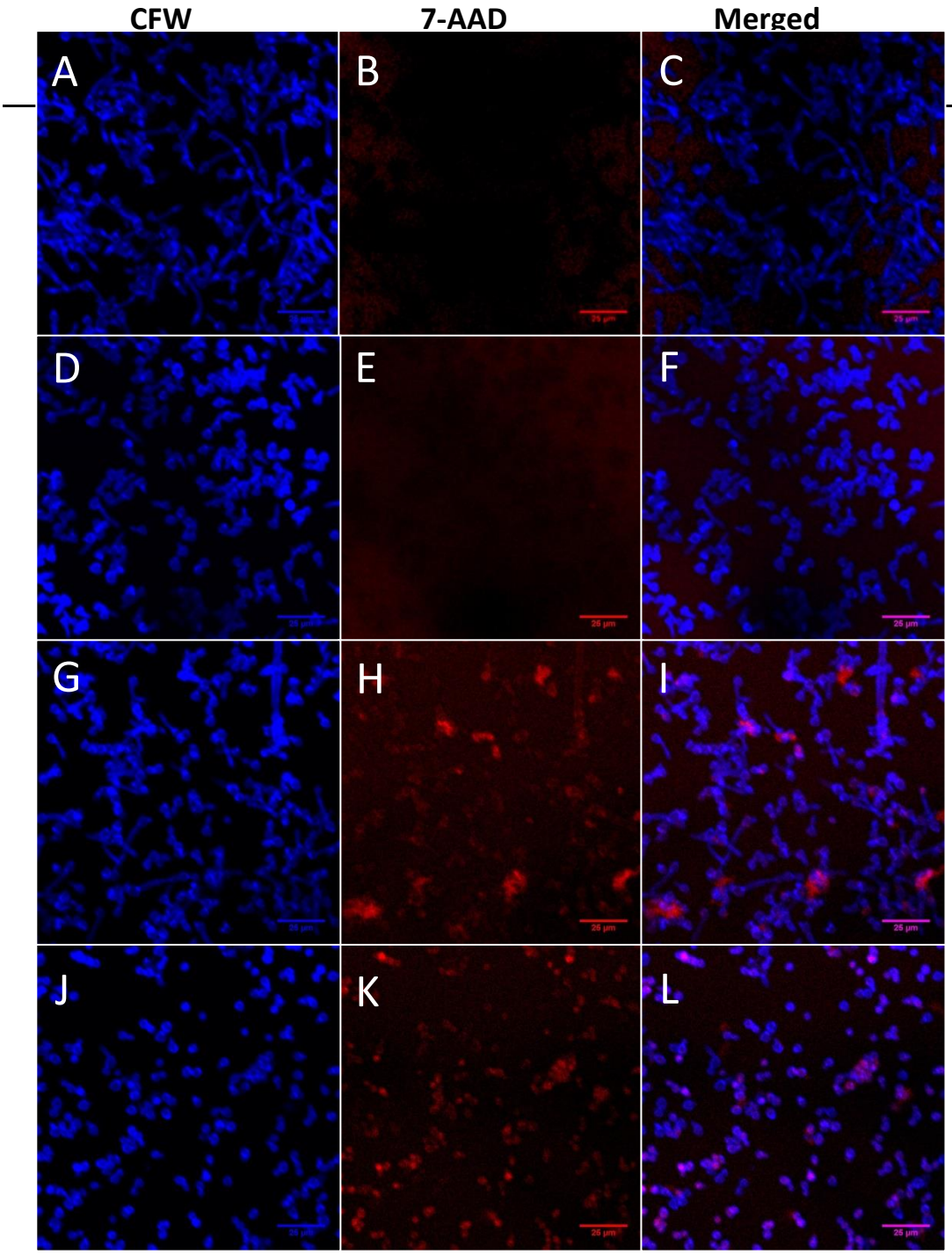

Figure 3.14 Confocal images of *C. albicans* viability test with 7-AAD. (A-C) Untreated dark culture. (D-F) Untreated culture exposed to 405nm confocal laser for 60min. (G-I) PPE-DABCO (20ug/mL) treated dark culture. (J-L) PPE-DABCO (20ug/mL) treated culture exposed to 405nm confocal laser for 60min. Images analyzed using ImageJ (1.48p, Java 1.7.0_07 (64-bit), NIH).

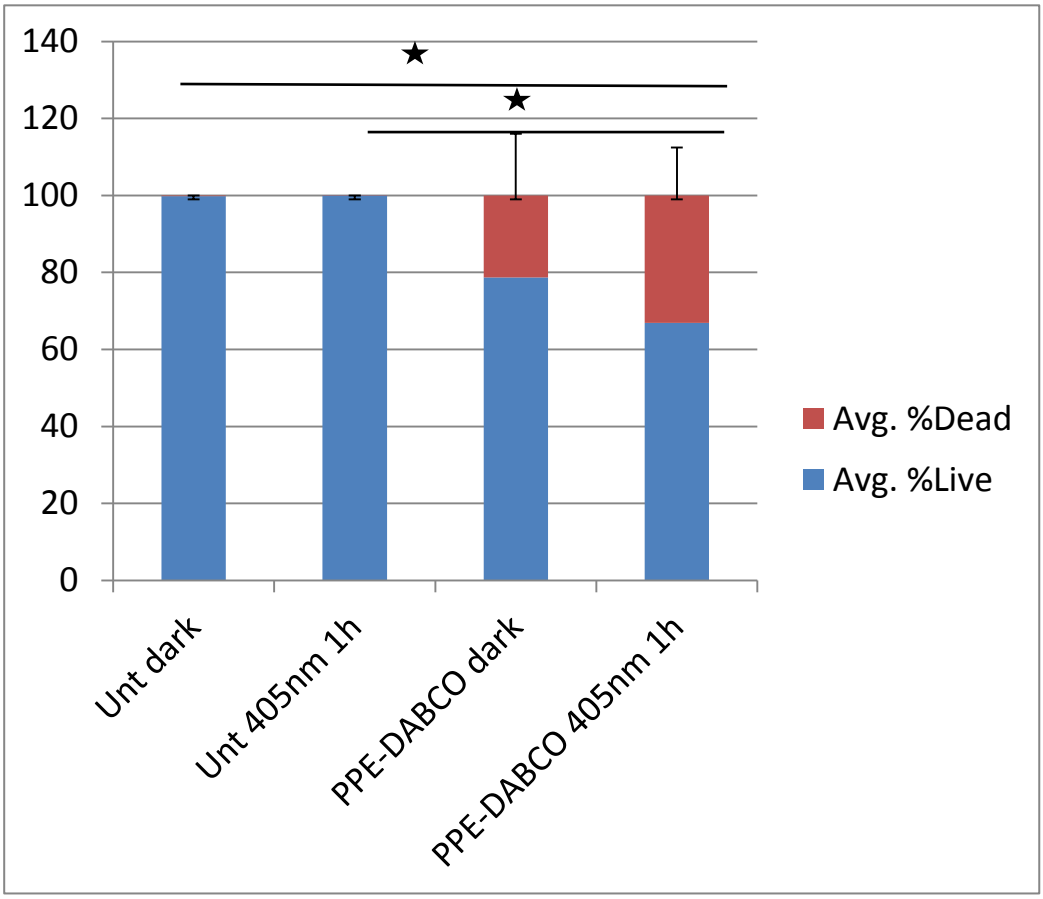

Figure 3.15. *C. albicans* viability test with 7-AAD. Quantification of images represented in Figure 3.11. Experiment performed in triplicate; three fields per sample per experiment were quantified. Images analyzed using ImageJ (1.48p, Java 1.7.0_07 (64-bit), NIH). Statistical significance assessed via a 2-sample, unequal variance T-test. Star indicates p-value<0.05.

3.6 Effect of PPE-DABCO and EO-DABCO on yeast to hyphal transition in surviving cells

While the antifungal effects of both compounds were evidenced by CFU reduction following light irradiation, we wanted to assess whether exposure to the agents and subsequent photoactivation results in a heritable loss of ability to make hyphae in the cells that are not acutely killed and then allowed to produce many generations of progeny. The yeast to hyphal transition is an essential component of the development of

C. albicans biofilms. To test whether treatment with 20ug/mL PPE-DABCO or EO-DABCO, followed by light irradiation of the cultures for 60 minutes, could inhibit this transition in surviving cells, or cause an observable morphological change in hyphal structure, dilutions of exposed cultures, including untreated controls, were plated on YPD agar plates and incubated at 37C for four days, then representative samples of each culture were incubated either at room temperature for 1h in the dark, or at 37C for 3h or 24h in the dark to induce hyphal growth and immediately imaged on the laser-scanning confocal microscope. All samples were able to grow hyphae after 3h incubation at 37C, indicating that neither exposure to light irradiation alone, nor light activation of the biocidal compounds, was sufficient to inhibit the yeast to hyphal transition (Figure 3.16).

In addition, all samples were able to effectively grow dense biofilm structures after 24h of exposure to hyphal growth inducing conditions (Figure 3.17), with no readily observable impediment to the biofilm development due to either exposure to 60 min light irradiation alone, or light activation of the compounds used to treat the original cultures. From this result, we were able to conclude that light-irradiation, with or without application of PPE-DABCO or EO-DABCO, of *C.albicans* suspension cultures did not result in inhibition of the yeast to undergo transition to hyphal form or the development of dense biofilm structures.

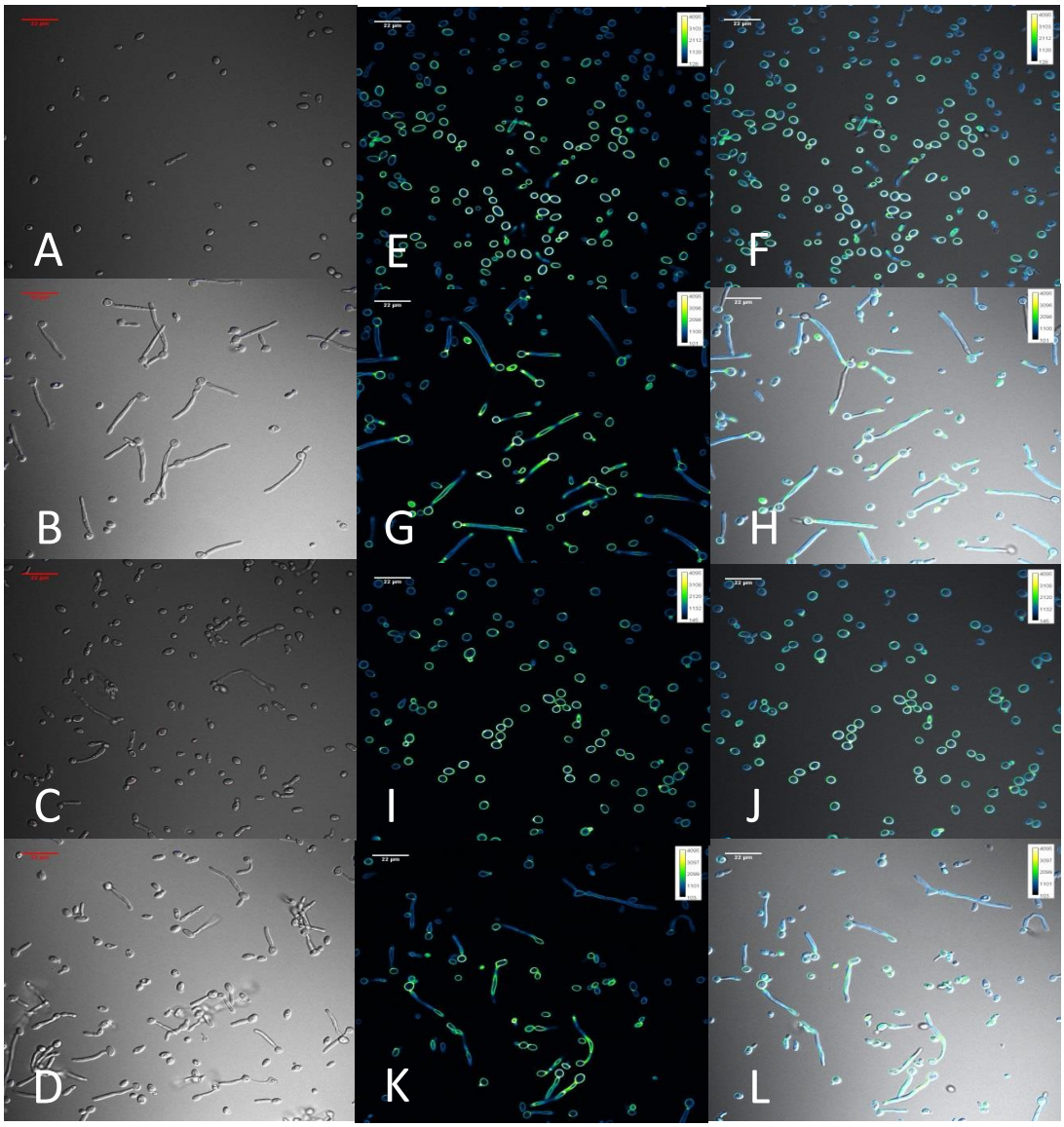

Figure 3.16 60 minutes of light-activation of PPE-DABCO and EO-DABCO is insufficient at preventing the yeast to hyphal transition in surviving cells. A) DIC image of an untreated culture after 1h incubation at 25C following exposure to 60 min UV-irradiation and B) after 3h of growth at 37C. C) DIC image of an untreated culture after 1h incubation at 25C following exposure to 420nm light for 60 min and D) after 3h of growth at 37C. (E-H) Culture treated with EO-DABCO (20µg/mL) and exposed to 60min UV-irradiation. E) EO-DABCO signal of culture after incubation for 1h at 25C and F) merged with DIC image. G) EO-DABCO signal of culture after incubation for 3h at 37C and H) merged with DIC image. (I-L) Culture treated with PPE-DABCO (20µg/mL) and exposed to 60min 420nm-irradiation. I) PPE-DABCO signal of culture after incubation for 1h at 25C and J) merged with DIC image. K) PPE-DABCO signal of culture after incubation for 3h at 37C and L) merged with DIC image.

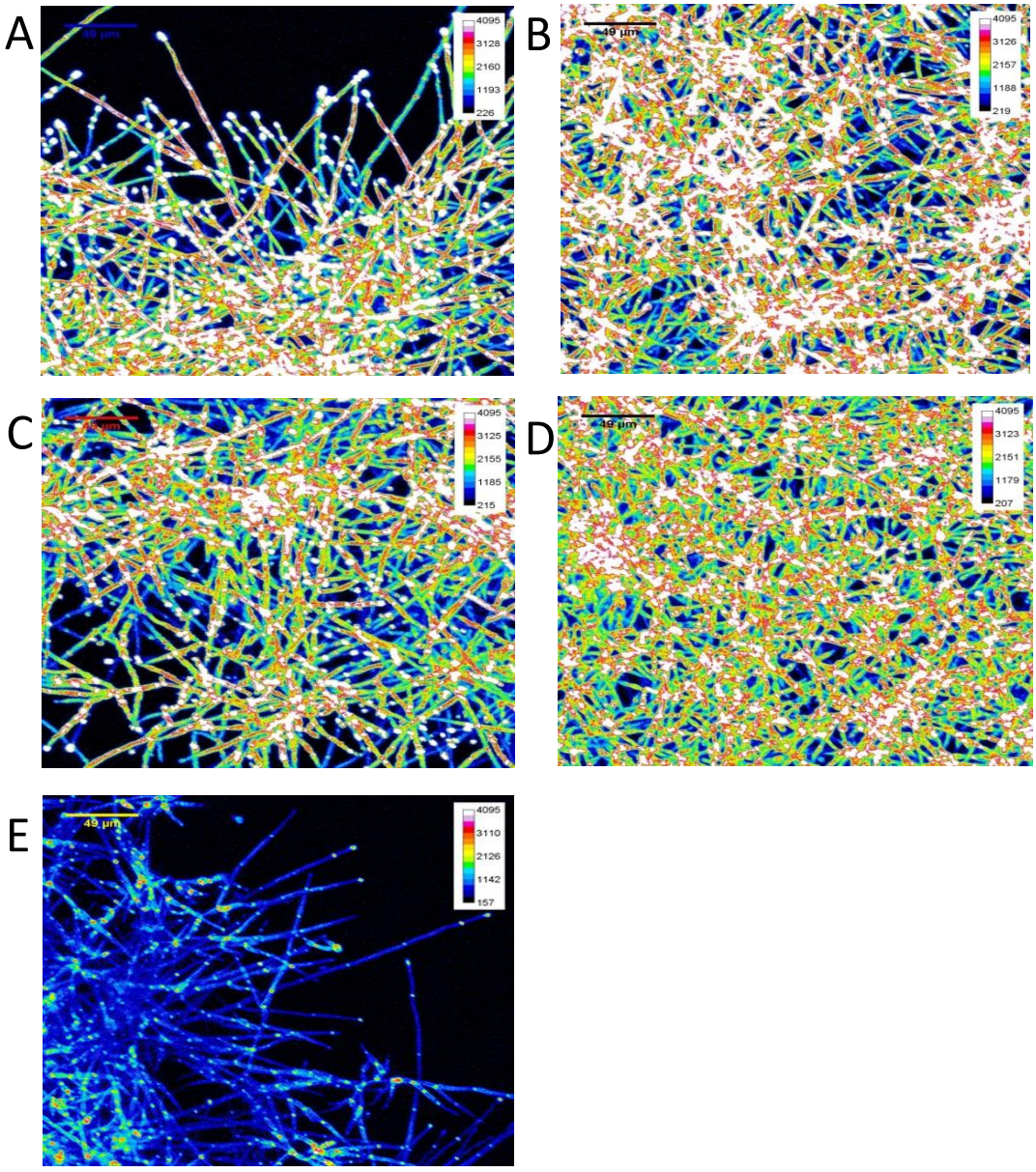

Figure 3.17. Light-irradiation alone, or with application of PPE-DABCO or EO-DABCO, is not sufficient to impede *C. albicans* biofilm development. *C. albicans* 24h biofilms were grown from suspension cultures exposed to 60min of light-irradiation. A) 24h biofilms grown from a 60 minute UV-irradiated untreated culture or B) a culture treated with 20µg/mL EO-DABCO and exposed to UV-irradiation for 60 minutes. C) 24h biofilms grown from an untreated culture exposed to 420nm light for 60 minutes or D) a culture treated with 20µg/mL PPE-DABCO and exposed to 420nm light for 60 minutes. E) A 24h biofilm grown from a scraping from the original *C. albicans* stock culture and unexposed to light irradiation. Images are Z-projections of 3D image stacks based on max intensity of CFW staining using ImageJ (1.48p, Java 1.7.0_07 (64-bit), NIH).

3.7 Effect of PPE-DABCO and EO-DABCO on *C. albicans* biofilm formation

After concluding that neither the yeast to hyphal transition nor the development of biofilm structure could not be fully impeded by light irradiation of either PPE-DABCO or EO-DABCO, we next decided to ascertain whether *C. albicans* treated with these compounds, in the dark or following 30 minutes light irradiation, could form biofilms with similar structural characteristics as untreated *C. albicans* biofilms. Biofilms were grown out to 25h from suspension cultures diluted to 1e6 cells/mL following treatment, stained the biofilms with calcofluor-white, and immediately imaged on the laser-scanning confocal microscope. To assess overall structural characteristics of the biofilms, we analyzed the distribution of the average cellularity of the biofilms as a function of Z-depth, which gave an estimation of the average thickness of the entire biofilm structure, as well as an estimation of cellular density at different depths of the structure (Figure 3.18). The untreated cultures unexposed to light irradiation showed a broader distribution of the cellular mass of the biofilm structure over a Z-thickness that ranged over 40um (Figure 3.18 A). The biofilms grown from cultures that were treated with 20ug/mL of either EO-DABCO or PPE-DABCO in the dark, had distributions of cellularity that were less broadly distributed than the untreated biofilm, with most of the cellular bulk of these biofilms ranging over a Z-thickness of roughly 35um. Interestingly, the biofilms grown from cultures treated with PPE-DABCO in the dark displayed a greater average percent area cellularity over a similar Z-thickness range as the untreated and EO-DABCO from cultures kept in the dark, which may indicate that treatment with PPE-DABCO may lead to the production of biofilms with a greater cellular density. All of the biofilms grown from cultures irradiated for 30 minutes with either 420nm or UVA light, with or without

the presence of PPE-DABCO or EO-DABCO, displayed a sharp peak of increased average percent area cellularity over a Z-thickness ranging from approximately 15-20um, compared to the biofilms grown from the untreated cultures that were kept in the dark. The mechanism governing this observation is unclear, but may represent a cellular response to stressful environmental conditions, either the presence of the compounds, light-irradiation, or a combined effect of both. To further analyze differences in biofilm structures between the samples, we next looked at the distribution of average percent area cellularity per 2um Z-slice (Figure 3.18 B). Notably, the biofilms grown from cultures that were treated with PPE-DABCO and exposed to 30 minutes UV-irradiation displayed a significant increase in the median average percent area cellularity per 2um Z-slice (Figure 3.18 C), while the median average percent area cellularity values for all other conditions were not significantly different from the untreated controls grown from cultures kept in the dark. To further examine differences in the distribution of average cellularity of the analyzed biofilms, we generated a density histogram of the average percent area cellularity per 2um Z-slice (Figure 3.18 D). The untreated dark biofilms displayed a mean of 4.339 average percent area cellularity per Z-slice. This value was similar to the means observed for the biofilms grown from cultures treated with EO-DABCO, both in dark conditions and following 30 minutes UV-irradiation, and biofilms grown from cultures treated with PPE-DABCO following light irradiation at 420nm, with the mean values ranging from 4.311 to 4.977. Notably, the biofilms grown from cultures treated with PPE-DABCO in the dark displayed a much higher observed mean of the average percent area cellularity per Z-slice than the untreated dark biofilms, 10.19. This also supports previous evidence that treatment with 20ug/mL PPE-DABCO in the

absence of light irradiation may lead to the development of a more densely packed biofilm structure. Surprisingly, it was observed that biofilms grown from untreated cultures that were irradiated with 420nm or UV-light also displayed a higher mean than the untreated dark biofilms, with values of 6.890 and 5.788, respectively. This may indicate that light irradiation alone may have some effect on the development of biofilm structure as well, although further testing and analysis need to be performed to confirm this observation.

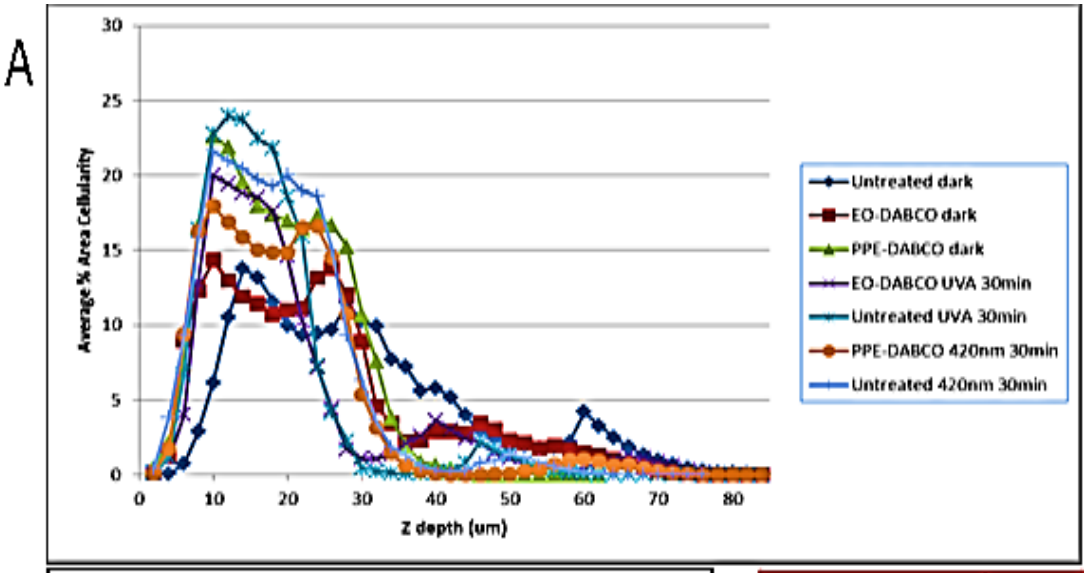

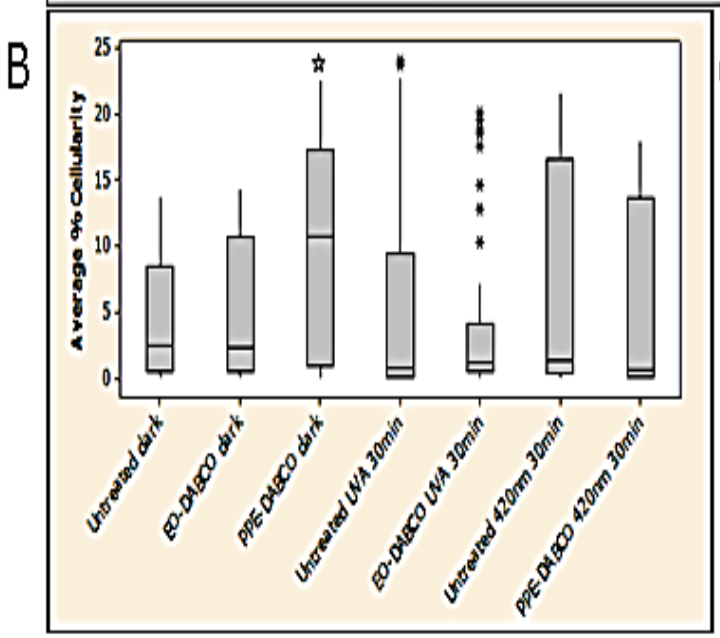

C

Variable	Median
Untreated-dark	2.496
EO-DABCO-dark	2.295
PPE-DABCO-dark	10.69
Untreated UVA 30min	0.83
EO-DABCO UVA 30min	1.231
Untreated 420nm 30min	1.35
PPE-DABCO 420nm 30min	0.72

Figure 3.18. Growth of 25h biofilms from *C. albicans* cultures. *C. albicans* cultures were treated with PPE-DABCO (20ug/mL) or EO-DABCO (20ug/mL) for 2h in the dark or 30 minutes irradiation with 420nm-light or UV-light (to activate PPE-DABCO or EO-DABCO respectively). Untreated controls were also exposed to 30 minutes irradiation with 420nm-light or UV-light. Biofilms were stained with 20ug/mL calcofluor-white and imaged at 25h. A) Distribution of the average cellular density of biofilms is represented by plotting the average percent area cellularity of three fields per biofilm, three biofilms per condition vs. Z depth (um). B) Boxplot representing the distributions of average percent area cellularity per 2um Z-slice of data from (A). The symbol ☆ represents statistical significance in a CI of 95.0%, as determined by Mann-Whitney nonparametric comparison of medians. C) Table of median average percent area cellularity per 2um Z-slice, quantified from data represented in (B). Data representative of the average of 3 fields per biofilm, 3 biofilms per condition.

Chapter 4. Conclusion

In this study, we determined that the light activation of PPE-DABCO and EO-DABCO could efficiently kill *C. albicans* planktonic cells in suspension. Furthermore, we were able to visualize and photoactivate the agents with a 405nm confocal laser, which allowed us to quantify time-dependent changes in the cells in response to the treatment. Furthermore, by washing out the excess PPE-DABCO in our viability assays, as well as our live-cell experiments, we were able to determine that the direct physical interaction of the agent with the cell was responsible for the antimicrobial effect, and not the result of singlet oxygen generation by activation of the free compound in solution. However, this study did not elucidate the extent to which the compounds are able to penetrate the cell wall of the yeast. It remains to be investigated whether the compounds are able to interact with the cell membrane of yeast and hyphal cells. Previous work has demonstrated that CPEs, particularly PPE-Th, another cationic conjugated polyelectrolyte with similar biocidal properties as the agents used in this and previous antifungal studies, possesses the ability to induce remodeling of the outer membrane of bacteria, as well as the peptidoglycan layer prior to causing the cytoplasmic membrane to collapse, killing the cell (119, 122). We did see a reduction in viability of *C. albicans* yeast with PPE-DABCO in the dark, but the mechanism by which this is occurring remains to be elucidated. It is possible that insertion of these compounds into the cell wall or cell membrane can induce remodeling of these features by activating cell wall stress response pathways or other mechanisms. The ability of *C. albicans* to remodel the cell wall in response to drug treatment has been well documented; low levels of treatment with echinocandins have been demonstrated to induce the synthesis of chitin, leading to an

increase of chitin in the cell wall and conferring a protective effect to the cell (123, 55). Furthermore, cell wall remodeling has also been observed with other compounds that interact directly with the cell wall, including calcofluor-white and Congo red by activating the HOG MAP kinase pathway in *S. cerevisiae* (124). If cell wall remodeling is occurring, it remains to be determined which cell wall remodeling pathway is activated, what implications this dynamic response may hold with regards to virulence of the surviving cells.

We demonstrated that single cell hyphal growth stops upon treatment with PPE-DABCO and photoactivation of the agent. While there was an inhibition of hyphal growth with photoactivation of the compounds, it is unclear to what extent this is due to the increase in cell death that occurs with photoactivation of PPE-DABCO. Preliminary experiments demonstrated that both compounds inhibited the development of hyphae after 2 hours of continuous activation using the 405nm laser. What appeared to be cell debris was visible in images of cultures treated with PPE-DABCO and irradiated every 5 minutes for 2 hours with the 405nm laser. However, cultures that were treated with the agents and exposed to light for 60 minutes in the photochamber were still able to produce surviving cells that effectively form hyphae. It remains to be elucidated the relative contribution of both the source of the irradiation (i.e. laser vs. lamp) and the time of light exposure to inhibiting this morphological transition.

The necessity of light activation of these compounds to both kill planktonic cells and inhibit the yeast to hyphal transition indicates that the induction of singlet oxygen is critical for full efficacy of the agents. However, the mechanism by which cell death may be occurring, the relative ability of individual compounds to interact with the cells and

generate singlet oxygen, and the contribution of the geometry and structure of the biocidal compounds to the ability of the agents to interact with and kill the cells remains to be investigated.

Our live cell experiments in which we activated PPE-DABCO with the 405nm confocal laser allowed us to not only visualize the effects to individual cells in response to treatment over time, it also enabled us to quantify the morphological cellular changes, and in so doing, assess the time-dependency of the cellular responses. However, this study failed to sufficiently elucidate the specific mechanistic effects of 405nm irradiation alone and the contribution of activation of PPE-DABCO to causing cellular damage. The detrimental effects of UV-light on *C. albicans* has been observed, both in experiments performed by our laboratory as well as others. A recent study by Risovic *et al.* provided evidence that the efficiency of using UV and visible light to eradicate *C. albicans* was wavelength dependent, with the strongest effect observed using light centered at 406nm (126). As our live-cell confocal experiments utilized the 405nm laser at a relatively high power, phototoxicity effects on untreated cultures became a confounding factor in analysis. Although we were able to provide evidence that the effects of PPE-DABCO activation could be isolated from phototoxicity effects, by limiting the time the cultures were irradiated with the 405nm laser to 20min, it remains unclear how the 405nm laser is affecting the cellular processes of the untreated and treated cells. A study by Farrell *et al.* demonstrated that low-level UV-pulsed light irradiation of clinical strains of *C. albicans* resulted in enhanced membrane permeability and an increase in the ROS localized to the mitochondria. The increase in intracellular ROS production resulted in a concurrent increase in apoptotic markers, including the abnormal condensation of chromatin and

exposure of phophatidylserine on the outer portion of the cell membrane. Increasing the UV dosage resulted in nuclear damage, activation of cellular repair mechanisms, irreversible cell membrane leakage, and an increase in apoptotic and necrotic cells (127). This indicates that even in our experiments in which the time of exposure to the 405nm laser was limited, it is likely that reversible and irreversible effects to the cells may be occurring, even in the absence of the photoactivating agent. Furthermore, it remains to be investigated whether the phototoxicity effects of 405nm light on EO-DABCO treated samples can be isolated from the effects of photoactivation of the compound. The time-dependent responses of EO-DABCO treated cultures, both irradiated and without photoactivation, needs to be assessed, perhaps in another set of live-cell imaging experiments.

Cultures that were previously exposed to PPE-DABCO and EO-DABCO and irradiated with light were still able to form biofilms subsequently, as were cultures that were irradiated with UV-visible light alone and cultures that were treated with the agents in the absence of photoactivation of the compounds. We observed quantifiable changes in the overall structural characteristics of biofilms exposed to PPE-DABCO in the dark, and among the biofilms exposed to light-irradiation. However, the implications of these observations remain unclear. Further characterization of biofilms grown under these conditions is necessary to fully elucidate any mechanistic and structural changes in the biofilm growth, which may affect the ability of small molecules to diffuse through the structure, the overall resistance of different biofilm structures to antifungal therapy, and the composition of both the cell wall of cells within the biofilms and the ECM.

One of the considerations for antimicrobial efficiency of agents is the ability to effectively penetrate and kill cells within a biofilm. Previous work by Dascier *et al.* demonstrated EO-OPE compounds with 1,4-diazabicyclo[2,2,2]-octane (DABCO) groups demonstrated greater efficiency at eradicating *E. coli* bacterial biofilms than EO-OPE compounds containing traditional quarternary ammonium side chains, which is thought to be related to the ability of the EO-DABCO compounds to more easily penetrate the biofilm structure. This study also demonstrated that the relative amount of singlet oxygen generation does not directly correlate to the effectiveness of the biocidal activity against biofilms, which may indicate that geometry of the compound influences the killing ability in addition to the efficiency of singlet oxygen generation (128). While the results of our study demonstrated the ability of these compounds to inhibit the yeast to hyphal transition, which is important for the attenuating the pathogenicity of *C. albicans*, we have not yet investigated the ability of PPE-DABCO and EO-DABCO to effectively penetrate and eradicate mature biofilms. It is possible that the antimicrobial ability of these compounds will be attenuated in a biofilm environment, where the presence of copious amounts of heterogeneous ECM may bind the compounds nonspecifically and inhibit diffusion. This may be influenced by the structure and physical properties of the agents, and it needs to be determined whether the molecular weight, geometry and charges of the compounds affect the activity against mature biofilms. For example, a study conducted by Ji *et al.* demonstrated that the increasing length of the chain of CPE compounds correlated to a reduction of effectiveness against bacteria; the relative chain length of polymerized compounds may affect the ability of the agent to diffuse through a biofilm structure (129). Furthermore, it has been demonstrated that 10-30 times the

concentration of EO-OPEs was required to show effectiveness against *E.coli* biofilms, which indicates that increasing the concentration of these agents when treating *C. albicans* biofilms may be necessary for full eradication (128). It has been previously demonstrated that UV-light irradiation increases the effectiveness EO-OPEs against *E. coli* biofilms (128). The efficiency of the compounds against *C. albicans* biofilms in both the light and dark needs to be assessed; the relative amount of biofilm eradication may be vastly different between the two conditions. This may aid in elucidating the mechanisms of the antimicrobial activities of the compounds against mature biofilms.

References

1. Martins, N. *et al.* Candidiasis: Predisposing Factors, Prevention, Diagnosis and Alternative Treatment. *Mycopathologia* **177,** 223–240 (2014).

2. Mikulska, M. *et al.* Occurrence, presentation and treatment of candidemia. *Expert Rev Clin Immunol.* **8,** 755-65 (2012).

3. Wisplinghoff, H. *et al.* Nosocomial bloodstream infections due to *Candida* spp. in the USA: species distribution, clinical features and antifungal susceptibilities. *Int. J. Antimicrob. Agents* **43,** 78–81 (2014).

4. Spampinato, C., Leonardi, D. *Candida* infections, causes, targets, and resistance mechanisms: traditional and alternative antifungal agents. *Biomed Res. Int.* **2013,** 1-13 (2013).

5. Bhattacharya, S. Early diagnosis of resistant pathogens: how can it improve antimicrobial treatment? *Virulence* **4,** 172–84 (2013).

6. Mayer, F. L., Wilson, D., Hube, B. *Candida albicans* pathogenicity mechanisms. *Virulence* **4,** 119–28 (2013).

7. Brown, A. J., Gow, N. A. Regulatory networks controlling *Candida albicans* morphogenesis. *Trends Microbiol.* **7,** 333–8 (1999).

8. Bramley, T.A. *et al*. Binding sites for LH in *Candida albicans*: comparison with the mammalian corpus luteum LH receptor. *J Endocrinol.* **130,** 177-90 (1991).

9. Zhao, X., Malloy, P.J., Ardies, C.M., Feldman, D. Oestrogen-binding protein in *Candida albicans*: antibody development and cellular localization by electron immunocytochemistry. *Microbiology* **141,** 2685-92 (1995)

10. Whiteway, M. Transcriptional control of cell type and morphogenesis in *Candida albicans*. *Curr. Opin. Microbiol.* **3,** 582–8 (2000).

11. Nantel, A. *et al*. Transcription Profiling of *Candida albicans* Cells: Undergoing the Yeast-to-Hyphal Transition. *Molecular Biology of the Cell* **13,** 3452–3465 (2002).

12. Berman, J., Sudbery, P. E. *Candida Albicans:* a molecular revolution built on lessons from budding yeast. *Nat. Rev. Genet.* **3,** 918–30 (2002).

13. Ernst, J. F. Transcription factors in *Candida albicans* – environmental control of morphogenesis. *Microbiology* **146,** 1763–1774 (2000).

14. Lo, H. J. *et al.* Nonfilamentous *C. albicans* mutants are avirulent. *Cell* **90,** 939–49 (1997).

15. Jacobsen, I. D. *et al. Candida* albicans dimorphism as a therapeutic target. *Expert Rev. Anti Infect. Ther.* **10,** 85–93 (2012).

16. Lionakis, M.S., Lim, J.K., Lee, C.C., Murphy, P.M. Organ-specific innate immune responses in a mouse model of invasive candidiasis. *J. Innate. Immun.* **3,** 180–199 (2011).

17. Baillie, G. S., Douglas, L. J. Role of dimorphism in the development of *Candida albicans* biofilms. *J. Med. Microbiol.* **48,** 671–9 (1999).

18. Kumamoto, C. A., Vinces, M. D. Alternative *Candida albicans* lifestyles: growth on surfaces. *Annu. Rev. Microbiol.* **59,** 113–33 (2005).

19. Sapaar, B. *et al.* Effects of extracellular DNA from *Candida albicans* and pneumonia-related pathogens on *Candida* biofilm formation and hyphal transformation. *J. Appl. Microbiol.* **116,** 1531-42 (2014).

20. Chandra, J. *et al.* Biofilm Formation by the Fungal Pathogen *Candida albicans*: Development, Architecture, and Drug Resistance. *J Bacteriol*. **183,** 5385–5394 (2001).

21. LaFleur, M.D., Kumamoto, C.A., Lewis, K. *Candida albicans* biofilms produce antifungal-tolerant persister cells. *Anti- microb Agents Chemother*. **50,** 3839–46 (2006).

22. Tobudic, S., Kratzer, C., Lassnigg, A., Presterl, E. Antifungal susceptibility of *Candida albicans* in biofilms. *Mycoses* **55,** 199–204 (2012).

23. Baillie, G.S., Douglas, L.J. Effect of growth rate on resistance of *Candida albicans* biofilms to antifungal agents. *Antimicrob. Agents Chemother.* **42,** 1900–5 (1998).

24. Baillie, G. S., Douglas, L. J. Matrix polymers of *Candida* biofilms and their possible role in biofilm resistance to antifungal agents. *J. Antimicrob. Chemother.* **46,** 397–403 (2000).

25. Martins, M. *et al.* Presence of extracellular DNA in the *Candida albicans* biofilm matrix and its contribution to biofilms. *Mycopathologia* **169,** 323–31 (2010).

26. Martins, M. *et al.* Addition of DNase Improves the In Vitro Activity of Antifungal Drugs against *Candida albicans* Biofilms. *Mycoses* **55,** 80–85 (2012).

27. Ramage, G. Investigation of multidrug efflux pumps in relation to fluconazole resistance in *Candida albicans* biofilms. *J. Antimicrob. Chemother*. **49,** 973–980 (2002).

28. Eddouzi, J. *et al.* Molecular mechanisms of drug resistance in clinical *Candida* species isolated from Tunisian hospitals. *Antimicrob. Agents Chemother*. **57,** 3182–93 (2013).

29. Shah, A.H. *et al.* Novel Role of a Family of Major Facilitator Transporters in Biofilm Development and Virulence of *Candida albicans. Biochem J.* [Epub ahead of print] (2014).

30. Yi, S. *et al.* Alternative mating type configurations (a/α versus a/a or α/α) of *Candida albicans* result in alternative biofilms regulated by different pathways. PLoS Biol. **9,** (2011).

31. Zhu, W., Filler, S.G. Interactions of *Candida albicans* with epithelial cells. *Cell Microbiol*. **12,** 273-82 (2010).

32. Phan, Q. T. *et al.* Als3 is a *Candida albicans* invasin that binds to cadherins and induces endocytosis by host cells. *PLoS Biol.* **5,** e64 (2007).

33. Sun, J. N. *et al.* Host cell invasion and virulence mediated by *Candida albicans* Ssa1. *PLoS Pathog.* **6,** e1001181 (2010).

34. Wächtler, B. *et al. Candida albicans*-epithelial interactions: dissecting the roles of active penetration, induced endocytosis and host factors on the infection process. *PLoS One* **7,** e36952 (2012).

35. Felk, A. *et al. Candida albicans* Hyphal Formation and the Expression of the Efg1-Regulated Proteinases Sap4 to Sap6 Are Required for the Invasion of Parenchymal Organs. *Infect.Immun.* **70,** 3689–3700 (2002).

36. Hoyer, L. L. The ALS gene family of *Candida albicans*. *Trends Microbiol.* **9,** 176–180 (2001).

37. Sundstrom, P. Adhesins in *Candida albicans*. *Curr. Opin. Microbiol.* **2,** 353–7 (1999).

38. Younes, S., Bahnan, W., Dimassi, H. I. & Khalaf, R. a. The *Candida albicans* Hwp2 is necessary for proper adhesion, biofilm formation and oxidative stress tolerance. *Microbiol. Res.* **166,** 430–6 (2011).

39. Fukazawa, Y., Kagaya, K., Molecular bases of adhesion of *Candida albicans. J. Med. Vet. Mycol.* **35,** 87-99 (1997).

40. Naglik, J. R., Challacombe, S. J. & Hube, B. *Candida albicans* Secreted Aspartyl Proteinases in Virulence and Pathogenesis. *Microbiol. Mol. Biol. Rev.* **67,** 400–428 (2003).

41. Staib, P., Kretschmar, M., Nichterlein, T., Hof, H. & Morschhäuser, J. Differential activation of a *Candida albicans* virulence gene family during infection. *Proc. Natl. Acad. Sci. U. S. A.* **97,** 6102–7 (2000).

42. White, T.C., Agabian, N. *Candida albicans* secreted aspartyl proteinases: isoenzyme pattern is determined by cell type, and levels are determined by environmental factors. *J Bacteriol*. **177,** 5215-221 (1995).

43. Felk, A. *et al. Candida albicans* Hyphal Formation and the Expression of the Efg1-Regulated Proteinases Sap4 to Sap6 Are Required for the Invasion of Parenchymal Organs. *Infect. Immun.* **70,** 3689–3700 (2002).

44. Wu, H. *et al. Candida albicans* secreted aspartic proteases 4-6 induce apoptosis of epithelial cells by a novel Trojan horse mechanism. *FASEB J.* **27,** 2132-44 (2013).

45. Ansell, G. B., Hawthorne, J.N. Phospholipids. *Catabolism.*, 152-174 (1964).

46. Ghannoum, M. A. Potential Role of Phospholipases in Virulence and Fungal Pathogenesis. *Clin. Microbiol. Rev.* **13,** 122–143 (2000).

47. Gácser, A. *et al.* Lipase 8 affects the pathogenesis of *Candida albicans*. *Infect. Immun.* **75,** 4710–8 (2007).

48. Schofield, D.A. *et al.* Differential *Candida albicans* lipase gene expression during alimentary tract colonization and infection. *FEMS Microbiol. Lett.* **244,** 359-65 (2005).

49. Kapteyn, J. C. *et al.* The cell wall architecture of *Candida albicans* wild-type cells and cell wall-defective mutants. *Mol. Microbiol.* **35,** 601–11 (2000).

50. Chaffin, W. L. *Candida albicans* cell wall proteins. *Microbiol. Mol. Biol. Rev.* **72,** 495–544 (2008).

51. Shepard, M.G., Cell envelope of *Candida albicans*. *Crit. Rev. Microbiol.* **15,** 7-25 (1987).

52. Brown, a J. & Gow, N. a. Regulatory networks controlling *Candida albicans* morphogenesis. *Trends Microbiol.* **7,** 333–8 (1999).

53. Ernst, J. F. Transcription factors in *Candida albicans* – environmental control of morphogenesis. *Microbiology* **146,** 1763–1774 (2000).

54. Andriole, V.T. Current and future antifungal therapy: new targets for antifungal therapy. *Int. J. Antimicrob. Agents* **16,** 317-21 (2000).

55. Keunsook, L. *et al.* Elevated Cell Wall Chitin in *Candida albicans* Confers Echinocandin Resistance In Vivo. *Antimicrobial Agents and Chemotherapy* **56,** 208-17 (2012).

56. Lipke, P.N., Ovalle, R. Cell wall architecture in yeast: new structure and new challenges. *J. Bacteriol.* **180,** 3735-40 (1998).

57. Ram, A.F.J. *et al.* Loss of the plasma-membrane bound protein Gas1p in *Saccharomyces cerevisiae* results in the release of β1,3-glucan into the medium and induces a compensation mechanism to ensure cell wall integrity. *J. Bacteriol.* **180,** 1418-24 (1998).

58. Bates, S., Hughes, H.B., Munro, C.A., Thomas, W.P.H., MacCallum, D.M., Bertram, G., Atrih, A., Ferguson, M.A., Brown, A.J.P., Odds, F.C., Gow, N.A.R., Outer chain N-glycans are required for cell wall integrity and virulence of *Candida albicans*. *J. Biol. Chem.* **281**, 90–98 (2006)

59. Prill, S.K., Klinkert, B., Timpel, C., Gale, C.A., Schröppel, K., Ernst, J.F. PMT family of *Candida albicans*: five protein mannosyltransferase isoforms affect growth, morphogenesis and antifungal resistance. *Mol. Microbiol.* **55,** 546–560 (2005).

60. Rouabhia, M., Schaller, M., Corbucci, C., Vecchiarelli, A., Prill, S.K.-H., Giasson, L., Ernst, J.F. Virulence of the fungal pathogen *Candida albicans* requires the five isoforms of protein mannosyltransferases. *Infect. Immun.* **73,** 4571–4580 (2005).

61. Cantero, P.D., Lengsfeld, C., Prill, S.K.-H., Subanovi´c, M., Román, E., Ernst, J.F. Transcriptional and physiological adaptation to defective protein-O-mannosylation in *Candida albicans. Mol. Microbiol.* **64,** 1115–1128 (2007).

62. Fuchs, B. B., Mylonakis, E. Our paths might cross: the role of the fungal cell wall integrity pathway in stress response and cross talk with other stress response pathways. *Eukaryot. Cell* **8,** 1616–25 (2009).

63. Ketela, T., Green, R., Bussey, H. *Saccharomyces cerevisiae* Mid2p is a potential cell wall stress sensor and upstream activator of the PKC1-MPK1 cell integrity pathway. *J. Bacteriol*. **181,** 3330–3340 (1999).

64. Ozaki, K. *et al.* Rom1p and Rom2p are GDP/ GTP exchange proteins (GEPs) for the Rho1p small GTP binding protein in *Saccharomyces cerevisiae. EMBO J.* **15,** 2196–2207 (1996).

65. Nonaka, H. *et al.* A downstream target of RHO1 small GTP- binding protein is PKC1, a homolog of protein kinase C, which leads to activation of the MAP kinase cascade in *Saccharomyces cerevisiae. EMBO J.* **14,** 5931–5938 (1995).

66. Watanabe, Y., Irie, K., Matsumoto, K. Yeast RLM1 encodes a serum response factor-like protein that may function downstream of the Mpk1 (Slt2) mitogen-activated protein kinase pathway. *Mol. Cell. Biol.* **15,** 5740–5749 (1995).

67. Bermejo, C. *et al.* The Sequential Activation of the Yeast HOG and SLT2 Pathways Is Required for Cell Survival to Cell Wall Stress. *Molecular Biology of the Cell* **19,** 1113–1124 (2008).

68. Delgado-Silva, Y. *et al.* Participation of *Candida albicans* transcription factor RLM1 in cell wall biogenesis and virulence. *PLoS One* **9,** e86270 (2014).

69. Hohmann, S. Osmotic stress signaling and osmoadaptation in yeasts. *Microbiol. Mol. Biol. Rev.* **66,** 300–372 (2002).

70. de Nadal, E., Alepuz, P. M., Posas, F. Dealing with osmostress through MAP kinase activation. *EMBO Rep*. **3,** 735–740 (2002).

71. Posas, F., Saito, H. Activation of the yeast SSK2 MAP kinase kinase kinase by the SSK1 two-component response regulator. *EMBO J*. **17,** 1385–1394 (1998).

72. Denning, D. W. Echinocandin antifungal drugs. *New Drug Classes* **362,** 1142–1152 (2003).

73. NCCLS. Reference method for broth dilution antifungal susceptibility testing of yeasts: approved standard. NCCLS document **M27-A2.** Wayne, PA: NCCLS, (2002).

74. NCCLS. Reference method for broth dilution antifungal susceptibility testing of conidial-forming filamentous fungi: approved standard. NCCLS **M38–A.** Wayne, PA: NCCLS, (2002).

75. Spampinato, C., Leonardi, D. *Candida* infections, causes, targets, and resistance mechanisms: traditional and alternative antifungal agents. *Biomed Res. Int.* **2013,** 204237 (2013).

76. Espinel-Ingroff, A. Mechanisms of resistance to antifungal agents: yeasts and filamentous fungi. *Rev. Iberoam. Micol.* **25,** 101–6 (2008).

77. Yoshida Y. Cytochrome P450 of fungi: primary target for azole antifungal agents. *Curr. Top. Med. Mycol.* **2,** 388–418 (1988).

78. Lamfon, H., Porter, S. R., McCullough, M. & Pratten, J. Susceptibility of *Candida albicans* biofilms grown in a constant depth film fermentor to chlorhexidine, fluconazole and miconazole: a longitudinal study. *J. Antimicrob. Chemother.* **53,** 383–5 (2004).

79. Delattin, N., Cammue, B. P., Thevissen, K. Reactive oxygen species-inducing antifungal agents and their activity against fungal biofilms. *Future Med. Chem.* **6,** 77–90 (2014).

80. Kobayashi D, Kondo K, Uehara N *et al.* Endogenous reactive oxygen species is an important mediator of miconazole antifungal effect. *Antimicrob. Agents Chemother.* **46,** 3113–3117 (2002).

81. Francois I.E.*et al.* Azoles: mode of antifungal action and resistance development. Effect of miconazole on endogenous reactive oxygen species production in *Candida albicans. Curr. Med. Chem.* **5,** 3–13 (2006).

82. Bink, A. *et al.* Superoxide dismutases are involved in *Candida albicans* biofilm persistence against miconazole. *Antimicrob. Agents Chemother.* **55,** 4033–7 (2011).

83. Gopinathan, S., Janagond, A. B., Agatha, D. *et al.* Detection of FUR1 Gene in 5-Flucytosine Resistant Candida Isolates in Vaginal Candidiasis Patients. *J. Clin. Diagn. Res.* **7,** 2452–5 (2013).

84. Steier, Z. *et al.* Flucytosine antagonism of azole activity versus *Candida glabrata*: role of transcription factor Pdr1 and multidrug transporter Cdr1. *Antimicrob. Agents Chemother.* **57,** 5543–7 (2013).

86. Vermitsky, J.P. *et al.* Pdr1 regulates multidrug resistance in *Candida glabrata:* gene disruption and genome-wide expression studies. *Mol. Microbiol.* **61,** 704–722 (2006).

87. Papon, N. *et al*. Molecular mechanism of flucytosine resistance in *Candida lusitaniae*: contribution of the FCY2, FCY1, and FUR1 genes to 5-fluorouracil and fluconazole crossresistance. *Antimicrob. Agents Chemother.* **51,** 369-371 (2007).

88. Caffrey, P. *et al.* Amphotericin biosynthesis in *Streptomyces nodosus*: deductions from analysis of polyketide synthase and late genes. *Chem. Biol.* **8,** 713–723 (2001).

89. Dick, J. D., Merz, W. G. & Saral, R. Incidence of polyene-resistant yeasts recovered from clinical specimens. *Antimicrob. Agents Chemother.* **18,** 158–63 (1980).

90. Chen, S. C., Slavin, M. a & Sorrell, T. C. Echinocandin antifungal drugs in fungal infections: a comparison. *Drugs* **71,** 11–41 (2011).

91. Ramage, G. Investigation of multidrug efflux pumps in relation to fluconazole resistance in *Candida albicans* biofilms. *J. Antimicrob. Chemother.* **49,** 973–980 (2002).

92. Pfaller, M. *et al.* In vitro susceptibility of invasive isolates of *Candida spp.* to anidulafungin, caspofungin, and micafungin: six years of global surveillance. *J. Clin. Microbiol.* **46,** 150–6 (2008).

93. Walker, L. a, Gow, N. a R. & Munro, C. a. Elevated chitin content reduces the susceptibility of *Candida* species to caspofungin. *Antimicrob. Agents Chemother.* **57,** 146–54 (2013).

94. Shields, R. K. *et al.* Paradoxical effect of caspofungin against *Candida* bloodstream isolates is mediated by multiple pathways but eliminated in human serum. *Antimicrob. Agents Chemother.* **55,** 2641–7 (2011).

95. Kobayashi, D., Kondo, K., Uehara, N. *et al.* Endogenous reactive oxygen species is an important mediator of miconazole antifungal effect. *Antimicrob. Agents Chemother.* **46,** 3113–3117 (2002).

96. Vandenbosch, D., Braeckmans, K., Nelis, H.J., Coenye, T. Fungicidal activity of miconazole against *Candida spp.* biofilms. *J. Antimicrob. Chemother.* **65,** 694–700 (2010).

97. Sokol-Anderson, M. L., Brajtburg, J., Medoff, G. Amphotericin B-induced oxidative damage and killing of *Candida albicans. J. Infect. Dis.* **154,** 76–83 (1986).

98. Pereira Gonzales, F., Maisch, T. Photodynamic inactivation for controlling *Candida albicans* infections. *Fungal Biol.* **116,** 1–10 (2012).

99. Bertoloni, G, *et al.* Factors influencing the haematoporphyrin-sensitized photoinactivation of *Candida albicans*. *J. Gen. Microbiol.* **135,** 957-66 (1989).

100. Pereira, CA, *et al*. Susceptibility *of Candida albicans*, *Staphylococcus aureus*, and *Streptococcus mutans* biofilms to photodynamic inactivation: an in vitro study. *Lasers Med. Sci.* **26,** 341-48 (2011).

101. Zeina B, *et al.* Cytotoxic effects of antimicrobial photodynamic therapy on keratinocytes in vitro. *Br. J. Dermatol.* **146,** 568-73 (2002).

102. Zeina, B. *et al.* Killing of cutaneous microbial species by photodynamic therapy. *Br J Dermatol.* **144,** 274-8 (2001).

103. Dai, T. *et al.* Photodynamic therapy for methicillin-resistant *Staphylococcus aureus* infection in a mouse skin abrasion model. *Lasers Surg. Med.* **42,** 38-44 (2010).

104. Maisch, T. *et al.* Antibacterial photodynamic therapy. A new treatment for superficial bacterial infections? *Hautarzt* **56,** 1048-55 (2005).

105. Schafer, M., Schmitz, C., Horneck, G. High sensitivity of *Deinococcus radiodurans* to photodynamically-produced singlet oxygen. *Int. J. Radiat. Biol.* **74,** 249-53 (1998).

106. Prates, R.A., *et al.* Influence of multidrug efflux systems on methylene blue-mediated photodynamic inactivation of *Candida albicans. J. Antimicrob. Chemother*. **66,** 1525-32 (2011).

107. Wysong, D. R. *et al.* Cloning and Sequencing of a *Candida albicans* Catalase Gene and Effects of Disruption of This Gene. *Infect. Immun.* **66,** 1953-61 (1998).

108. Martchenko, M., Alarco, A., Harcus, D., Whiteway, M. Superoxide Dismutases *in Candida albicans* : Transcriptional Regulation and Functional Characterization of the Hyphal-induced SOD5 Gene. *Mol. Biol. Cell* **15,** 456–467 (2004).

109. Nantel, A. *et al.* Transcription profiling of *Candida albicans* cells undergoing the yeast-to-hyphal transition. *Mol Biol Cell.* **13,** 3452-65 (2002).

110. Nicholls, S. *et al.* Activation of the heat shock transcription factor Hsf1 is essential for the full virulence of the fungal pathogen *Candida albicans. Fungal Genet. Biol.* **48,** 297-305 (2011).

111. Mayer, F. L. *et al.* Small but crucial: the novel small heat shock protein Hsp21 mediates stress adaptation and virulence in *Candida albicans*. *PLoS One* **7,** (2012).

112. Carmona-Ribeiro, A. M., de Melo Carrasco, L. D. Cationic antimicrobial polymers and their assemblies. *Int. J. Mol. Sci.* **14,** 9906–46 (2013).

113. Kenawy, E.-R., Worley, S. D., Broughton, R. The chemistry and applications of antimicrobial polymers: a state-of-the-art review. *Biomacromolecules* **8,** 1359–84 (2007).

114. Wilde, K. N., Whitten, D. G., Canavan, H. E. In vitro cytotoxicity of antimicrobial conjugated electrolytes: interactions with mammalian cells. *ACS Appl. Mater. Interfaces* **5,** 9305–11 (2013).

115. Lu, L. *et al.* Biocidal activity of a light-absorbing fluorescent conjugated polyelectrolyte. *Langmuir* **21,** 10154–9 (2005).

116. Ji, E., Parthasarathy, A., Corbitt, T. S., Schanze, K. S. & Whitten, D. G. Antibacterial activity of conjugated polyelectrolytes with variable chain lengths. *Langmuir* **27,** 10763–9 (2011).

117. Wang, Y. *et al.* Dark Antimicrobial Mechanisms of Cationic Phenylene Ethynylene Polymers and Oligomers against *Escherichia coli*. *Polymers (Basel).* **3,** 1199–1214 (2011).

118. Wang, Y. *et al.* Understanding the dark and light-enhanced bactericidal action of cationic conjugated polyelectrolytes and oligomers. *Langmuir* **29,** 781–92 (2013).

119. Wang, Y., Chi, E. Y., Natvig, D. O., Schanze, K. S., Whitten, D. G. Antimicrobial activity of cationic conjugated polyelectrolytes and oligomers against *Saccharomyces cerevisiae* vegetative cells and ascospores. *ACS Appl. Mater. Interfaces* **5,** 4555–61 (2013).

120. Tang, Y.L. *et al.* Synthesis, Self-Assembly, and Photophysical Properties of Cationic Oligo(p-phenyleneethynylene)s. *Langmuir* **27**, 4945–4955 (2011).

121. Tang, Y.L. *et al.* Synthesis, self-assembly, and photophysical behavior of oligo phenylene ethynylenes: from molecular to supramolecular properties. *Langmuir* **25,** 21-5 (2009).

122. Wang, Y. *et al.* Direct visualization of bactericidal action of cationic conjugated polyelectrolytes and oligomers. *Langmuir* **28,** 65–70 (2012).

123. Walker, L. *et al.* Stimulation of Chitin Synthesis Rescues *Candida albicans* from Echinocandins. *PLoS Pathog.* **4,** (2008).

124. Roman, E. *et al.* The Sho1 adaptor protein links oxidative stress to morphogenesis and cell wall biosynthesis in the fungal pathogen *Candida albicans. Mol.Cell Bio.* **25,** 10611-27 (2005).

126. Risovic, D. *et al.* Quantitative investigation of efficiency of ultraviolet and visible light in eradication of *Candida albicans* in vitro. *Photomed. Laser Surg.* **32,** 232-9 (2014).

127. Farrell, H. *et al.* Studies on the relationship between pulsed UV light irradiation and the simultaneous occurrence of molecular and cellular damage in clinically-relevant *Candida albicans. J. Microbiol. Methods* **84,** 317-26 (2011).

128. Dascier, D., Ji, E., Parthasarathy, A., Schanze, K. S., Whitten, D. G. Efficacy of end-only-functionalized oligo(arylene-ethynylene)s in killing bacterial biofilms. *Langmuir* **28,** 11286–90 (2012).

129. Ji, E., Parthasarathy, A., Corbitt, T. S., Schanze, K. S., Whitten, D. G. Antibacterial activity of conjugated polyelectrolytes with variable chain lengths. *Langmuir* **27,** 10763–9 (2011).

Appendix A. Supplemental Figures and Methods

A. Supplemental Methods

A.1. Limiting dilution assay

C. albicans 5314 were grown overnight (16-18h) in 5mL YPD broth (scraping taken from LiN2 ATCC stock) at 30C in the orbital shaker, 300rpm. For light exposure experiments, yeast suspension (1e6 cell/mL in PBS) were transferred to VWR Glass Vials, Short Form Style, Phenolic Cap on, 0.5 Dr. For dark experiments, , yeast suspension (1e6 cell/mL in PBS) were transferred to 1.5uL polypropylene centrifuge tubes. PPE-DABCO was added to a final concentration of 20µg/mL to cultures suspended in PBS at 1e6 cells/mL. Cultures were incubated with PPE-DABCO for 30 minutes prior to washing 3 times in PBS by centrifugation at 10,000xg for 5 minutes, followed by siphoning off the supernatant and resuspending cells in PBS, at 1e6cells/mL. Untreated controls included for both dark and light exposure experiments. The light irradiation experiments were carried out in a photoreactor (4 UV-lamps, LZC-ORG, Luzchem Research Inc., Ottawa, Canada). LZC-420 (centered at ~420 nm) was used to activate PPE-DABCO treated cultures and untreated cultures for 30min at room temperature. For dark exposure experiments, yeast were incubated, following pretreatment with PPE-DABCO and washing, for 30 minutes at room temperature in the dark. Following the 30 minute incubation in the dark or in the photochamber, the samples at 1e6cells/mL were diluted to the following ratios: undiluted (1:1e6), 1:1e3, 1:1e5, 1:1e6, 1:1e7. 1 µL of each sample, including the original undiluted sample was plated in triplicate on YPD agar plates, which were incubated for four days at 30C. Digital

photographs were taken periodically and analyzed in ImageJ (1.48p, Java 1.7.0_07 (64-bit), NIH).

A.2 FUN1 Metabolic Assay

C. albicans 5314 were grown overnight (16-18h) in 5mL YPD broth (scraping taken from LiN2 ATCC stock) at 30C in the orbital shaker, 300rpm. Yeast suspension (1e6 cell/mL in PBS) were transferred to 1.5uL polypropylene centrifuge tubes. PPE-DABCO was added to a final concentration of 20µg/mL to cultures suspended in PBS at 1e6 cells/mL. Cultures were incubated with PPE-DABCO or left untreated for 30 minutes prior to washing 3 times in PBS by centrifugation at 10,000xg for 5 minutes, followed by siphoning off the supernatant and resuspending cells in in RPMI+300mg/L L-glutamine+0.165M MOPS+0.2% glucose (pH 7.4) containing 20uM fluorescein at 1e6 yeast/mL. FUN1 was added to a final concentration of 10uM. 150µL of yeast were added to each of two channels, one containing the untreated suspension and the other channel containing the PPE-DABCO treated yeast, of an Ibidi µ-slide $VI^{0.4}$ luer (80601) using a pipette. The slide was incubated at 30C for 1h to allow yeast to adhere. a single field of the PPE-DABCO culture and untreated culture were exposed to the 405nm laser (14%, HV 830V, Gain 1) to activate the PPE-DABCO for a total of 4 scans per field (1024x1024, 0.207µm/pixel, Z depth 20 slices, 1.5µm/slice, scanning speed 2.0µs/pixel). The cultures were simultaneously scanned with the 473nm laser to fluoresce the fluorescein. Following this scan, the 405nm laser was shut off, and the PPE-DABCO and untreated fields previously exposed to the 405nm laser, along with a PPE-DABCO and untreated field not previously exposed to the 405nm laser, continued to be scanned for a following 2h, Z-stacks of each field taken every 10min (PLAPON 60X O NA:1.42,

0.207µm/pixel x 0.207µm/pixel, Z depth 20 slices, 1.5µm/slice, Sampling speed 2.0µs/pixel). The 473nm laser was used to visualize the fluorescein to generate a negative image of the growing cells that was used for image processing (1%, HV 610V, Gain 1). Experiment was performed once. Analysis of images was performed in ImageJ (1.48p, Java 1.7.0_07 (64-bit), NIH).

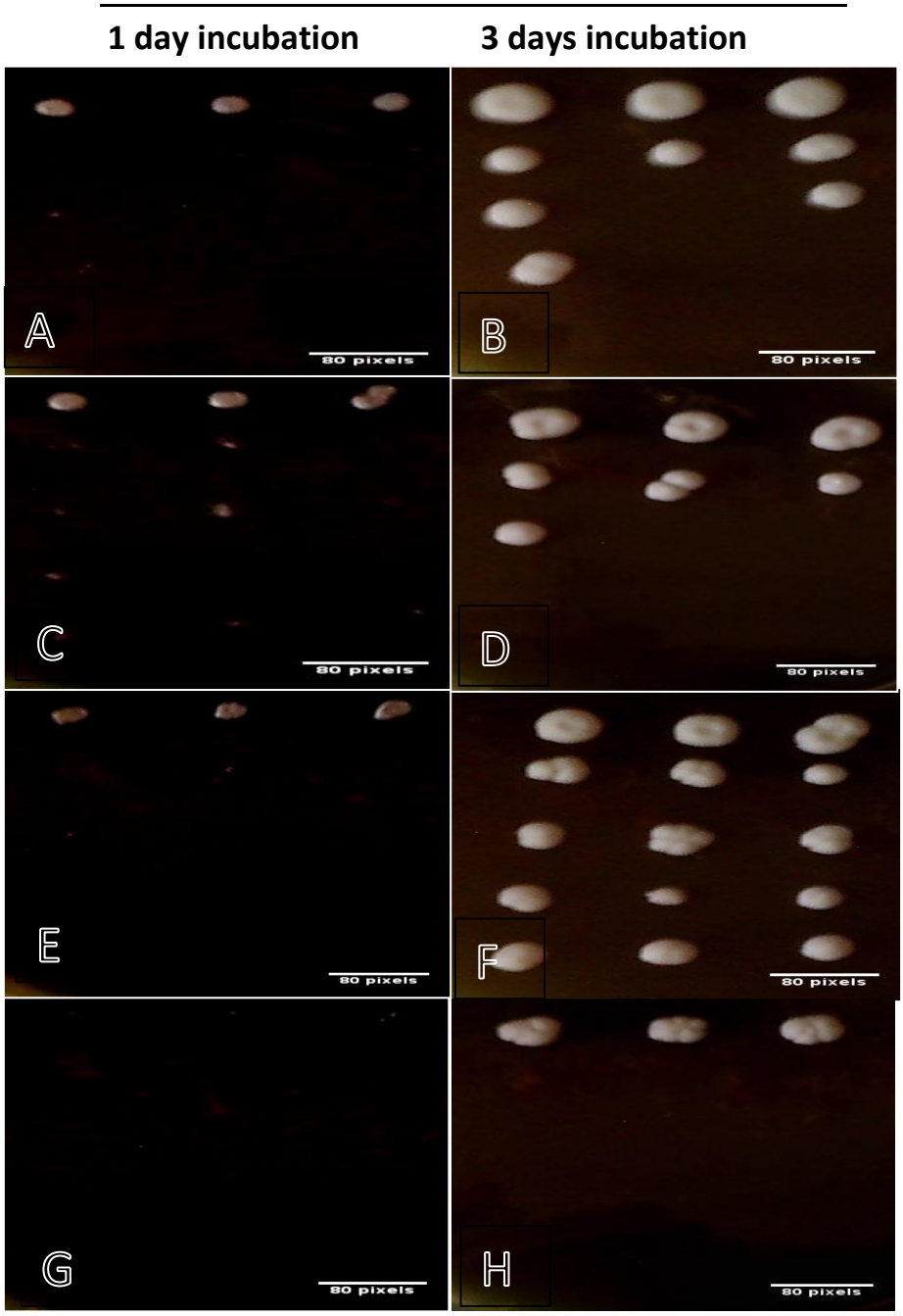

Figure A.1. Limiting dilution assay. *C.albicans* colonies on YPD agar following one or three days incubation at 30C. A-B) Untreated dark culture. C-D) Untreated culture exposed to 420nm light-irradiation for 30 minutes. E-F) PPE-DABCO dark treated culture. G-H) PPE-DABCO treated culture following 420nm light-irradiation for 30 minutes. Experiment performed in triplicate. Images representative of a single experimental repeat.

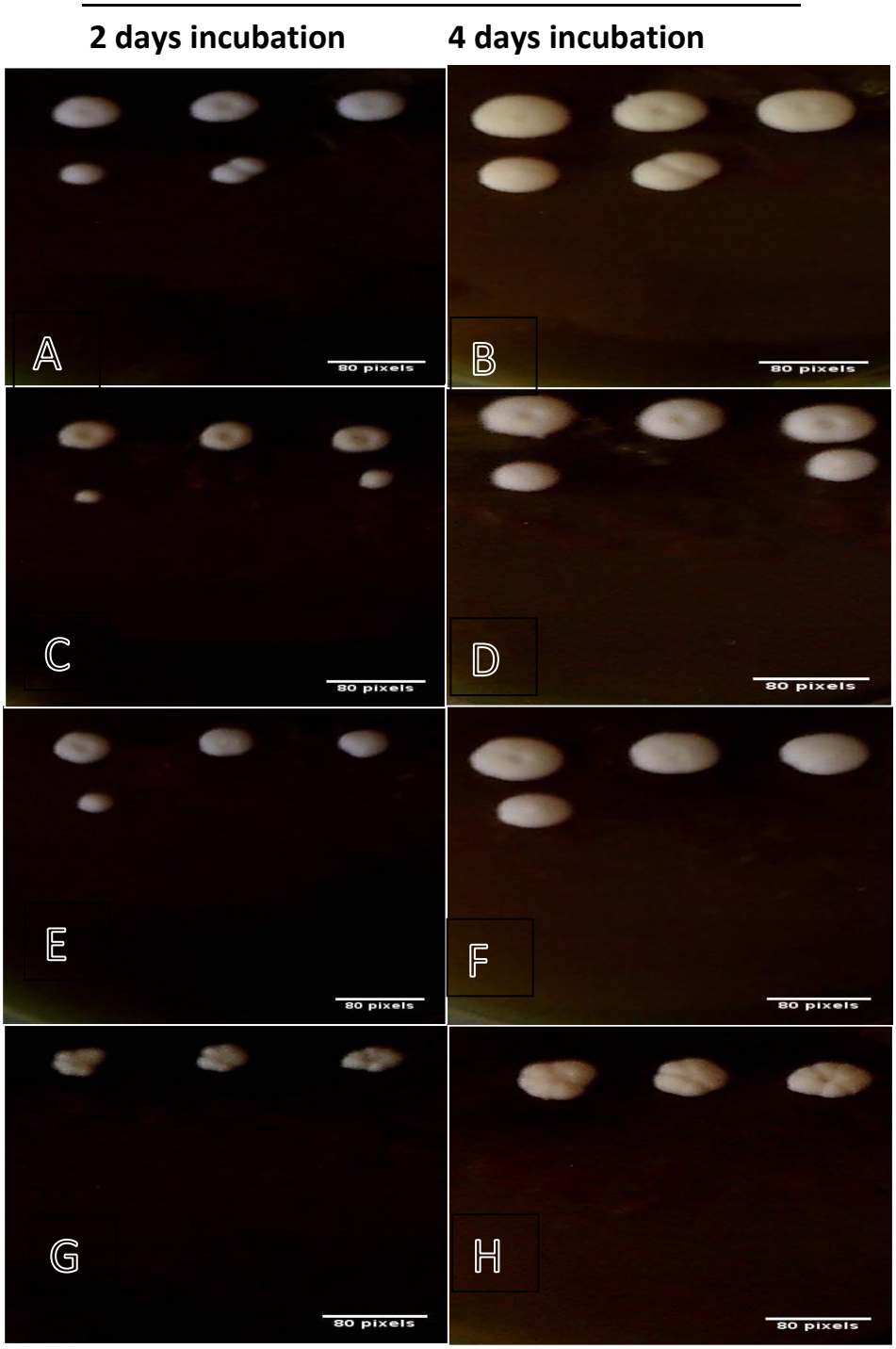

Figure A.2. Limiting dilution assay. *C.albicans* colonies on YPD agar following two or four days incubation at 30C. A-B) Untreated dark culture. C-D) Untreated culture exposed to 420nm light-irradiation for 30 minutes. E-F) PPE-DABCO dark treated culture. G-H) PPE-DABCO treated culture following 420nm light-irradiation for 30 minutes. Experiment performed in triplicate. Images representative of a single experimental repeat.

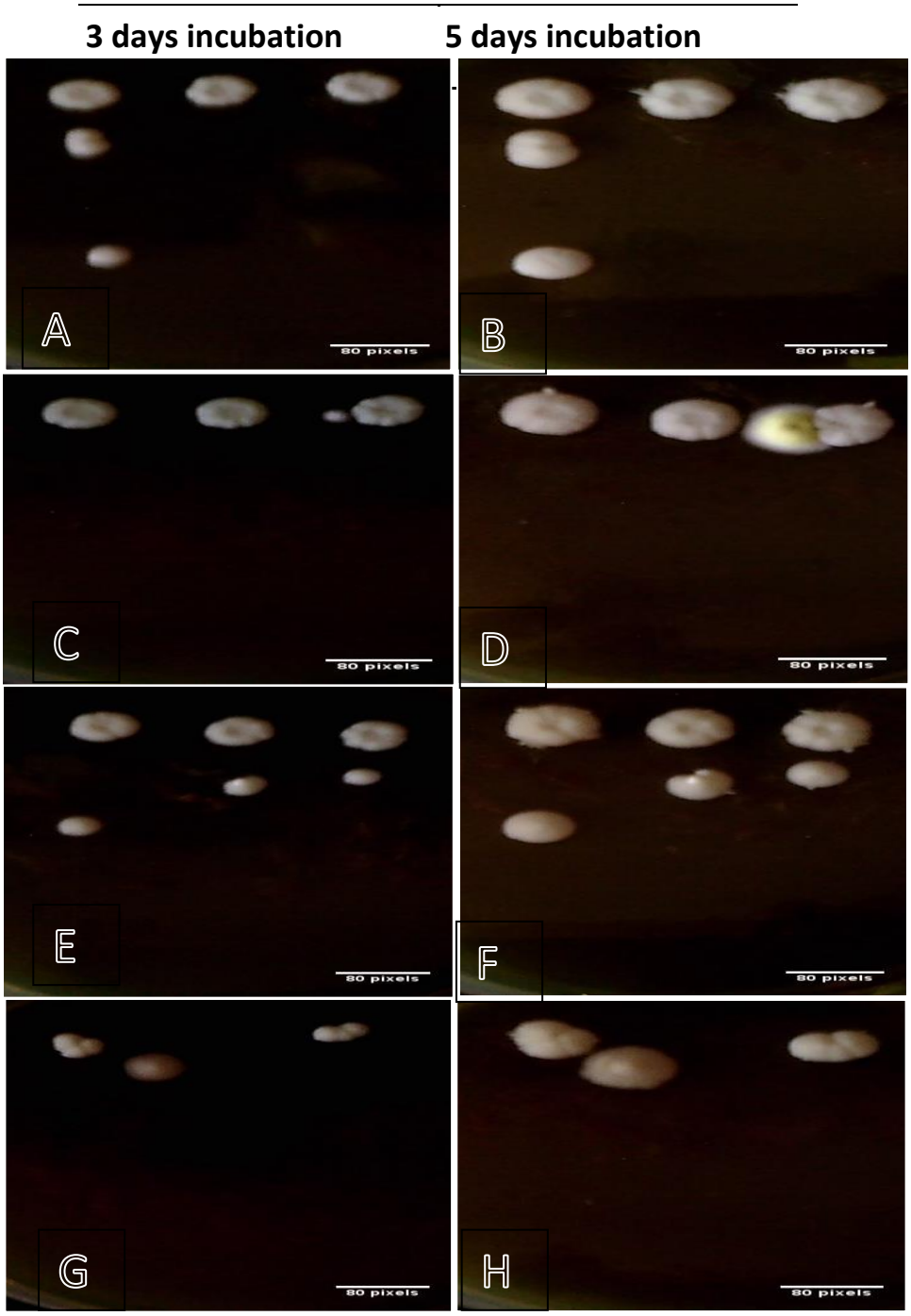

Figure A.3. Limiting dilution assay. *C.albicans* colonies on YPD agar following three or five days incubation at 30C. A-B) Untreated dark culture. C-D) Untreated culture exposed to 420nm light-irradiation for 30 minutes. E-F) PPE-DABCO dark treated culture. G-H) PPE-DABCO treated culture following 420nm light-irradiation for 30 minutes. Experiment performed in triplicate. Images representative of a single experimental repeat.

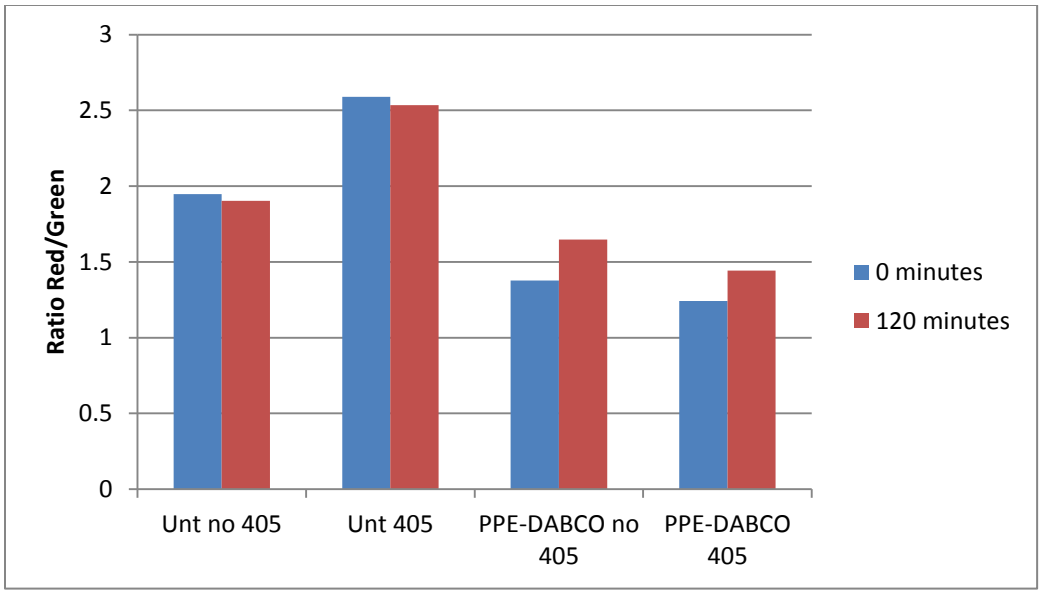

Figre A.4. FUN1 was added to *C.albicans* cultures (1e6 cells/mL) at a final concentration of 10µM. Quantification performed after two hours of growth following the 20 minute pre-exposure of the untreated and PPE-DABCO treated field to the 405nm laser. Experiment was performed once.

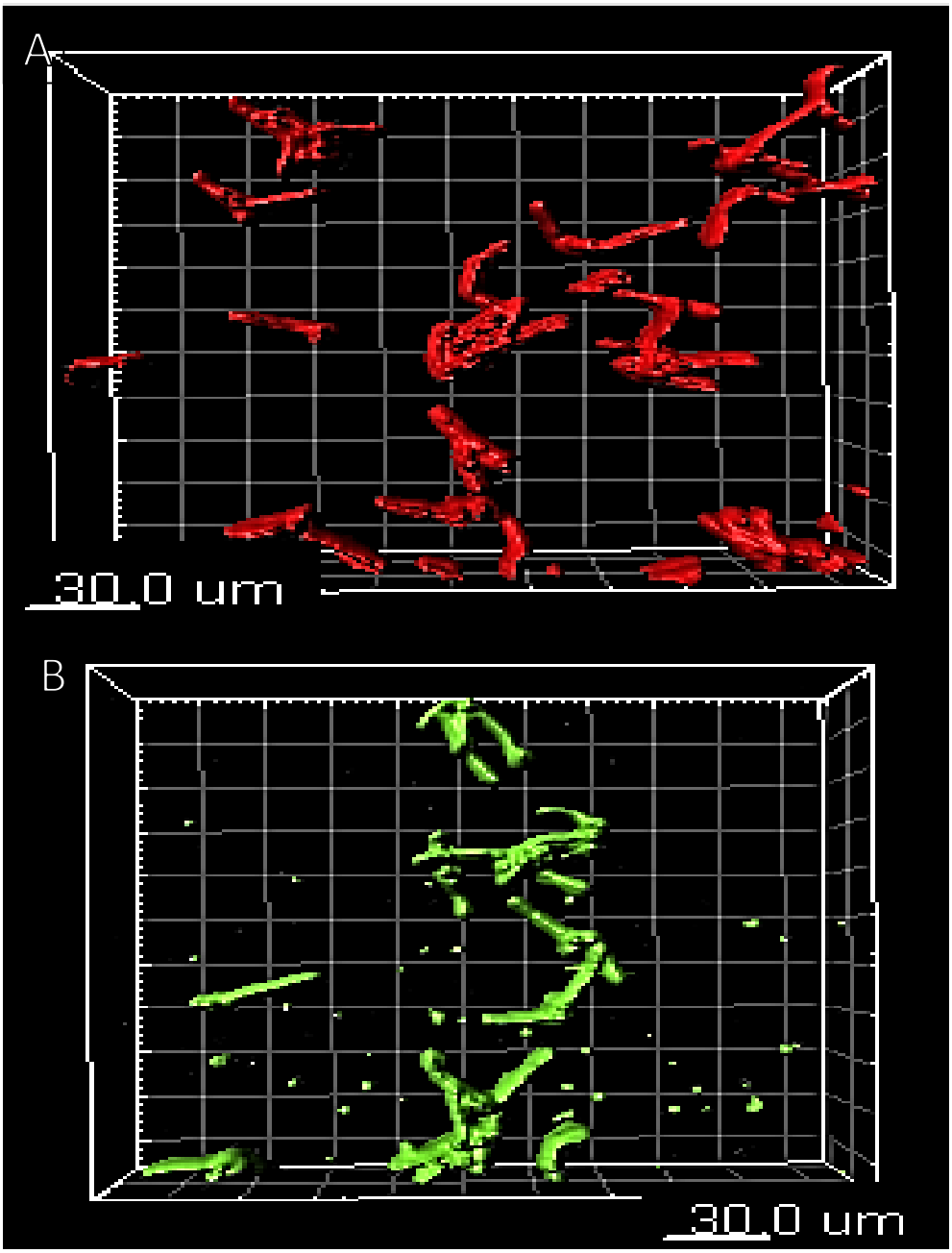

Figure A.5. Imaris surface rendering of *C.albicans* hyphal growth from live-cell confocal experiments with 405nm laser. A) Untreated culture after 2h of growth without 405nm laser activation. B) PPE-DABCO (20ug/mL) treated culture after 2h of growth without 405nm laser exposure. Experiment performed in duplicate. Images representative of a single experimental repeat.

Appendix B. *C. albicans* growth under flow

B. Supplemental Methods

B.1. Growth of *C. albicans* biofilms under flow conditions

C. albicans 5314 were grown under flow conditions using either an Ibidi µ-slide I $^{0.2}$ Luer uncoated (80161), channel height 200 µm, 50 µL volume or an Ibidi µ-slide I $^{0.8}$ Luer uncoated (80191), channel height 800 µm, 200 µL volume. The slide was first prepared the day prior to live imaging by attaching 2 dams constructed from two 15mL polypropylene tubes, which were cut at the 14mL mark with a narrow notch cut into the dams from the top to the middle (about 2-3mm wide). The dams were positioned around the inlet and outlet of the slide, with both notches positioned in the same direction 90 degrees perpendicular to the narrow side of the slide; the notches hold the vacuum lines in place as a precaution against leakage overflow of media. The dams were attached to the slide using DAP® brand 100% Silicone All-Purpose Adhesive Sealant to prevent leakage of media during media flow through the slide. The slide was then filled with sterile fetal bovine serum with two 1mL syringes, leaving the syringes in the inlet and outlet after injection. The slide was incubated overnight at room temperature and handled exclusively in the BSC. *C. albicans* 5314 were grown overnight (16-18h) in 5mL YPD broth (scraping taken from LiN2 ATCC stock) at 30C in the orbital shaker, 300rpm. The following day, the media, pump and all components of the microfluidics were preheated on the microscope stage, set to 37C. The slide was washed with 5mL of PBS, using two 5mL syringes in the inlet and outlet. The yeast were counted with a hemocytometer and 1.0-1.5e6 yeast were washed in 1mL PBS one time at 10,000xg for 5min. The pellet was

resuspended in 1mL RPMI+300mg/L L-glutamine+0.165M MOPS+0.2% glucose (pH 7.4). The yeast were added to the slide using two 1mL syringes and allowed to adhere by incubation the slide at 37C for 1h. For biofilms grown with 0.1ug/mL calcofluor white, calcofluor white was added to warmed RPMI media at a final concentration of 0.1ug/mL. For biofilms grown in fluorescein, fluorescein was added to warmed RPMI media at a final concentration of 10uM. For biofilms grown in caspofungin, casofungin was added to the warmed RPMI media at final concentrations of 0.015ug/mL. The media was flown through the slide at a rate of 0.1mL/min using a Watson Marlow 120 pump. The confocal stage was kept at 37C for the duration of imaging. The imaging was performed using an Olympus FV1000 confocal microscope (PLAPON 60X O NA:1.42, 0.207um/pixel x 0.207um/pixel x 2.0um/slice, Sampling speed 2.0us/pixel), with Z stacks imaged every 5 min. Analysis performed using Imaris software (X63, 6.1.5, Bitplane, Zurich, Switzerland), Minitab® (16.2.4, LEADTOOLS © 1991-2004, LEAD Technologies, Inc.) and Microsoft® Excel® 2010 (14.0. 7109.5000).

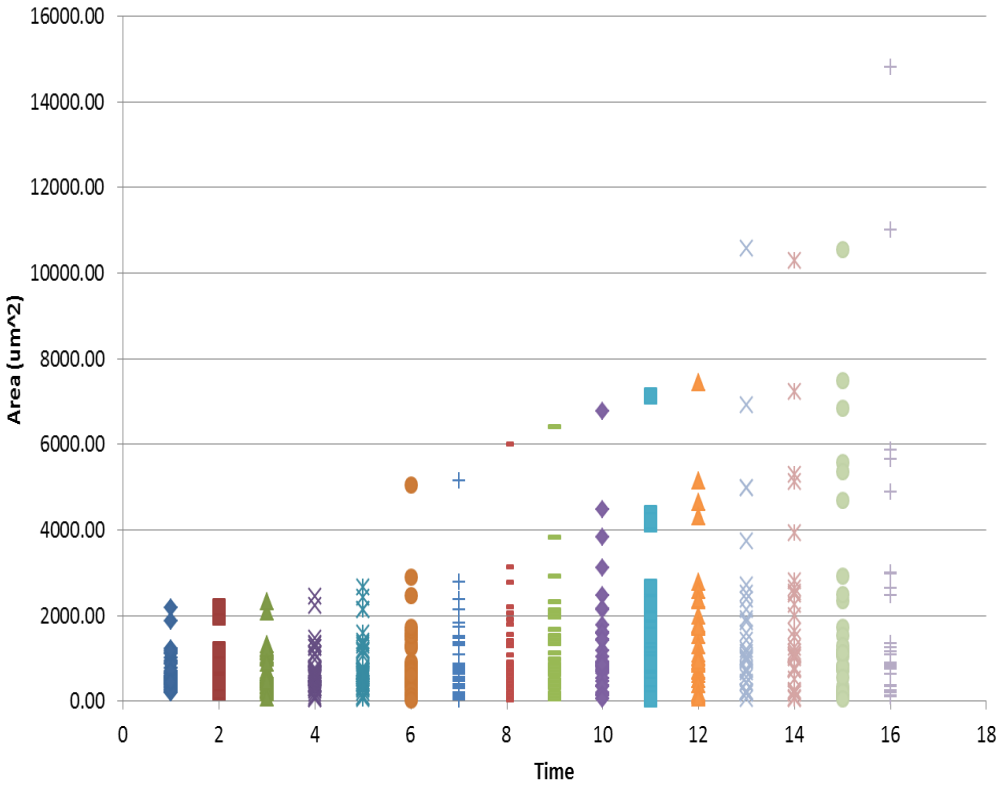

Figure B1. *C.albicans* growth over time under flow. Imaris surface-rendered objects from a single experimental repeat of a flow experiment performed with fluorescein and calcofluor-white. Objects with an initial area greater than 500µm^2 were excluded from further analysis, based upon the position of the centroid of the object. Each time point equals 5 minutes.

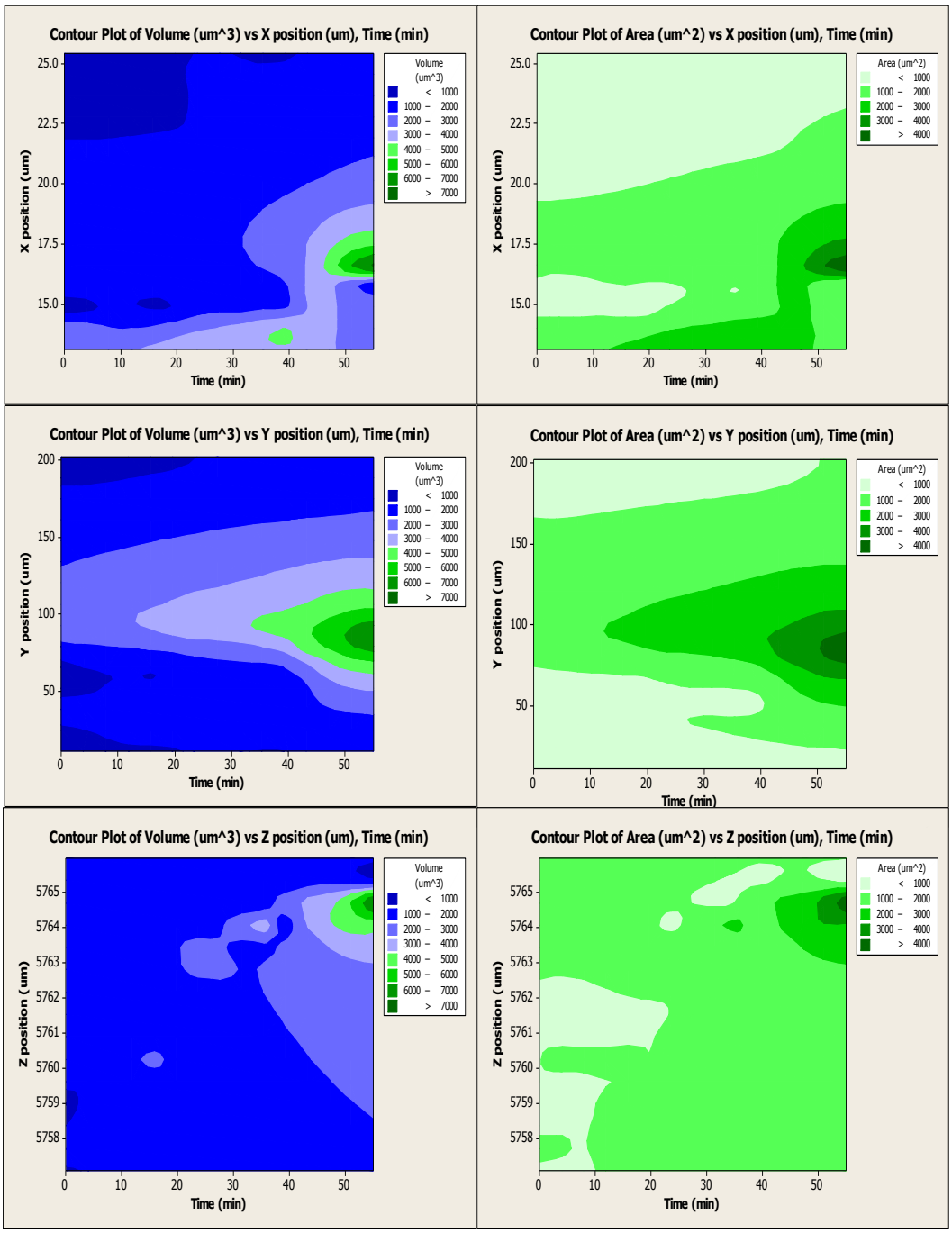

Figure B2. Live-cell imaging and activation of untreated *C. albicans* culture with fluorescein allows spatial and temporal analysis of hyphal growth. A) Area (μm$^{\wedge 2}$) and B) Volume (μm$^{\wedge 3}$) of surface-rendered cells vs. X position (μm) over time (min). C) Area (μm$^{\wedge 2}$) and D) Volume (μm$^{\wedge 3}$) of surface-rendered cells vs. Y position (μm) over time (min). E) Area (μm$^{\wedge 2}$) and F) Volume (μm$^{\wedge 3}$) of surface-rendered cells vs. Z position (μm) over time (min). Experiment performed in triplicate. Graphs representative of a single experimental repeat.

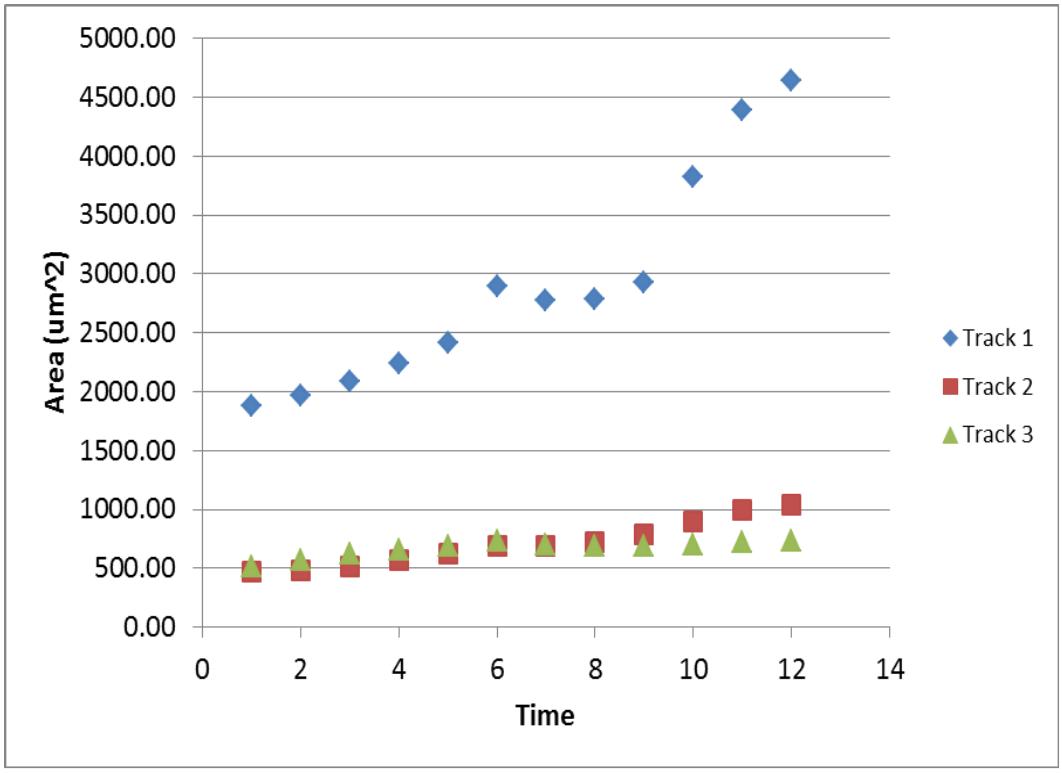

Figure B3. *C.albicans* growth over time under flow. Imaris surface-rendered objects from a single experimental repeat of a flow experiment performed with fluorescein and calcofluor-white. Objects with an initial area greater than 500µm^2 were excluded from further analysis, based upon the position of the centroid of the object. Graphical example of tracked surface-rendered objects change in area (µm^2) over time. Each time point equals 5 minutes.

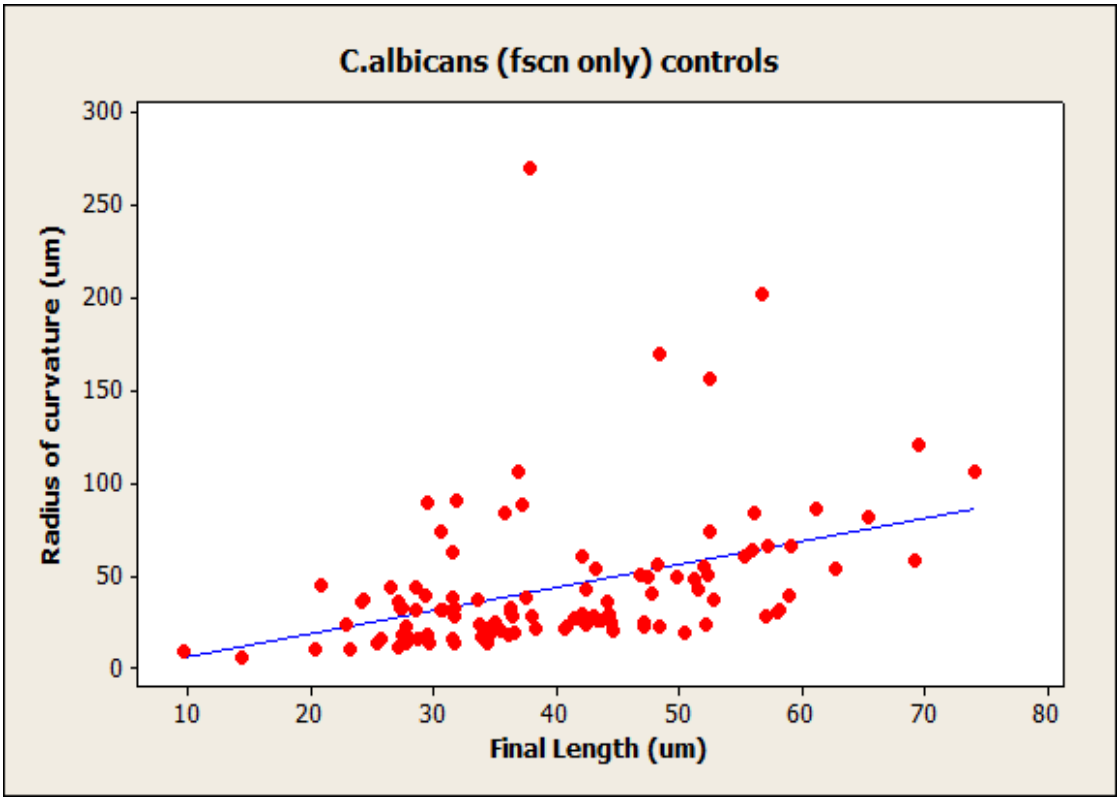

Figure B4. *C.albicans* radius of curvature of hyphae following 2h of growth under flow. Imaris surface-rendered objects from a single experimental repeat of a flow experiment performed with fluorescein only. Radius of curvature determined using three points along the entire length of the surface-rendered object. Calculation of radius of curvature performed using Excel formula from Newton Excel Bach: ArcCenP3.

Appendix C. *C. albicans* growth with sub-MIC caspofungin

C. Supplemental Methods

C.1. C. albicans dosage response to caspofungin under static conditions

C. albicans 5314 were grown overnight (16-18h) in 5mL YPD broth (scraping taken from LiN2 ATCC stock) at 30C in the orbital shaker, 300rpm. The yeast were counted with a hemocytometer, and washed in 1mL PBS one time at 10,000xg for 5min. Approximately 4e5 yeast/mL were resuspended RPMI+300mg/L L-glutamine+0.165M MOPS+0.2% glucose (pH 7.4). Yeast were seeded on MatTek Glass Bottom 35mm Microwell Dish, No. 1.5 coverglass (0.16-0.19mm), by adding 2mL of the yeast suspension to each dish. Caspofungin was added in the following concentrations to individual dishes: 0, 0.02, 0.03 and 0.04ug/mL. The dishes were incubated at 37C, 5% CO2 for 1h. The cells were then fixed by addition of 4% PFA for 20min at room temperature. The dishes were washed three times in PBS to remove non-adherent cells and excess PFA by rinsing with PBS and using vacuum suction. Following washing, 2mL of PBS was added to each dish and remaining cells were stained with calcofluor-white at a final concentration of 10ug/mL. The yeast were immediately imaged on an Olympus FV1000 confocal microscope (UPLSAPO 40X 2 NA:0.95, 0.31 um/pixel x 0.31 um/pixel x 1.5um/slice, Sampling speed 2.0us/pixel). Experiment performed in triplicate, 7-10 fields analyzed per dish using Imaris software (X63, 6.1.5, Bitplane, Zurich, Switzerland) and Minitab® (16.2.4, LEADTOOLS © 1991-2004, LEAD Technologies, Inc.).

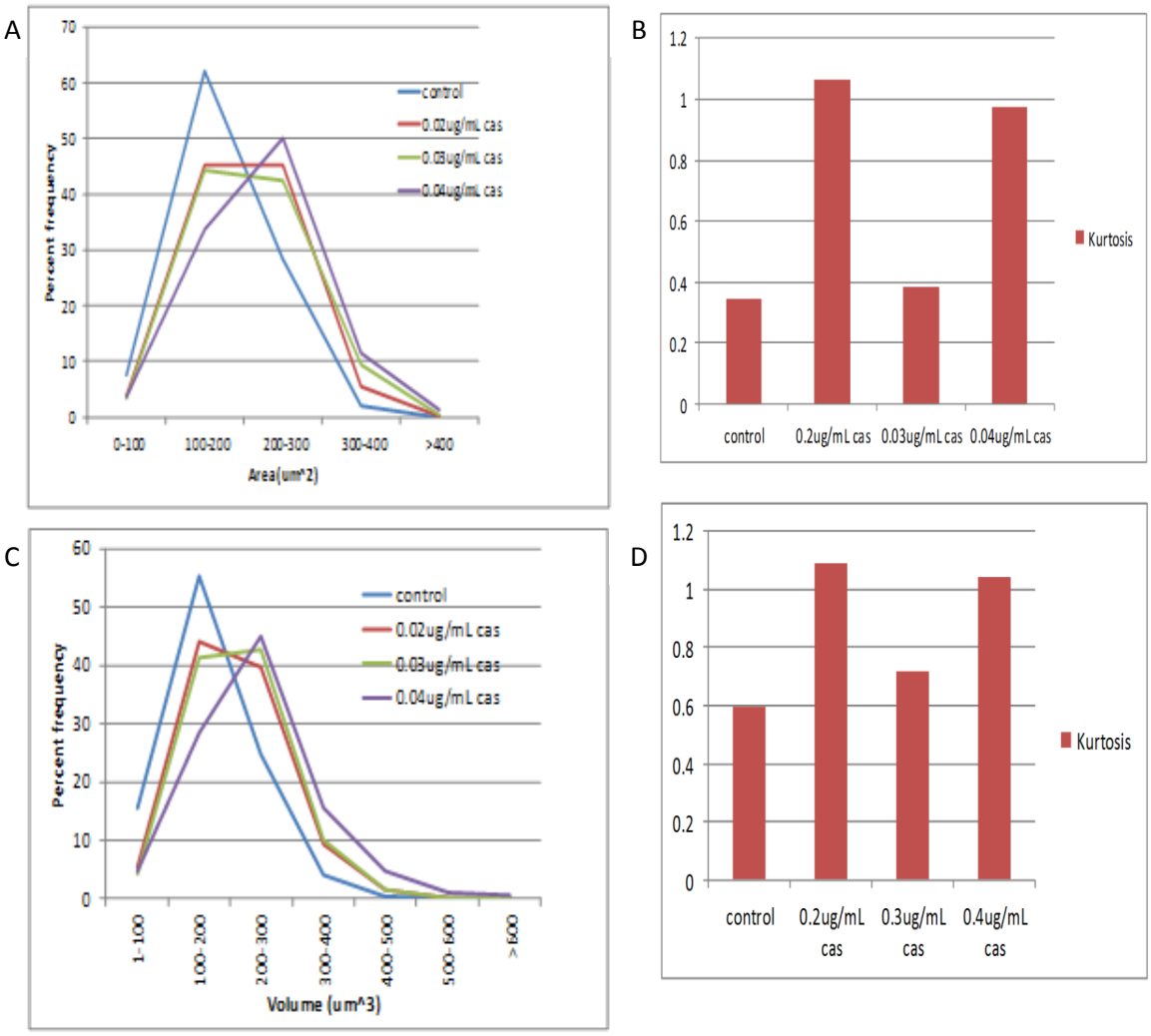

Figure C.1. Quantifiable, dose-dependent changes in the distribution of hyphal elongation in the presence of sub-MIC concentrations of caspofungin. A) Distribution of area (μm^2) of hyphae following 1h of growth with indicated concentrations of caspofungin. B) Kurtosis of (A). C) Distribution of volume (μm^3) of hyphae following 1h of growth with indicated concentrations of caspofungin. D) Kurtosis of (C). Hyphae fixed in 4% PFA following 1h of growth at 37C, stained with 10µg/mL calcofluor white and imaged with laser-scanning confocal microscopy. Data from three independent experiments (N=763, 946, 902, 827 individual cells for control, 0.02µg/mL, 0.03µg/mL, 0.04µg/mL caspofungin respectively).

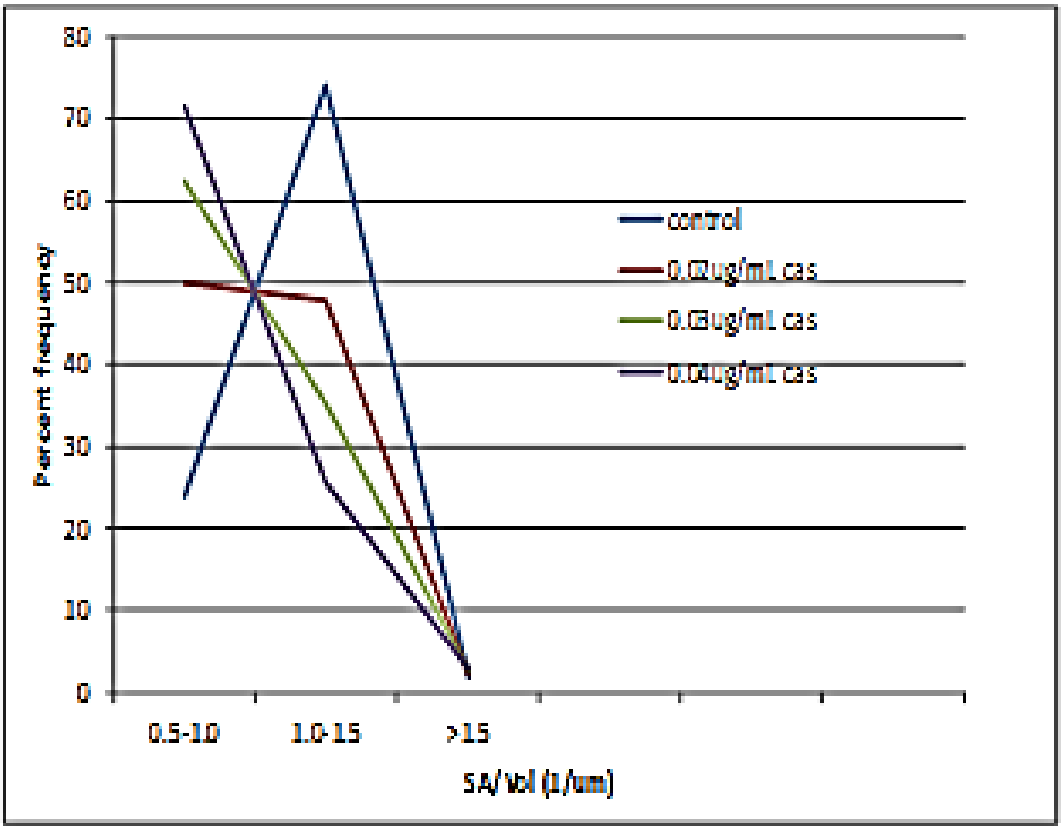

Figure C.2. Quantifiable, dose-dependent changes in the distribution of hyphal elongation in the presence of sub-MIC concentrations of caspofungin. Graphical representation of surface area to volume ratio. Hyphae fixed in 4% PFA following 1h of growth at 37C, stained with 10µg/mL calcofluor white and imaged with laser-scanning confocal microscopy. Data from three independent experiments (N=763, 946, 902, 827 individual cells for control, 0.02µg/mL, 0.03µg/mL, 0.04µg/mL caspofungin respectively).

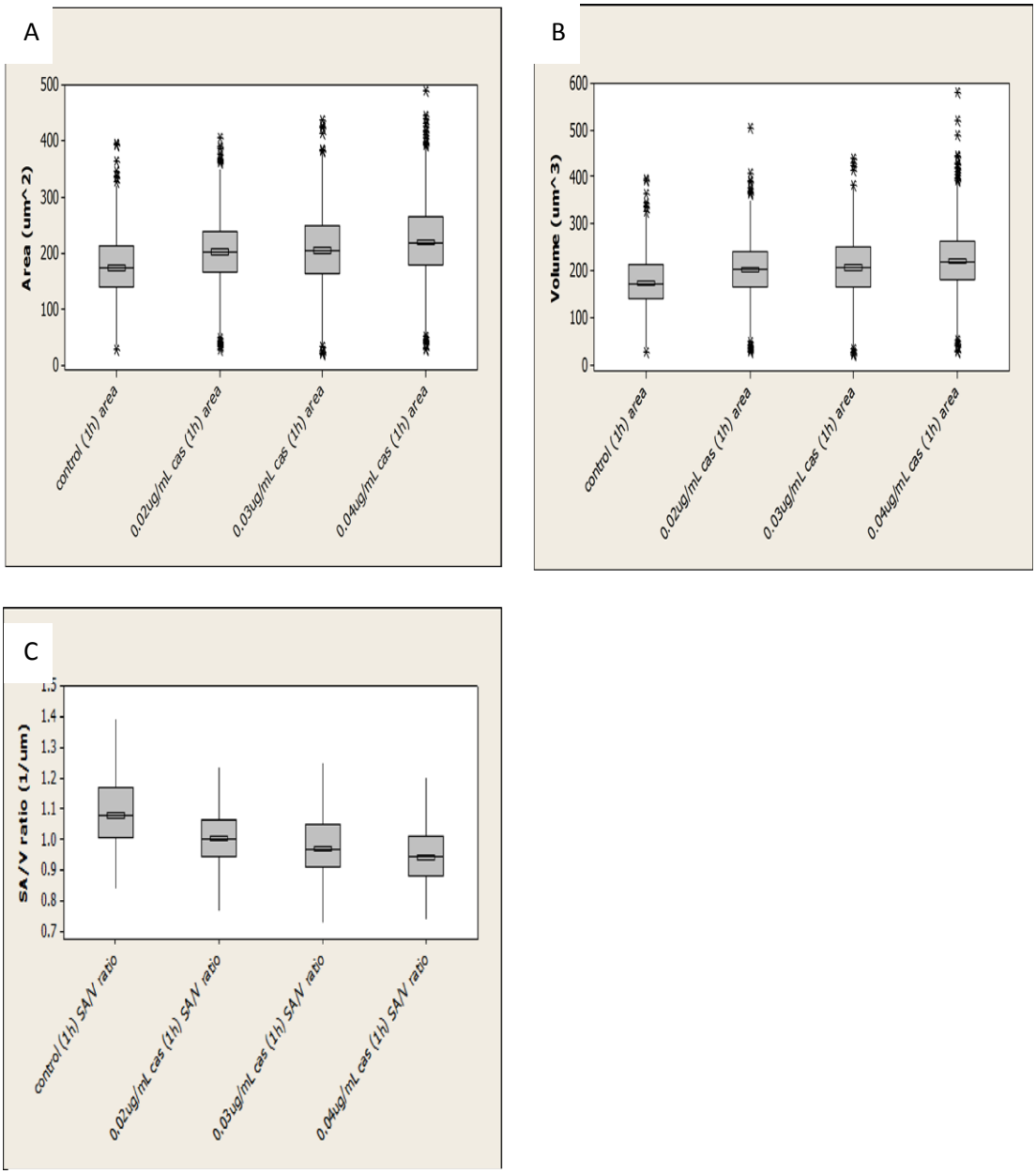

Figure C.3. Morphological differences observable in hyphae in presence of increasing doses of caspofungin. A) Area (μm^2) B) Volume (μm^3) and C) Surface area to volume ratio (μm^{-1}) of hyphae grown for 1h at 37C in presence of indicated concentrations of caspofungin. Hyphae fixed with 4% PFA for 20 minutes, stained with 10µg/mL calcofluor white and imaged with laser-scanning confocal microscopy. Data from three independent experiments (N=763, 946, 902, 827 individual cells for control, 0.02µg/mL, 0.03µg/mL, 0.04µg/mL caspofungin respectively). Statistical significance at 95% CI determined by Mann-Whitney nonparametric comparison.

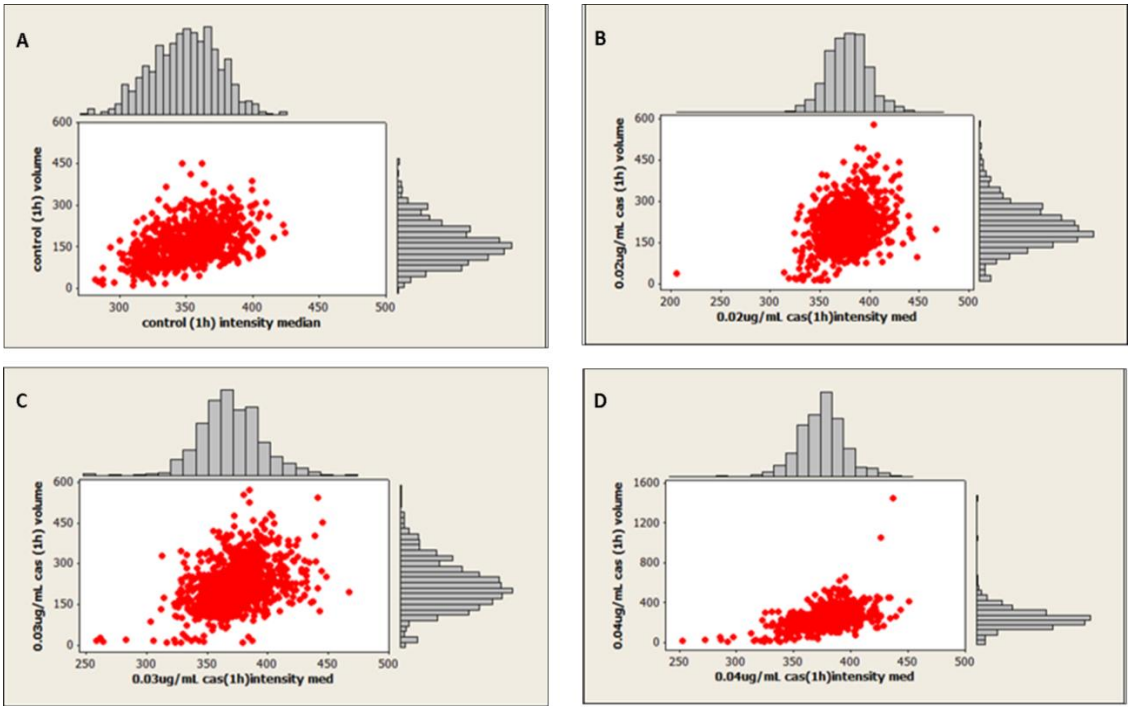

E	Regression Analysis			
Condition	Equation	P	R^2	R-Sq(adj)
Control	control (1h) volume = - 299 + 1.32 control (1h) intensity median	0.000	21.30%	21.20%
0.02µg/mL cas	0.02µg/mL cas (1h) volume = - 297 + 1.34 0.02µg/mL cas(1h) intensity med	0.000	13.70%	13.60%
0.03µg/mL cas	0.03µg/mL cas (1h) volume = - 311 + 1.43 0.03µg/mL cas(1h) intensity med	0.000	17.00%	16.90%
0.04µg/mL cas	0.04µg/mL cas (1h) volume = - 724 + 2.58 0.04µg/mL cas(1h) intensity med	0.000	25.90%	25.80%

Figure C.4. Chitin content of hyphal cell wall correlates to an increase in hyphal volume. A-D) Marginal plots of hyphal volume (μm^3) vs. intensity median of calcofluor-white fluorescence for populations treated with indicated concentrations of caspofungin. E) Regression analysis for data presented in A-D. Hyphae fixed in 4% PFA following 1h of growth at 37C, stained with 10µg/mL calcofluor white and imaged with laser-scanning confocal microscopy. Data from three independent experiments (N=763, 946, 902, 827 individual cells for control, 0.02µg/mL, 0.03µg/mL, 0.04µg/mL caspofungin respectively) *Outliers excluded from analysis of D.

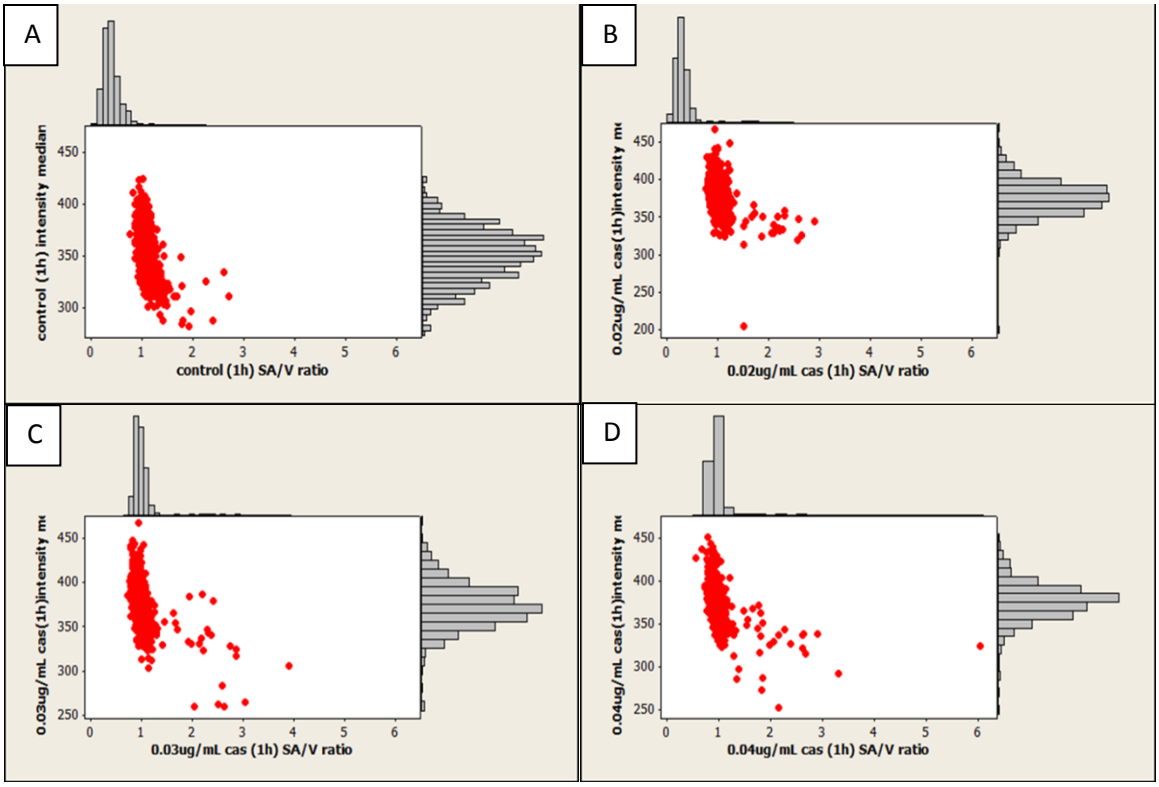

Figure C.5. Increased chitin content of hyphal cell wall correlates to a decrease in SA:Vol ratio of hyphae. A-D) Marginal plots of hyphal SA:Vol ratios (μm^{-1}) vs. intensity median of calcofluor-white fluorescence for populations treated with indicated concentrations of caspofungin. E) Regression analysis for data presented in A-D. Hyphae fixed in 4% PFA following 1h of growth at 37C, stained with 10µg/mL calcofluor white and imaged with laser-scanning confocal microscopy. Data from three independent experiments (N=763, 946, 902, 827 individual cells for control, 0.02µg/mL, 0.03µg/mL, 0.04µg/mL caspofungin respectively)

Regression Analysis				
Condition	Equation	P	R^2	R-Sq(adj)
Control	control (1h) SA/V ratio = 2.66 - 0.00438 control (1h) intensity median	0.000	35.6%	35.5%
0.02µg/mL cas	0.02µg/mL cas (1h) SA/V ratio = 2.44 - 0.00374 0.02µg/mL cas(1h)intensity med	0.000	16.9%	16.8%
0.03µg/mL cas	0.03µg/mL cas (1h) SA/V ratio = 2.90 - 0.00506 0.03µg/mL cas(1h)intensity med	0.000	25.4%	25.3%
0.04µg/mL cas	0.04µg/mL cas (1h) SA/V ratio = 3.43 - 0.00652 0.04µg/mL cas(1h)intensity med	0.000	22.9%	22.9%

Figure C.6. Increased chitin content of hyphal cell wall correlates to a decrease in SA:Vol ratio of hyphae. Regression analysis for data presented in Figure C.5 (A-D). Hyphae fixed in 4% PFA following 1h of growth at 37C, stained with 10µg/mL calcofluor white and imaged with laser-scanning confocal microscopy. Data from three independent experiments (N=763, 946, 902, 827 individual cells for control, 0.02µg/mL, 0.03µg/mL, 0.04µg/mL caspofungin respectively)